

Curriculum Vitae

Shaneen Baxter

ssbaxter85@gmail.com

Doctor of Philosophy, 2020

EDUCATION

- 2012 – 2020 University of Maryland, Baltimore; PhD in Molecular Medicine
- 2005 – 2008 Midwestern University, Downers Grove, IL; MS in Biomedical Science
- 1995 – 1997 University of Illinois at Urbana-Champaign; BS in General Biology

EXPERIENCE

- 2012 – 2020 **Graduate Research Assistant;** University of Maryland, Baltimore
- 2009 – 2012 **Research Technologist;** University of Chicago, IL 60637
- 2005 – 2008 **Graduate Research Assistant;** Midwestern University, IL 60515

PUBLICATIONS

Manuscripts

Li L and Baxter SS, Zhao P, Gu N, Zhan X. Differential interactions of MIM and IRTKS with Rab proteins in endocytosis of CXCR4. *Journal of Biological Chemistry*. 2019 Apr 19; 294(16):6494-6505

Li L, Baxter SS, Gu N, Ji M, Zhan X. Missing-in-metastasis protein downregulates CXCR4 by promoting ubiquitination and Rab-mediated intracellular trafficking. *Journal of Science*. 2017 Apr 15;130(8):1475-1485

Li L, Liu H, Baxter SS, Gu N, Ji M, Zhan X. The SH3 domain distinguishes the role of I-BAR proteins IRTKS and MIM in chemotactic response to serum. *Biochem Biophys Res Commun*. 2016 Oct 28;479(4):787-792. doi: 10.1016/j.bbrc.2016.09.131. Epub 2016 Sep 28

Kariuki SN, Maranville JC, Baxter SS, Jeong C, Nakagome S, Hrush CL, Witonsky DB, Sperling AI, Di Rienzo A. Mapping Variation in Cellular and Transcriptional Response to 1,25-Dihydroxyvitamin D3 in Peripheral Blood Mononuclear Cells. *PLoS One*. 2016; 11(7): e0159779

Kupfer SS, Maranville JC, Baxter SS, Huang Y, Rienzo AD. Comparison of cellular and transcriptional responses to 1,25-dihydroxyvitamin d3 and glucocorticoids in peripheral blood mononuclear cells. *PLoS One*. 2013 Oct 8;8(10):e76643. doi: 10.1371/journal.pone.0076643; PMID: 24116131

Maranville JC, Baxter SS, Witonsky DB, Chase MA, Di Rienzo A. Genetic mapping with multiple levels of phenotypic information reveals determinants of lymphocyte glucocorticoid sensitivity. *Am J Hum Genet*. 2013 Oct 3;93(4):735-43. doi: 10.1016/j.ajhg.2013.08.005. Epub 2013 Sep 19; PMID: 24055111

Maranville JC, Baxter SS, Torres JM, Di Rienzo A. Inter-ethnic differences in lymphocyte sensitivity to glucocorticoids reflect variation in transcriptional response. *Pharmacogenomics J*. 2011 Dec 13; DOI 10.1038/tpj.2011.55

Maranville JC, Luca F, Richards AL, Wen X, Witonsky DB, Baxter S, Stephens M, Di Rienzo A. Interactions between glucocorticoid treatment and cis-regulatory polymorphisms contribute to cellular response phenotypes. *PLoS Genet*. 2011 Jul; DOI 10.1371/journal.pgen.1002162

Baxter SS, Carlson LA, Mayer AMS, Hall ML, Fay MJ. Granulocytic Differentiation of HL-60 Promyelocytic Leukemia Cells is Associated with Increased Expression of Cul5. *In Vitro Cell Dev Biol Anim*. 2009 Jan; DOI 10.1007/s11626-008-9163-4.

Abstract

Fay, MJ; Tan, GK; Baxter, SS; Hall, ML; Mayer, AMS; Carlson, LA. Differential expression of full-length and truncated cullin-5 is associated with granulocytic differentiation of HL-60 leukemia cells. *In Vitro Cell Dev Biol*. 2009; 45:S42.

Baxter, SS; Carlson, LA; Mayer, AMS; Hall, ML; Fay MJ. Granulocytic Differentiation of HL-60 Promyelocytic Leukemia Cells is Associated with Increased mRNA Expression for Components of the Cullin-5-Containing E3 Ubiquitin Ligase. *In Vitro Cell Dev Biol*. Spring 2008; 44:S43

SOCIETY MEMBERSHIP AND LEADERSHIP

- 2019 Member, American Society for Biochemistry and Molecular Biology
- 2017 Recruitment activities for the Molecular Medicine Program at UMB
- 2017 Seminar peer review, CVID Research in Progress Meeting, UMB
- 2016 Recruitment activities for the Molecular Medicine Program at UMB
- 2014 Lab supervision of a high school student for summer internship
- 2008 – 2015 Member, The Society of *In Vitro* Biology

PRESENTATIONS

Molecular Medicine Seminar, University of Maryland, Baltimore, November 15th, 2018; Title: The Role of MIM in intracellular Membrane Trafficking; Oral PPT Presentation

9th Annual Cancer Biology Research Retreat, University of Maryland, Baltimore, April 30th, 2018; Title: MTSS1 Facilitates Intracellular Vesicle Trafficking; Poster

Center for Vascular and Inflammatory Diseases Research in Progress Meeting; University of Maryland, Baltimore; March 1st, 2018; Title: Role of MIM in Intracellular Trafficking; Oral PPT Presentation

8th Annual Cancer Biology Research Retreat, University of Maryland, Baltimore, June 13th, 2017; Title: Pro-inflammatory Cytokines Regulate the Gene Expression and Function of MTSS1; Poster

2016 Molecular Medicine Retreat; University of Maryland, Baltimore, October 6th, 2016; Title: The role of the MTSS1 Gene in Macrophage Function and Tumor-promoting Inflammation; Poster

2016 ASH Meeting on Lymphoma Biology, Colorado Springs, Co; June 18-21; Title: The Role of the MTSS1 Gene in Macrophage Function and Tumor-Promoting Inflammation; Poster

2016 NCI CRCHD Professional Development Workshop; Bethesda, MD; May 22-24; Title: The Role of the MTSS1 Gene in Macrophage Function and Tumor-Promoting Inflammation; Poster

Center for Vascular and Inflammatory Diseases Research in Progress Meeting; University of Maryland, Baltimore; May 20th, 2016; Title: The role of the MIM gene in macrophage function and tumor-promoting inflammation; Oral PPT Presentation

2008 World Congress on In Vitro Biology, Tucson, AZ, June 14-18, 2008; Title: Granulocytic Differentiation of HL-60 Promyelocytic Leukemia Cells is Associated with Increased mRNA Expression for Components of the Cullin-5-Containing E3 Ubiquitin Ligase; Poster

2008 Student Research Day, Northwestern University, Downers Grove, IL, May 2008; Title: Granulocytic Differentiation of HL-60 Promyelocytic Leukemia Cells is Associated with Increased mRNA Expression for Components of the Cullin-5-Containing E3 Ubiquitin Ligase; Poster

AWARDS

2008 Honor B. Fell Award, The Society for In Vitro Biology, Tucson, AZ

2008 Student Travel Award, The Society of In Vitro Biology, Tucson, AZ

2008 2nd Place Award, Student Poster Competition, Society for In Vitro Biology, Tucson, AZ

Abstract

Title: Investigating the Role of Metastasis Suppressor 1 (MTSS1/ MIM) in Cancer Biology

Shaneen Baxter, Doctor of Philosophy, 2020

Dissertation Directed by: Steven Zhan, PhD, Professor, Department of Pathology, Molecular Medicine Program

Metastasis suppressor 1 (MTSS1/ MIM) is a multi-domain, membrane-associated protein that has been linked to progression and poor prognosis of several types of cancer. It was initially thought to be metastasis suppressor, but it has been shown to be overexpressed as well as downregulated in both metastatic and non-metastatic cancer, making its role in tumorigenesis unclear. There are also questions about how MIM becomes deregulated in certain types of cancer. In this study, we hypothesized that factors within the microenvironment such as inflammation, nutrient availability, chemokine gradients and autophagy are major contributors to the role of MIM in cancer progression and metastasis.

As a member of the BAR domain superfamily, a family of proteins that bind and deform membranes, MIM is thought to be involved in intracellular membrane trafficking pathways such as endocytosis and autophagy. This lab previously reported that MIM interacts with E3 ubiquitin ligase, AIP4, and endocytic Rabs to regulate cell surface expression of the CXCR4 receptor. In this study, we further investigated the role of MIM in CXCR4 endocytosis by examining the interaction of MIM with Rab7 and Rab11. Upon internalization, CXCR4 may be guided into the lysosomal degradation pathway or the recycling pathway. We found that an interaction with Rab7 (a marker for late

endosomes of the lysosomal pathway) is necessary for MIM to function in CXCR4 endocytosis. We also found that MIM does not interact with Rab11 (a marker for recycling endosomes), instead, another I-BAR domain protein, IRTKS, seems to mediate CXCR4 recycling. We examined the role inflammation may play in aberrant MIM expression and function, and discovered that inflammatory cytokines downregulate MIM in macrophages, indirectly leading to CXCR4 cell surface overexpression and increased migration of these cells towards a SDF-1 gradient. This is of significance because SDF-1 is often secreted by stromal cells within the tumor microenvironment and at common metastatic sites. We also investigated the role of MIM in autophagy, and found that overexpression of MIM inhibits basal autophagy, which has the potential to promote tumorigenesis. Overall, our results provided further insights into how MIM deregulation can lead to cancer progression and metastasis.

Investigating the Role of Metastasis Suppressor1 (MTSS1/ MIM) in Cancer Biology

by
Shaneen Baxter

Dissertation submitted to the Faculty of the Graduate School of the
University of Maryland, Baltimore in partial fulfillment
of the requirements for the degree of
Doctor of Philosophy
2020

©Copyright 2020 by Shaneen Baxter

All rights Reserved

Table of Contents

List of Tables.....	vii
List of Figures.....	viii
List of Abbreviations.....	x
CHAPTER 1: INTRODUCTION.....	1
1.1 MTSS1/ MIM and Cancer.....	1
1.2 Regulation of MIM.....	5
1.3 Physiological Role of MIM.....	8
1.4 The BAR domain superfamily.....	9
1.4.1 Structural Characteristics of BAR domain proteins.....	11
1.4.2 The I-BAR subfamily.....	13
1.5 Protein Structure and Cellular Function of MIM.....	15
1.6 Overview of Work.....	17
1.7 Thesis Aims.....	21
CHAPTER 2: INFLAMMATION DOWNREGULATES MIM EXPRESSION IN MOUSE MACROPHAGES.....	25
2.1 Introduction.....	25
2.2 Materials and Methods.....	27

2.3 Results.....	35
2.3.1 Pro-inflammatory cytokines downregulate MIM in RAW 264.7 cells.....	35
2.3.2 LPS downregulates MIM in mouse bone marrow-derived macrophages.....	38
2.3.3 IL-6-induced downregulation of MIM results in impaired CXCR4 internalization and increased chemotactic response to SDF-1.....	40
2.3.4 Pro-inflammatory cytokines have no effect on MIM expression in B cells...	42
2.3.5 LPS-induced inflammation in mice does not alter MIM expression in liver..	44
2.4 Discussion.....	46
 CHAPTER 3: RAB7 IS REQUIRED FOR MIM-MEDIATED LYSOSOMAL DEGRADATION OF CXCR4.....	
3.1 Introduction.....	50
3.2 Materials and Methods.....	53
3.3 Results.....	59
3.3.1 MIM promotes CXCR4 internalization and reduces SDF-1 chemotactic response in multiple cell types.....	59
3.3.2 Rab7 is indispensable for MIM-mediated CXCR4 internalization.....	63
3.3.3 Rab7 is required for MIM-mediated recruitment of CXCR4 to late endosomes.....	66

3.3.4 Rab7 is required for recruitment of MIM into late endosomes.....	68
3.3.5 MIM regulates CXCR4 degradation while IRTKS regulates CXCR4 recycling.....	70
3.3.6 The SH3 domain determines the interaction with Rab11.....	73
3.4 Discussion.....	75
 CHAPTER 4: OVEREXPRESSION OF MIM SUPPRESSES BASAL AUTOPHAGY.....	
4.1 Introduction.....	80
4.2 Materials and Methods.....	82
4.3 Results.....	85
4.3.1 MIM overexpression induces LC3 accumulation.....	85
4.3.2 MIM overexpression inhibits autophagic degradation.....	88
4.3.3 MIM overexpression induces accumulation of autophagosomes.....	91
4.3.4 Overexpression of MIM alters autophagic response to starvation.....	93
4.3.5 RNAi-mediated reduction of MIM in RAW 264.7 cells increases LC3-II degradation under normal conditions.....	96
4.3.6 Overexpression of MIM impedes C2-ceramide-induced autophagy and promotes ceramide-mediated cytotoxicity.....	99

4.4 Discussion.....	102
CHAPTER 5: SUMMARY AND CONCLUSION.....	106
REFERENCES.....	111

List of Tables

Table 1: Summary of MIM-linked Cancers.....	4
---	---

List of Figures

Figure 1.1	The domain structures of BAR family members.....	1
Figure 1.2	Schematic models for membrane deformation.....	1
Figure 1.3	Schematic of domain organization of I-BAR proteins	1
Figure 1.4	Schematic of domain organization of MIM.....	1
Figure 2.1	Certain pro-inflammatory cytokines downregulate MIM expression in RAW 264.7 cells.....	1
Figure 2.2	LPS downregulates MIM expression in mouse bone marrow-derived macrophages	1
Figure 2.3	IL-6 treated RAW 264.7 cells show impaired CXCR4 internalization and increased chemotactic response to SDF-1	1
Figure 2.4	Inflammation has no effect on MIM expression in B cells.....	1
Figure 2.5	LPS-induced inflammation has no effect on MIM expression in mice liver ...	1
Figure 3.1	MIM promotes CXCR4 internalization and inhibits chemotactic response to SDF-1	1
Figure 3.2	Rab7 is required for MIM-mediated CXCR4 internalization	1
Figure 3.3	Rab7 is essential for MIM to promote CXCR4 sorting into late endosomes ..	1
Figure 3.4	RAB7 is indispensable for recruitment of MIM into late endosomes.....	1
Figure 3.5	MIM and IRTKS are targeted by different Rabs.....	1
Figure 3.6	The SH3 domain determines recruitment of IRTKS to Rab11	1
Figure 3.7	A model depicting the function of I-BAR domain proteins in the regulation of CXCR4	1
Figure 4.1	MIM overexpression induces LC3 accumulation	1

Figure 4.2 MIM overexpression inhibits autophagic degradation	1
Figure 4.3 MIM overexpression prevents autophagosome maturation/ fusion.....	1
Figure 4.4 Starvation induces autophagy in MIM-overexpressing cells	1
Figure 4.5 siMIM-treated RAW 264.7 cells show increased LC3-II degradation.....	1
Figure 4.6 MIM overexpression inhibits autophagy activation and enhances cytotoxicity induced by C2-ceramide	1
Figure 5.1 A model depicting the role of the tumor microenvironment in MIM expression and function.....	1

List of Abbreviations

5-Aza-dC	5-aza-2-deoxycytidine
ABBA	Actin-Bundling with BAIAP2 homology
AIP4	Atrophin-1 Interacting Protein 4
AKT	RAC-alpha serine/threonine-protein kinase
AML	Acute myeloid leukemia
AML1-ETO	Acute Myeloid Leukemia 1/Eight Twenty One
BA1	Bafilomycin A1
BAIAP2	Brain-specific Angiogenesis Inhibitor 1-Associated Protein 2
BAR	Bin-Amphiphysin-Rvs
BCA	Bicinchoninic acid
BMDM	Bone marrow-derived macrophages
BSA	Bovine serum albumin
β -TRCP	β -Transducin Repeat-Containing Protein
CCD	Coiled coil domain
CKI δ	Casein Kinase I δ
CMA	Chaperone-mediated autophagy
CO ₂	Carbon dioxide
Co-IP	Co-immunoprecipitation
CXCL12	C-X-C motif chemokine ligand 12
CXCR4	C-X-C chemokine receptor type 4
CXCR5	C-X-C chemokine receptor type 5
DLBCL	Diffuse Large B Cell Lymphoma

DMEM	Dulbecco's modified Eagle's medium
DMSO	Dimethyl sulfoxide
DNA	Deoxyribonucleic acid
DNMT3B	DNA methyltransferase 3B
EDTA	Ethylenediaminetetraacetic acid
EEA1	Early Endosome Antigen 1
EGFR	Epidermal growth factor receptor
ELISA	Enzyme-linked immunosorbent assay
FACS	Fluorescence activated cell sorting
F-BAR	Extended Fes-CIP4 homology (EFC)/FCH-BAR
FBS	Fetal bovine serum
GFP	Green fluorescent protein
GPCR	G-protein coupled receptor
GTP	Guanosine triphosphate
HA	Hemagglutinin
HRP	Horseradish peroxidase
I-BAR	IRSp53-MIM homology domain/inverse-BAR
IFN γ	Interferon gamma
IgG	Immunoglobulin G
IL-6	Interleukin 6
IP	Immunoprecipitation
IRSp53	Insulin Receptor Substrate p53
IRTKS	Insulin Receptor Tyrosine Kinase Substrate

ITCH	Itchy E3 ubiquitin protein ligase
Ivy1	Interaction with VPS33 and YPT7 protein 1
LDH	Lactate dehydrogenase
LPS	Lipopolysaccharide
MAP1LC3/ LC3	Microtubule-associated protein 1 light chain 3
M-CSF	Macrophage colony-stimulating factor
MIM	Missing in Metastasis
MIM-KO	MIM knockout
MiR	MicroRNA
mTOR	Mammalian target of rapamycin
MTSS1	Metastasis suppressor 1
MVB	Multivesicular bodies
N-BAR	N-terminal amphipathic helix BAR
NEDD4	Neural Precursor Cell Expressed, Developmentally Downregulated 4, E3 Ubiquitin Protein Ligase
NSCLC	Non-small-cell Lung Carcinoma
p62	Sequestosome-1
PAGE	Polyacrylamide gel electrophoresis
PBS	Phosphate-buffered saline
PCR	Polymerase chain reaction
PDAC	Pancreatic Ductal Adenocarcinoma
PE	Phycoerythrin
PI3K	Phosphoinositide 3-kinase

PINKBAR	Planar Intestinal and Kidney specific BAR domain
PML-RARA	Promyelocytic Leukemia/Retinoic Acid Receptor Alpha
PRD	Proline-rich domain
PTEN	Phosphatase and tensin homolog
PVDF	Polyvinylidene difluoride
qPCR	Quantitative PCR
Rab11	Ras-related protein Rab-11A
Rab5	Ras-related protein Rab-5A
Rab7	Ras-related protein Rab-7A
RAC1	Rac family small GTPase 1
RFP	Red fluorescent protein
RT-PCR	Reverse transcription PCR
RIPA	Radio-immunoprecipitation assay
RNA	Ribonucleic acid
SCF	Skp1-Cullin1-F-box
SDF-1	Stromal cell derived factor 1
SDS	Sodium dodecyl sulfate
SH3	Src Homology 3
siRNA	Small interfering RNA
SRD	Serine-rich domain
TAMs	Tumor-associated macrophages
TBST	Tris-buffered saline with Tween 20
TGF- β 1	Transforming growth factor beta 1

TNF α	Tumor necrosis factor alpha
TNM	Tumor-Node-Metastasis
Ub	Ubiquitin
WH2	Wiskott-Aldrich homology 2

Chapter 1: Introduction

1.1 MTSS1/ MIM and Cancer

The focus of conventional cancer therapies over the last few decades has been on targeting oncogenes, DNA synthesis, and aberrant signaling pathways for cell growth. A major challenge faced by the field with these therapies is that they are often ineffective in the case of metastatic cancer. Metastasis is a multistep process that involves detachment of cells from the primary tumor, intravasation into the circulatory and lymphatic systems, evasion of immune surveillance, extravasation at distant capillary beds and invasion of distant organs [1]. Once at a secondary site, metastatic cells establish a microenvironment that favors angiogenesis and proliferation, resulting in secondary tumors [2]. Metastasis is estimated to be responsible for 90% of cancer deaths [3]. Even in cancers that are highly treatable, the survival rate falls significantly once metastasis has occurred. For example, luminal A breast cancer subtype has a 100% 5-year survival rate when localized, but this falls to 29.8% for metastatic disease [4]. Consequently, for most types of cancer, patient prognosis is more favorable if diagnosis and treatment are performed at early stages before lymphatic involvement and metastasis has taken place.

Contributing factors to the challenges in treating metastatic cancer include deactivation of metastasis suppressors, the bidirectional interaction between tumor cells and the surrounding microenvironment and chemotherapy resistance [5]. In the case of a deactivated or downregulated metastasis suppressor gene, treatment approaches become more complicated since most therapeutic strategies target gain-of-function mechanisms. Approaches to targeting a downregulated gene often involve focusing on upstream

regulators or downstream mediators of the gene as well as microenvironmental factors that may influence gene expression. Therefore, a thorough understanding of how a loss-of-function gene contributes to tumorigenesis is important in developing effective therapeutic strategies.

A gene that is often found to be downregulated in metastatic cancer is metastasis suppressor 1 (MTSS1) (also known as missing-in-metastasis (MIM)). In a 2002 study, a 5.3kB transcript that was shown to be expressed in multiple low-grade bladder cancer cell lines, but missing in a metastatic cell line, was given the name Missing In Metastasis (MIM) [6]. The same study also showed reduced expression of the gene in metastatic breast and prostate cancer cell lines, leading to it being described as a potential metastasis suppressor gene. However, subsequent studies have shown that MIM is reduced in non-metastatic tumor cell lines and samples [7], [8], [17], [9]–[16] as well as overexpressed in tumors compared to normal tissue [17]–[24], making the exact role of MIM in tumor progression uncertain.

Several studies also show that aberrant expression of MIM is associated with poor prognosis for multiple cancer types, with both overexpression and reduced expression linked to treatment failure. **Table 1** provides a summary of the type of dysregulation and prognostic outcomes for MIM-linked cancers. MIM has been reported to be overexpressed in at least 7 tumor types. However, for multiple tumor types with MIM overexpression, there have also been studies that show MIM downregulation. These seemingly contradictory reports may be due to a number of possible factors, including cohort sizes, the heterogeneity of tumor samples, the grade of the tumors, and the Tumor-Node-Metastasis (TNM) staging of the patient. The trend that emerges from these studies

is that high MIM expression correlates with low-grade tumors, while low MIM expression correlates with late TNM stages and metastasis. Only a small number of cases show a correlation of overexpression of MIM with metastasis.

Given the association of low MIM expression with late TNM stages and metastasis, it is not surprising that poor prognosis of cancer correlates strongly with reduced expression of MIM. Of the 45 studies referenced in **Table 1**, 24 found a correlation between MIM dysregulation and poor prognosis, but only 4 of the 24 studies described an association of high MIM expression with poor prognosis. These studies highlight the clinical relevance of MIM and several suggest utilizing MIM as either a target for cancer therapy or a prognostic marker for cancer progression. However, a proper way to target MIM is yet to be identified. Given the challenges of targeting a downregulated gene, a better understanding of the role of MIM in cancer biology is necessary to developing therapeutic strategies that involve MIM.

Tumor Type	Expression (tumor vs healthy)	Associated with Metastasis	Associated with Poor Prognosis	References
Acute Myeloid Leukemia	+/-		yes (-)	[13]
Bladder Cancer	-			[9]
Bladder Uroepithelium Cell Carcinoma	-	yes (-)	yes (-)	[15]
Breast Cancer	-		yes (-)	[25]
Breast Cancer	-	yes (-)	yes (-)	[26]
Breast Cancer	-		yes (-)	[27]
Breast Cancer	-			[28]
Breast Cancer (basal, ER-)	-		yes (-)	[29]
Breast Cancer (HER2+)	-	yes (-)	yes (-)	[30]
Cervical Cancer	+	no		[21]
Chronic Myeloid Leukemia	-			[14]
Colorectal Cancer	+	yes (+)	yes (+)	[19]
Colorectal Cancer		yes (+)		[31]
Colorectal Cancer	-	yes (-)		[32]
Colorectal Cancer		yes (-)	yes (-)	[33]
Colorectal Cancer	-			[34]
Diffuse Large B Cell Lymphoma (DLBCL)	-			[35]
Gastric Cancer	-			[36]
Gastric Cancer	-	yes (-)	yes (-)	[37]
Gastric Cancer	-			[38]
Glioblastoma	-		yes (-)	[39]
Glioblastoma	-			[40]
Head and Neck Squamous Cell Carcinoma	+			[20]
Hepatitis B-related Hepatocellular Carcinoma	+	yes (+)	yes (+)	[23]
Hepatocellular Carcinoma	+			[17]
Hepatocellular Carcinoma	-	yes (-)	yes (-)	[41]
Hepatocellular Carcinoma	+	yes (+)	yes (+)	[24]
Hilar Cholangiocarcinoma	-	yes (-)	yes (-)	[42]
Intrahepatic Cholangiocarcinoma	-	yes (-)	yes (-)	[43]
Kidney Cancer	-			[44]
Lung Adenocarcinoma	-		yes (-)	[45]
Lung Giant-Cell Carcinoma	+			[16]
Melanoma	+	yes (+)	yes (+)	[18]
Non-small-cell Lung Carcinoma		yes (-)	yes (-)	[46]
Non-small-cell Lung Carcinoma	-	yes (-)		[47]
Non-small-cell Lung Carcinoma	+	yes (-)	yes (-)	[22]
Oesophageal Squamous Cell Carcinoma	-	yes (-)	yes (-)	[10]
Osteosarcoma	-			[48]
Ovarian Cancer	-		yes (-)	[49]
Ovarian Cancer	-	yes (-)		[12]
Pancreatic Cancer	-	yes (-)	yes (-)	[50]
Prostate Cancer	-			[8]
Prostate Cancer	-			[51]
Prostate Cancer	-			[52]
Tongue Squamous Cellular Carcinoma	-			[53]

Table 1: Summary of MIM-linked cancers. List of clinicopathological studies related to MIM dysregulation in tumors. (+) overexpression, (-) downregulation.

1.2 Regulation of MIM

Discerning the underlying mechanism of MIM deregulation is one of the first steps in developing therapeutic options for MIM-linked cancers, and several modes of MIM regulation have already been identified. As one of the most common modes of gene silencing, DNA methylation of CpG islands was the first mechanism to be explored for MIM downregulation [7], [54]. In a 2004 study, Nixdorf *et al* concluded that MIM downregulation is unlikely to be due to DNA methylation as treatment of representative cell lines with the deoxyribonucleoside, 5-aza-2-deoxycytidine (5-Aza-dC), failed to induce MIM expression [7]. However, this was later contradicted in a 2006 study, where Utikal *et al* discovered that the MIM promoter is methylated in its 5' region in cells and tissue samples with low MIM expression, and that inhibition of DNA methylation by 5-Aza-dC led to upregulation of MIM expression in a low expressing cell line [54]. The cells that Nixdorf *et al* treated with 5-Aza-dC were bladder cell lines T24, SW1710, VMcub3, and J82, while Utikal *et al* used prostate cancer cell line, LNCap. The different cancer type is the most likely reason for the dissimilar results. Later studies confirmed that downregulation of MIM can be due to promoter hyper-methylation in certain cancer types, as 5-Aza-dC treatment was shown to also restore MIM expression in a gastric cancer cell line [36] and glioma cell lines [40]. Also, a 2013 study identified MIM as one of the genes that are hyper-methylated across various types of B-cell Non-Hodgkin lymphoma [55].

As seen with the Nixdorf bladder cancer cell lines study, DNA hyper-methylation does not explain all cases of MIM deregulation in cancer. MIM has been shown to be regulated through other mechanisms such as DNA methyltransferase downregulation,

ubiquitination-driven proteosomal destruction, upregulation by a transcription factor, and targeting by microRNAs. MIM was found to be a target of DNA methyltransferase 3B (DNMT3B) in hepatocellular carcinoma, where it is negatively associated with overexpression of DNMT3B, but the mechanism through which DNMT3B downregulates MIM seems to be methylation-independent [11], [13]. Schemionek *et al* recently described a DNMT3B-mediated mechanism of regulation in acute myeloid leukemia (AML), where DNMT3B binds to the MIM promoter in the PML-RARA (t(15;17) translocation) positive AML subset, but not AML1-ETO (t(8;21) translocation) positive cells, resulting in higher expression of MIM in the AML1-ETO subset [13]. This finding has interesting clinical implications, as patients with high MIM and low DNMT3B expression showed a highly significant increased overall survival rate compared to those with low MIM and high DNMT3B expression.

Another mechanism of MIM regulation was described in a 2013 study, where MIM was identified as a substrate for the SCF β -TRCP E3 ubiquitin ligase complex, which marks it for degradation in the 26S proteasome [56]. The interaction between MIM and β -TRCP is triggered by casein kinase I δ (CKI δ)-mediated phosphorylation of MIM, which makes inhibition of CKI δ a yet to be explored therapeutic possibility in treating MIM-linked cancer. This study, along with most studies on MIM regulation, describes a mechanism through which MIM is downregulated. An exception to this is a 2015 study by Giacobbe *et al.* that reported the transcriptional upregulation of MIM expression by Δ Np63, an isoform of the transcription factor, p63 [57].

Several studies describe the targeting of MIM by microRNAs in MIM deregulation. MicroRNA-182 is thought to downregulate MIM in a number of cancers,

including breast cancer [58], hepatocellular carcinoma [41], esophageal cancer [59], ovarian cancer [60] and prostate cancer [61]. Overexpression of miR-96 is also linked to reduced MIM expression in breast cancer [28], prostate cancer [51] and tongue squamous cellular carcinoma [53]. Other microRNAs that are linked to MIM include miR-135 in colorectal cancer [32], [62] and hepatocellular carcinoma [63], miR-23 in colorectal cancer [31] and DLBCL [35], miR-411 in osteosarcoma [48], miR-15 in breast [29] and colorectal cancer [33], and miR-29a in NSCLC [47]. MicroRNA-mediated regulation of MIM is another potential target for cancer therapy. For example, miR-29b has been shown to target DNMT3B, and thus could indirectly increase the expression MIM [64]. This could be of therapeutic significance as there is an ongoing clinical trial for a miR-29 mimic, Remlarsen (MRG-201), for treatment of keloids [65], which if approved, could be repurposed for treatment of MIM-linked cancers.

Another avenue for stabilizing the expression of MIM is to target the PTEN/PI3K/AKT signaling pathway. Two recent papers independently showed that MIM is positively regulated by phosphatase and tensin homolog (PTEN) in gastric cancer [38] and pancreatic ductal adenocarcinoma (PDAC) [66]. Another study showed that loss of Akt2 resulted in stabilization of MIM, possibly through the PTEN/PI3K/AKT signaling pathway [34]. It was also proposed that an inflammatory microenvironment could indirectly result in MIM downregulation through the PTEN signaling pathway [67]. Zeleniak, *et al* demonstrated that the highly inflammatory microenvironment of PDAC tumor bulk is capable of downregulating PTEN expression through secretion of miRNA-23b, which could potentially lead to MIM downregulation [67]. Therefore, exploring the

effect of inflammation on MIM expression also could provide therapeutic options for MIM-linked cancer.

1.3 Physiological Role of MIM

While there are several studies that present strong evidence of MIM-link cancers and MIM-associated poor prognosis, determining how MIM contributes to tumorigenesis is hindered by a lack of knowledge about the physiological function of MIM. It is ubiquitously expressed in human tissues, with abundant expression in the cerebellum, endocrine tissues, bone marrow and immune system [68]–[70]. Given its association with tumorigenesis, it is thought to have a role in development. In non-cancer-related studies, evidence points to a role in nervous system development, with reports of roles in differentiation and maintenance of cerebellar neurons [69], [71], shaping of neuronal membranes [70], neural tube closure [72], dendritic spine initiation and morphogenesis [73], [74], and regulation of neurite outgrowth [75].

Mice deficient in MIM display some organ defects including spleen, heart, kidney, bone, and brain abnormalities [71], [73], [74], [76]–[78]. In studies using knockout mouse models that were generated by different methods, MIM has been shown to contribute to the maintenance of the integrity of cell-cell contacts of the kidney epithelia [77] and to the development and function of B lymphocytes [78], while the mice were found to develop a progressive kidney disease [77], age-related B-cell lymphoma [78] and progressive ataxia [79]. Despite these notable defects, MIM-deficient mice are viable and fertile, with no gross abnormalities to clearly indicate its physiological role.

1.4 The BAR domain superfamily

MIM is a member of the BAR (Bin-Amphiphysin-Rvs) domain superfamily, a family of proteins that are known to bind and deform curved membranes. The BAR domain initially was defined as the conserved region found in vertebrate proteins BIN and amphiphysin, and yeast proteins Rvs161 and Rvs167 [80]. This conserved region has since been identified in more than 220 proteins which can be grouped into four structurally distinct subclasses: classical BAR, N-BAR/BAR (N-terminal amphipathic helix BAR), F-BAR (extended Fes-CIP4 homology (EFC)/FCH-BAR), or I-BAR (IRSp53-MIM homology domain/inverse-BAR) (**Figure 1.1**) [81].

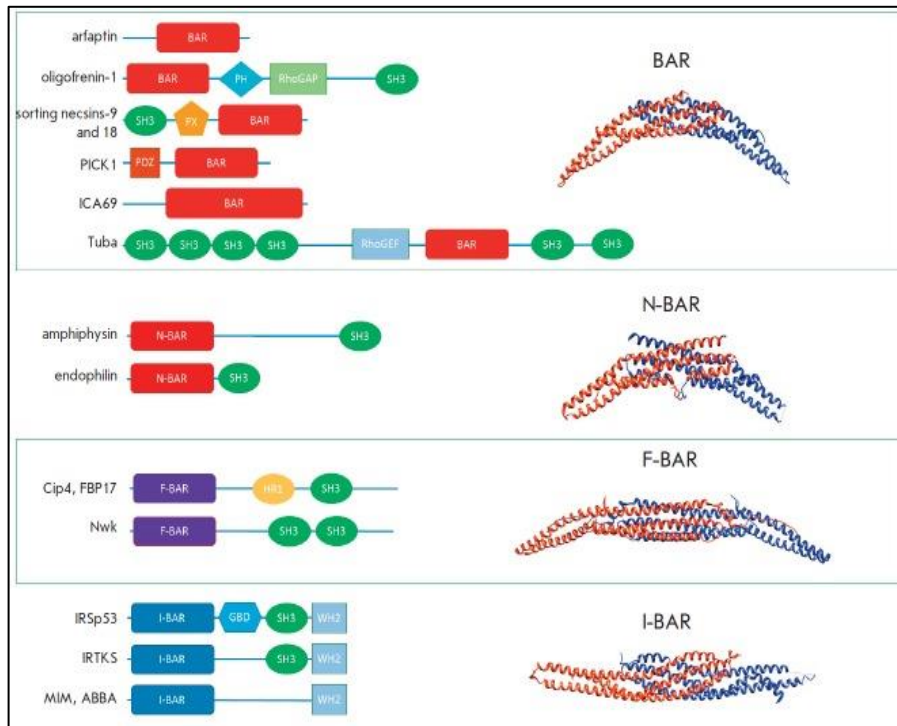


Figure 1.1 The domain structures of BAR family members (left side) and the structures of BAR domain dimers (right side). Reprinted from “Stanishneva-Konvalova TB, *et al*, (2016) The Role of BAR Domain Proteins in the Regulation of Membrane Dynamics. *Acta naturae* 8(4):60-69” with permission.

1.4.1 Structural Characteristics of BAR domain proteins

The overarching feature of proteins of the BAR domain superfamily is that they are crescent-shaped dimers that induce membrane curvature and bind to curved membrane regions. Classical BAR, N-BAR, and F-BAR contain clusters of positively charged amino acids on the concave surface of the crescent-shaped dimer, which binds to the negatively charged phospholipids of membranes (**Figure 1.2 A**) [82]. I-BAR proteins inversely bind membranes through the convex surface of the dimer, as the positively charged amino acids are located convexly rather than on the concave surface (**Figure 1.2 B**). N-BAR proteins differ from classical BAR in that they contain an N-terminal amphipathic helix, while F-BAR proteins feature an N-terminal Fes/CIP4 homology (FCH) and a coiled-coil domain as part of the BAR domain. Classical BAR, N-BAR and F-BAR proteins also differ in the level of curvature they bind or induce. Classical BAR and N-BAR proteins have the highest degree of intrinsic curvature, and thus bind/induce highly curved membranes. In comparison, the intrinsic curvature of F-BAR proteins varies from high to slightly curved, allowing them to bind to a wide range of membrane curvatures [83] (**Figure 1.1**).

In addition to the signature crescent-shaped domain, another marked feature of the BAR domain proteins is that almost all members contain at least one other domain, giving them the ability to act as a scaffold. The most common additional domain is the Src Homology 3 domain (SH3) which binds to proline-rich sequences of target proteins [84]. In addition to attracting binding partners, the SH3 domain seems to serve an auto-inhibitory role in most BAR domain proteins [84].

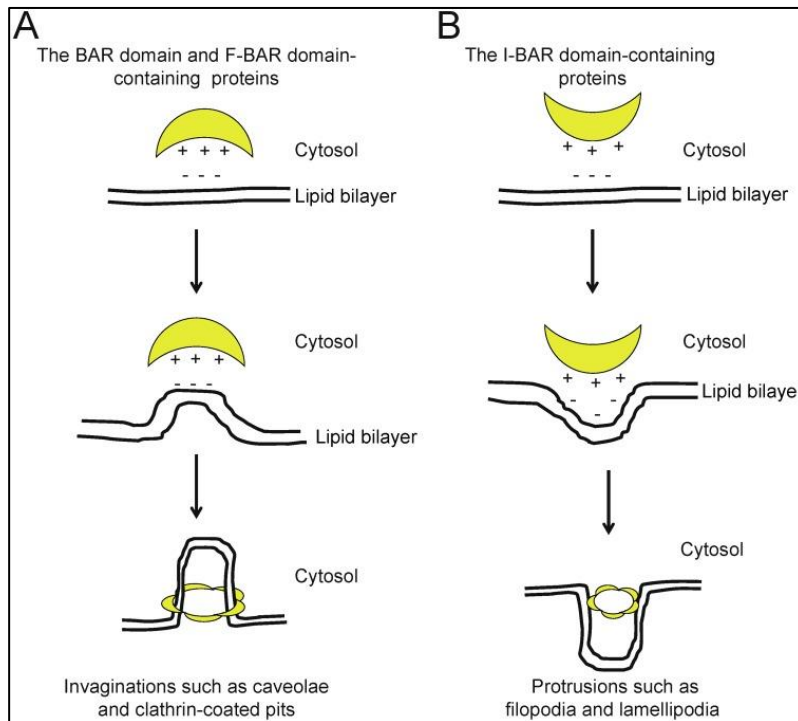


Figure 1.2 Schematic models for membrane deformation, based on the geometries of basic-charged amino acid residues that correspond to the structures of the membrane-binding surface of the F-BAR domain-containing proteins. (A) BAR or F-BAR proteins bind to the membrane to generate invaginations, such as caveolae and clathrin-coated pits; **(B)** I-BAR proteins deform the membrane to generate protrusions, such as filopodia and lamellipodia. Reprinted from “Safari F & Suetsugu S (2012) The BAR Domain Superfamily Proteins from Subcellular Structures to Human Diseases. *Membranes* 2(1):91-117” with permission.

1.4.2 The I-BAR subfamily

The I-BAR subfamily consists of five known members: **MIM**, **ABBA** (Actin-Bundling with BAIAP2 homology), also known as metastasis suppressor 1-like (MTSS1L), **IRSp53** (Insulin Receptor Substrate p53), also known as brain-specific angiogenesis inhibitor 1-associated protein 2 (BAIAP2), **IRTKS** (Insulin Receptor Tyrosine Kinase Substrate), also known as brain-specific angiogenesis inhibitor 1-associated protein 2-like protein 1 (BAIAP2L1) and **PINKBAR** (Planar Intestinal And Kidney specific BAR domain), also known as Brain-specific angiogenesis inhibitor 1-associated protein 2-like protein 2 (BAIAP2L2) (**Figure 1.3**) [82]. The I-BAR domain subgroup is further divided based on the presence of a SH3 domain, with MIM and structurally similar ABBA both lacking an SH3 domain. Along with the I-BAR domain, which is located at the N-terminus, all five members contains a C-terminal WASP-Homology 2, or Wiskott-Aldrich homology 2 (WH2)-like domain. The WH2 motif interacts with actin, which gives I-BAR proteins the ability to link actin to the interior phospholipid bilayer of the cell membrane [85]. The SH3 domain of IRSp53, IRTKS, and PINKBAR is known to recruit actin polymerization regulators such as Rac family small GTPase 1 (Rac1), Wiskott-Aldrich syndrome family proteins, and Arp2/3 complex [82]. MIM lacks an SH3 domain and consequently may not participate in actin polymerization in the same manner as the SH3-containing I-BAR proteins.

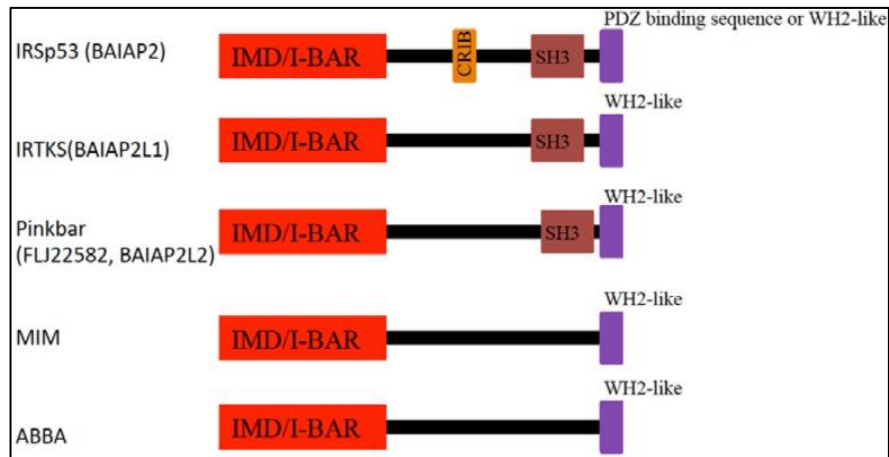


Figure 1.3 Schematic of domain organization of I-BAR proteins. IRSp53-MIM homology domain (IMD)/inverse-BAR (I-BAR); CRIB: Cdc42-Rac interactive binding region; SH3: Src homology 3 domain; WH2: Wasp homology 2 (verprolin homology) domain. Reprinted from “Safari F & Suetsugu S (2012) The BAR Domain Superfamily Proteins from Subcellular Structures to Human Diseases. *Membranes* 2(1):91-117” with permission.

1.5 Protein Structure and Cellular Function of MIM

MIM is thought to have several splice variants, with full-length MIM, predicted to be ~759 amino acids in length, having multiple protein-protein interacting regions that allow it to act as a cytoskeletal scaffold [86]. Other than the I-BAR and WH2 domains, full-length MIM consists of a coiled coil domain (CCD) within the I-BAR domain, a lysine-rich domain (LRD), a serine-rich domain (SRD) and a proline-rich domain (PRD) [68], [86] (**Figure 1.4**).

MIM has been shown to interact with various molecules involved in cytoskeletal rearrangements such as Rac1 [30], [75], [87], [88], cortactin [89], receptor protein tyrosine phosphatase delta (RPTP δ) [90], [91], disheveled-associated activator of morphogenesis 1 (DAAM1) [73], and cell membrane phosphatidylinositol 4,5-bisphosphate tyrosine (PIP₂) [74], [92], [93], establishing it as a cytoskeletal scaffold protein. Overexpression of MIM in various cell lines shows that it interacts with both monomeric actin (G-actin) and F-actin, and results in the disassembly of actin stress fibers as well as the induction of actin-enriched lamellipodia-like protrusions and filopodia-like extensions [8], [73], [77], [87], [89], [90], [94]–[97]. Through its function as a cytoskeletal scaffold, it is thought to participate in processes that involve membrane deformation and remodeling such as cell migration and endocytosis [29], [30], [39], [46], [57], [61], [98], [99]. MIM is also thought to be involved in a number of cell signaling pathways, including platelet-derived growth factor (PDGF) [18], [99], [100], epidermal growth factor (EGF) [20], [29], [99], C-X-C chemokine receptor type 5 (CXCR5) [78], C-X-C chemokine receptor type 4 (CXCR4) [101], and sonic hedgehog (SHH) signaling [91], [102], [103].

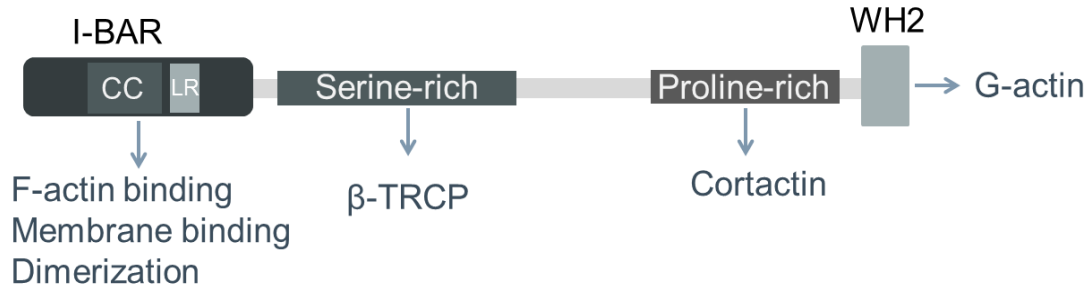


Figure 1.4 Schematic of domain organization of MIM. IRSp53-MIM homology domain (IMD)/inverse-BAR (I-BAR); coiled-coil domain (CC); lysine-rich domain (LR); Wasp homology 2 domain (WH2)

1.6 Overview of Work

There is a vast amount of evidence in the literature to support MIM playing a role in cancer progression and metastasis, but little is known about the exact function of MIM in tumor biology. This study aims to identify and elucidate the primary molecular mechanisms that underlie the role of MIM in cancer progression.

In clinicopathologic studies that examined MIM expression in cancers, there is often heterogeneity in MIM expression within a cancer type. For example, in a NSCLC study, MIM was overexpressed in the tumor when compared with normal lung, but varied from high to low expression within the cancer samples [22]. In another study (pancreatic cancer), where MIM expression was categorized into high and low based on immunohistochemical staining, low MIM expression in non-tumor and tumor tissues were observed in 6.6% and 27% of patients, respectively [50]. This differential expression of MIM in tumor samples raises the possibility that downregulation of MIM expression is caused by factors in the microenvironment. To explore this possibility, we examined the effect of inflammation on MIM expression. We found that certain inflammatory cytokines reduced MIM expression in mice bone marrow-derived macrophages (BMDM) and RAW 264.7 cells (a mouse macrophage-like cell line). We also observed that in addition to lower MIM expression, RAW 264.7 cells that were exposed to the inflammatory cytokine, interleukin 6 (IL-6), had higher CXCR4 cell surface expression, and increased migratory response to SDF-1. These results indicate that inflammation could be a contributing factor to MIM downregulation in the tumor milieu and to the role of MIM in metastasis.

MIM is involved in a number signaling pathways. Given this diversity, it's likely that MIM participates in signaling events that are common to multiple pathways. Several receptor-mediated signaling pathways share lysosomal degradation or recycling of the receptor as a regulatory mechanism. The lysosomal degradation pathway involves packaging and sorting of proteins into intracellular vesicles and trafficking them into lysosomes. As a member of the I-BAR subfamily, MIM can induce and bind to negative curvature. This feature would make it possible for MIM to tether other proteins to the interior surface of the lipid bilayer of vesicles, and thus facilitate intracellular vesicle trafficking. We proposed that the main function of MIM is as a scaffold protein in intracellular membrane trafficking pathways such as endocytosis and autophagy.

A role in intracellular trafficking could explain the diverse effects of MIM dysregulation in cancer. As a participant in endocytic pathways, MIM could influence the activity of growth factors and chemokines that signal through receptor-mediated endocytosis, thus affecting growth and proliferation signals as well as migration of cells within the tumor microenvironment. Deregulated MIM could also affect many aspects of cancer through an involvement in autophagy. Autophagy is essential for maintaining cellular homeostasis, and dysregulation of proteins that are involved in this pathway can impact processes such as proliferation, invasion, metastasis, and drug resistance [104].

Previous studies in this lab indicate that MIM has a regulatory role in CXCR4 cell surface expression. Bone marrow cells from MIM knockout (MIM-KO) mice showed a higher surface expression of CXCR4, increased motility in response to CXCR4 ligand, stromal-derived factor 1 (SDF-1; also known as C-X-C motif chemokine ligand 12 (CXCL12)) and impaired ability to internalize CXCR4 upon receptor activation [101].

We also found that MIM formed a complex with CXCR4 by binding to Itchy E3 Ubiquitin Protein Ligase (ITCH; also known as Atrophin-1 Interacting Protein 4 (AIP4)) in response to stimulation by SDF-1, and interacted with well-known endocytic regulators, Rab5 and Rab7 [105]. Additionally, in response to SDF-1, MIM facilitated CXCR4 ubiquitination and sorting into endocytic vesicles [105]. In this study, we further explored the role of MIM in the CXCR4 endocytic pathway by investigating the importance of the MIM–Rab7 interaction in CXCR4 downregulation and analyzing the interaction between MIM and Rab11, a small GTPase that plays an important role in the pathway leading to receptor recycling [106].

The relationship between MIM and Rab7/Rab11 was investigated by immunofluorescence microscopy, co-IP assays, immunoblot analyses, cell migration assays, and flow cytometry analysis. We found that Rab7 is required for MIM-mediated internalization of CXCR4 and for the recruitment of MIM and CXCR4 into late endosomes [107]. We also found that MIM did not interact with Rab11. Instead, another I-BAR protein, IRTKS, interacted with Rab11 upon SDF-1 stimulation [107]. Unlike MIM, IRTKS contains a SH3 domain, which seems to mediate the interaction with Rab11 [107]. These findings suggest that IRTKS participates in the recycling pathway, while MIM mediates the lysosomal degradation pathway, with the presence or absence of SH3 being the determining factor in the Rab7/Rab11 interaction.

Several yeast studies link Ivy1 (yeast ortholog of MIM) to autophagy, but a role for MIM in mammalian autophagy is yet to be fully characterized. In this study, we sought to establish a function for MIM in mammalian autophagy. By utilizing immunofluorescence assays and immunoblot analyses, we found that overexpression of

MIM promoted the accumulation of autophagosomes during basal autophagy and altered the normal autophagic response of cells to nutrient starvation. Additionally, we found that RNAi-mediated reduction of MIM expression increased the sensitivity of RAW 264.7 cells to rapamycin-induced autophagy. Western blot analysis of MIM expression revealed that both nutrient starvation and rapamycin treatment reduced the expression of endogenous as well as exogenous MIM. Interestingly, the synthetic ceramide, *n*-acetylsphingosine (C2-ceramide), which is a known autophagy inducer [108], had no significant effect on MIM expression and overexpression of MIM inhibited autophagy induced by this compound while enhancing its cytotoxic effect. Ceramides are the building blocks of sphingolipids (membrane lipids). In addition to providing structural support for membranes, ceramides can act as secondary messengers in regulating different cellular processes, including cell proliferation, differentiation, and cell death [109]. As such, ceramides have garnered interest as an anti-cancer therapeutic agent. However, ceramides are also linked to resistance to chemotherapy, possibly by inducing autophagy to prolong cell survival [110]. Our findings indicate that high MIM expression could reduce the effect of ceramide-induced autophagy, thus promoting cell death.

This study demonstrated the effect of an inflammatory or nutrient deprived microenvironment on regulating MIM expression, highlighted the importance of the interaction of MIM with Rabs in CXCR4 endocytosis and established a role for MIM in autophagy. Overall, our results provide further insight into the role of MIM in cancer progression that could have beneficial implications for cancer therapy.

1.7 Thesis Aims

There is a wealth of literature that link dysregulated MIM to cancer progression, metastasis and poor prognosis, but the mechanism through which MIM contributes to cancer is not yet fully understood. MIM has been found to be overexpressed as well downregulated in several types of cancer, but despite the large number of studies focused on aberrant MIM expression, there is still a lack in knowledge about how MIM becomes deregulated and the pathways that are impacted by MIM deregulation. The overall goal of this study is to improve our knowledge of MIM regulation and function in order to better understand how MIM deregulation contributes to cancer progression and metastasis.

Cues from the tumor microenvironment play a crucial role in all stages of cancer development, progression and metastasis [3]. Factors such as inflammation and nutrient availability can alter the expression of genes that regulate tumor-promoting processes such as angiogenesis, EMT and autophagy [111]. Evidence in the literature suggests that MIM expression may be regulated by microenvironment factors such as inflammation, but this has not yet been confirmed [67]. As a member of the I-BAR domain family of proteins, MIM is thought to be involved in membrane remodeling processes such as cell migration, endocytosis and autophagy. These processes are integral to the bidirectional communications within the tumor microenvironment. Given all the above, **we hypothesized that interactions in the tumor microenvironment are major contributors to the role of MIM in cancer progression and metastasis.** The following specific aims were used to test the predictions of this central hypothesis:

Aim 1: To determine if inflammation downregulates MIM expression.

Tumorigenesis is associated with changes in the tumor microenvironment that lead to the development of physical and biochemical gradients within the primary tumor [112]. This includes gradients in hypoxia, pH, nutrients and soluble molecules such as cytokines and chemokines. These gradients contribute to tumor heterogeneity [112]. MIM is often heterogeneously expressed within the tumor bulk, suggesting that its expression is impacted by gradients created within the microenvironment. A recent study identified MIM as an inflammation-responsive gene in a mouse model of PDAC [66]. Given this, **we predicted that pro-inflammatory cytokines reduces the expression of MIM.** MIM is highly expressed in macrophages and B-cells, which are often well-represented within the tumor microenvironment. To assess the effect of inflammation on MIM expression, RAW 264.7 cells, and mouse bone marrow-derived macrophages and B cells were exposed to LPS and various pro-inflammatory cytokines. Protein and mRNA expression of MIM were analyzed by Western blots and reverse transcription PCR (RT-PCR) respectively. Mice were also injected with LPS, and liver tissue harvested and analyzed for MIM expression.

Aim 2: To investigate the role of Rab GTPases in MIM-mediated CXCR4 endocytosis.

Previous work in this lab showed that in response to SDF-1, MIM interacts with the E3 ubiquitin ligase, AIP4, to facilitate ubiquitination and lysosomal degradation of CXCR4 [105]. We also found that MIM interacts with endocytic Rab GTPases, Rab5

and Rab7, in response to SDF-1 stimulation [105]. However, the interactions with Rabs were not fully explored. Rabs play a critical role in endocytic vesicle trafficking where different Rabs are associated with early endosomes, late endosomes and recycling endosomes. We observed that the interaction of MIM with Rab5 and Rab7 was time-dependent, correlating with the formation of early and late endosomes, respectively. This suggests that the MIM-Rab relationship may be significant to MIM function. Therefore, **we hypothesized that the interaction of MIM with Rabs is vital to the role of MIM in CXCR4 endocytosis.** To test this hypothesis, we performed siRNA-mediated knockdown of Rab7 in HeLa cells and assessed the interaction between MIM and Rab7 using co-IP and immunofluorescence assays. We also used co-IP assays to determine if MIM interacts with Rab11, which is associated with recycling endosomes. Additionally, we utilized IRTKS, another protein in the same family as MIM, to further interrogate MIM-Rab7 and MIM-Rab11 binding by creating fusion mutants of the two proteins.

Aim 3: To investigate the role of MIM in mammalian autophagy.

There are several studies in yeast that suggest a regulatory role for MIM in autophagy, but there is as yet very little evidence to support this in mammals. As intracellular membrane trafficking pathways, endocytosis and autophagy share many similarities. Previous studies in our lab show that MIM promotes the maturation of late endosomes or MVBs during SDF-1-induced CXCR4 endocytosis [105]. Given this, **we hypothesized that MIM is involved in autophagosome maturation during mammalian autophagy.** To determine if MIM participates in mammalian autophagy, we

modulated the expression of MIM in HeLa and RAW 264.7 cells and assessed the expression of autophagy markers by Western blots or immunofluorescence assays. We examined basal autophagy as well as autophagy induced by starvation, rapamycin, or C2-ceramide, and inhibited by bafilomycin A1.

Chapter 2: Inflammation Downregulates MIM Expression in Mouse Macrophages

2.1 Introduction

In cancer development, interactions between tumor cells and the surrounding environment are critical for survival, proliferation and dissemination of the tumor cells. Along with the malignant cells, the tumor mass consists of extracellular matrix proteins, secreted factors, and an assortment of local and infiltrating cells [113]. The non-malignant cells and proteins of the cancer milieu are collectively termed the tumor microenvironment. Key cellular components of the tumor microenvironment include T lymphocytes, B lymphocytes, natural killer and natural killer T cells, tumor-associated macrophages, myeloid-derived suppressor cells, dendritic cells, tumor-associated neutrophils and cancer-associated fibroblasts [114]. Non-cellular factors include extracellular matrix molecules, hypoxia, pH, nutrient availability, oxygen tension and interstitial pressure [115]. These cellular and non-cellular elements, along with secreted factors such as cytokines, chemokines, growth factors and proteases, help to provide the support necessary for tumor growth and progression. Microenvironment factors can also impact the expression of tumor promoting genes, tumor suppressors and metastasis suppressors, thus altering the genetic characteristics of the cancer cells [116]. The interactions of cancer cells with the microenvironment can ultimately determine whether the tumor is successfully eradicated, or whether treatment failure and metastasis occur. Therefore, the tumor microenvironment can influence therapeutic responses and resistance, making crosstalk between cancer cells and the microenvironment a major target of cancer therapy.

Several studies show that the expression of the *MIM* gene is often dysregulated in primary or metastatic tumors, with significant correlation between downregulation and poor patient prognosis (**Table 1**). Despite the wealth of literature that provides evidence of this link between MIM deregulation and tumor progression, the exact role of MIM plays in tumorigenesis is not fully determined. This includes gaps in the knowledge of how MIM is deregulated. There is evidence to show that MIM expression can be regulated in multiple ways, including DNA methylation [40], microRNAs [31], ubiquitination-driven proteosomal destruction [56], PTEN/PI3K/AKT pathway-driven deregulation [67], and p63 transcriptional regulation [57], but there are also indications of other modes of regulation that are yet to be elucidated. For instance, a recent publication identified MIM as an inflammation-responsive gene using a Mouse/Human Affymetrix Array comparison analysis, but experiments to validate this were not presented in the study [66]. The same group speculated in a later article that the highly inflammatory microenvironment of PDAC could be driving downregulation of MIM through a microRNA-dependent mechanism of downregulation [67]. If it is confirmed that MIM expression is regulated by inflammation, anti-inflammatory agents could be an option for adjuvant therapy in PDAC or other inflammation-associated cancers that are also linked to MIM-related poor prognosis.

Though expression is predominantly reduced, MIM sometimes shows a heterogeneous expression pattern for different stages of cancer, and also seems to have a range of expression within the tumor mass at a given stage [17], [22]. A possible explanation for this heterogeneity is that microenvironment factors such as inflammation, hypoxia, or nutrient deprivation may drive MIM deregulation. During tumor development

and progression, uncontrolled cell proliferation, altered metabolism and abnormal blood vessels often result in uneven distribution of microenvironment factors to cancer and stromal cells [113]. Therefore, a gene that is highly responsive to these factors could have varying degrees of expression throughout the tumor mass and surrounding stroma.

In this study, we examined the effect of inflammation on MIM expression. We found that pro-inflammatory cytokines reduced the mRNA and protein expression of MIM in macrophages, but may not regulate MIM in other cell types. Inflammation-induced downregulation of MIM resulted in increased chemotactic response of macrophages to SDF-1, which could have significant implications for the dissemination of tumor-associated macrophages.

2.2 Materials and Methods

Animals

Wild type C57BL/6J mice were bred and maintained in the animal facility at the University of Maryland School of Medicine. All the animals were used in accordance with the University of Maryland Institutional Animal Care and Use Committee guidelines under approved protocols.

Cells and cell lines

RAW 264.7 cells (a gift from Dr. Toni Antalis) were cultured in Dulbecco's modified Eagle's medium (DMEM) (Corning; Corning, NY) supplemented with 10% fetal bovine serum (FBS) (Hyclone; Logan, UT) and 100 unit/mL penicillin / 100 µg/mL streptomycin (pen/strep) (Life Technologies, Grand Island, NY; Cat. No. 15140-122) at

5% CO₂ and 37°C. Farage and Reh cells were a gift from Dr. Curt Civin. Mouse B cells, as well as human Reh, Farage, and THP-1 (ATCC, Gaithersburg, MD) cell lines were cultured at 37 °C, 5% CO₂ in RPMI 1640 medium supplemented with 10% FBS and pen/strep.

Antibodies and Reagents

Lipopolysaccharide (LPS) (Cat. No. L4391) and recombinant mouse tumor necrosis factor alpha (TNF α) (Cat. No. T7539) were obtained from SIGMA (St. Louis, MO). Recombinant mouse IL-6 (Cat. No. 575702), recombinant human IL-6 (Cat. No. 570802), PerCP/Cy5.5 anti-mouse/human CD11b (Cat. No. 101227), phycoerythrin (PE)-conjugated anti-mouse F4/80 (Cat. No. 123109), and mouse IL-6 ELISA MAXTM Standard Set (Cat. No. 431301) were purchased from BioLegend (San Diego, CA). Murine interferon gamma (IFN γ) (Cat. No. 315-05) and murine macrophage colony stimulating factor (M-CSF) (Cat. No. 315-02) were obtained from PeproTech (Rocky Hill, NJ). Anti-Mouse CD16/CD32 (eBioscience; Cat. No. 14-0161-85), mouse CD40L recombinant protein (Cat. No. RP-8641), and F(ab')₂ anti-mouse IgM (eBioscienceTM; Cat. No. 16-5092-85) were from Invitrogen (Carlsbad, CA). Mouse anti-Stat3 monoclonal antibody (Cat. No. 9139S) and rabbit anti-P-Stat3 polyclonal antibody (Cat. No. 9131S) were purchased from Cell Signaling Technology (Danvers, MA).

Western Blot analysis

Harvested cells were washed with phosphate-buffered saline (PBS) and lysed in radio-immunoprecipitation assay (RIPA) buffer supplemented with protease and phosphatase inhibitors. After 10 minutes of incubation on ice and centrifugation at 12,000g for 15 minutes at 4°C, the protein concentration was determined by

bicinchoninic acid (BCA) Assay. Protein samples were loaded on 10% (v/v) sodium dodecyl sulfate (SDS) polyacrylamide gels and transferred on a polyvinylidene difluoride (PVDF) membrane. Primary antibodies against MIM (Invitrogen; Cat. No. PA517047), Stat3, p-Stat3, or β -actin (SIGMA; Cat. No. A5441) were used for protein detection, followed by a secondary goat anti-rabbit horseradish peroxidase (HRP)-conjugated antibody or anti-mouse HRP-conjugated antibody. The proteins probed were visualized using X-autoradiography, and densitometry analysis was performed with gel images from three independent experiments using ImageJ software.

Quantitative RT-PCR

RNA was isolated using RNeasy kit (QIAGEN, Hilden, Germany) according to the manufacturer's instructions. The RNA yield and purity were measured using a spectrometer (Nanodrop). RNA (100 ng) was reverse transcribed using the High Capacity cDNA Reverse Transcription Kit from Applied Biosystems (Thermo Fisher Scientific, Waltham, MA; Cat. No. 4368814) following the manufacturer's recommendations. The cDNA synthesis was performed using an Eppendorf Mastercycler Gradient thermal cycler (Hamburg, Germany). The synthesized cDNA was used in quantitative polymerase chain reactions (qPCR) for gene expression of mouse *Mim* and *Gapdh* or human MIM and β -actin. Quantitative PCR was performed using Power SYBR® Green PCR Master Mix from Applied Biosystems (Life Technologies, Carlsbad, CA; Cat. No. 4367659) on an ABI 7900HT Real-Time PCR System (Applied Biosystems, Foster City, CA). The following primer pairs were used: mouse *Mtss1* forward 5'-GCG TCT TGG ATT GGG ACT TG-3' and *Mtss1* reverse 5'-TCC TTC TCG ATC ACA GCC TC-3'; mouse *Gapdh* forward 5'-CCG CAT CTT CTT GTG CAG TG-3' and *Gapdh* reverse 5'-GAC TGT

GCC GTT GAA TTT GC-3'; human MTSS1 forward 5'-TCT GCT CTC ACC AGG ATG TG-3' and MTSS1 reverse 5'-CCC TTT TGC GTG GTC TTT A-3'; human β -actin forward 5'-GGC ATG GGT CAG AAG GAT T-3' and β -actin reverse 5'-CAC ACG CAG CTC ATT GTA GA-3'. For each primer pair, a standard curve was generated by serial dilution of a pooled reference sample with a minimum efficiency more than or equal to 90%. Relative mRNA expression was calculated as gene of interest expression normalized to reference gene expression. Samples were run in triplicate.

Isolation of Mouse Bone Marrow Cells

Bone marrow cells were isolated as outlined by Zhang *et.al* [117]. In summary, female mice (8 weeks old) were euthanized by CO₂ inhalation. Under aseptic conditions, the abdomen and hind legs were sterilized with 70% ethanol, and the skin peeled from the top of each hind leg and down over the foot. The foot along with the skin was removed and discarded. The hind legs were cut at the hip joint with scissors, leaving the femur and tibia intact, which were placed in a petri dish containing sterile Dulbecco's modified Eagle's Medium / Ham's F-12 50/50 Mix with 10 mM L-glutamine (DMEM/F12 medium) (Corning; Cat. No. 10-090-CV). Excess muscle was removed from the legs, and using sharp scissors or razor blade soaked in ethanol, leg bones proximal to each joint were carefully severed. A 10 mL syringe was attached to a 25-G needle and the syringe filled with cold sterile Dulbecco's phosphate-buffered saline without calcium and magnesium (dPBS). The needle was then inserted into the bone marrow cavity of the femur or tibia and flushed with 2 to 5 mL of dPBS until bone cavity appeared white. The wash medium was collected in a sterile 50 mL Falcon tube kept on ice, and the cells were centrifuged for 10 minutes, 500 x g at room temperature. The supernatant was discarded,

and the pellet re-suspended in 1 mL sterile Red Blood Cell (RBC) Lysis Buffer (eBioscience Cat. No. 00-4333-57). After incubation at room temperature for 4-5 minutes, the reaction was stopped by diluting the Lysis Buffer with 9 mL of dPBS. Cells were filtered through a sterile 70 μ m cell strainer, and then centrifuged at 400 x g, 4°C for 5 minutes. Cells were re-suspended in DMEM/F12 medium supplemented with FBS and pen/strep until ready for further experimentation.

Macrophage Expansion Assay

To induce macrophage differentiation, mouse bone marrow cells were first cultured in DMEM/F12 media supplemented with 10% FBS and pen/strep in tissue culture-treated 100 mm dishes, and incubated in 37°C, 5% CO₂ incubator for 4 hours. After 4 hours, non-adherent cells were collected and live cells based on Trypan Blue exclusion were counted in a hemocytometer. Cells were then re-suspended in 10 mL macrophage complete medium (DMEM/F12 medium supplemented with 10% FBS and pen/strep plus 20 ng/mL recombinant murine M-CSF) at $\sim 6 \times 10^6$ cells/mL in sterile non-tissue culture-treated 100mm dishes. After 3 days another 5 mL of macrophage complete medium was added to each dish. After 5 days, 5 mL of media was removed and replaced with 5 mL fresh macrophage complete medium. On day 7, media was aspirated, and cells were gently washed with 5 mL dPBS (pre-warmed to 37°C). Cells were dislodged with non-enzymatic cell dissociation solution (Gibco Cat. No. 13151-014) and removed from the dish by pipetting. Cells were re-suspended in DMEM/F12 in preparation for further experimentation.

Flow cytometry Analysis

For genotyping of mouse BMDM, 400,000 cells for each sample were re-suspended in FACS buffer (200 μ L PBS containing 0.75% bovine serum albumin (BSA) (SIGMA-Aldrich; Cat. No. A4503) and 5 mM EDTA), and mouse FCR block (mouse CD16/CD32 antibody) was added to each tube and incubated for 10 minutes. To label the cells, PE anti-mouse F4/80 or PerCP/Cy5.5 anti-mouse CD11b or both was added to the appropriate tube. The treated cells were incubated for 30 minutes in the dark, washed with FACS buffer, fixed in 4% paraformaldehyde and stored at 4°C in the dark until ready for analysis.

Flow cytometry analysis was also performed to assess CXCR4 internalization. Briefly, after 24 hours treatment with 50 ng/mL IL-6, RAW 264.7 cells were detached using a non-enzymatic cell dissociation solution and stimulated with 100 ng/mL SDF-1 for 30 minutes. The treated cells were stained with PE-conjugated anti-human-CXCR4 antibody (1 μ g/mL) diluted in FACS buffer and incubated at 4°C for one hour in the dark. As control, cells were stained with PE-conjugated anti-IgG antibody in parallel. After washing, the cells were fixed with 4% paraformaldehyde and stored at 4°C in the dark until ready for analysis. Flow cytometry analysis was performed using a BD LSRFortessa flow cytometer. The data was analyzed by using FlowJo software version 8.8.7.

Cell migration assay

After 24 hours treatment with 50 ng/mL IL-6, RAW 264.7 cells were detached using a non-enzymatic cell dissociation solution and seeded in Transwell inserts (Corning; Cat. No. 3421) in serum-free media at the density of 2×10^5 cells/well. The inserts were then placed in wells containing DMEM plus SDF-1 at various

concentrations. Following incubation at 37°C and 5% CO₂ for 16 hours, the media was removed. The cells on each insert were washed with PBS twice, fixed with 4% paraformaldehyde and were stained with 0.1% Crystal Violet. Cotton swabs were used to remove non-migrated cells from the upper surface of the inserts, and cells within nine microscopic fields were counted under a microscope at 20x magnification.

Single Cell Suspension from Mouse Spleen

Female mice (8-10 weeks old) were euthanized by CO₂ inhalation. The left side of the sacrificed mouse was sterilized using 70% ethanol, and the body cavity was cut open with scissors. The spleen was removed using forceps and added to a 70 µm cell strainer that was previously placed in a sterile 60 mm petri dish containing 8-10 mL of complete medium (DMEM supplemented with 10% FBS and pen/strep). Using the plunger end of a sterile disposable syringe, the spleen was mashed through the cell strainer. The cell strainer was rinsed with 5 mL complete medium to remove any remaining cells. To create a single cell suspension, the cells were passed through a 16-gauge, 21-gauge, and 25-gauge needle in succession from largest to smallest, using a 10 mL syringe. The suspended cells were transferred to a 50 mL conical tube after passing through a 40 µm cell strainer and centrifuged at 800 x g for 3 minutes at room temperature. The pellet was re-suspended in 1 mL lysis buffer and incubated at room temperature for 5 minutes. Nine milliliters of complete medium was added to stop the RBC lysis reaction. The cell solution was spun at 400 x g for 5 minutes at 4°C, and the pellet re-suspended in complete medium until ready for further experimentation.

Enrichment of mouse B cells

Mouse splenic B cells were isolated and enriched using Magnetic-activated Cell Sorting (MACS) mouse B Cell Isolation Kit (Cat. No. 130-090-862) from Miltenyi Biotec (Bergisch Gladbach, Germany), according to manufacturer's instructions. Briefly, splenic cells were re-suspended in cold MACS buffer (PBS-2%FBS + 2mM EDTA) at a density of 10×10^6 cells per 40 μ L. Subsequently, 10 μ L of Biotin-Antibody Cocktail per 10×10^6 cells was added to the cell suspension, and incubated for 5 minutes at 4°C. Next, 30 μ L of MACS buffer and 20 μ L of Anti-Biotin MicroBeads per 10×10^6 cells were added to each reaction tubes. Each suspension was incubated for an additional 10 minutes at 4°C before MACS buffer (500 μ L) was added and the B cells isolated by magnetic separation.

In vivo LPS challenge, serum cytokine detection, and harvesting of liver from mice

Female C57BL/6J mice (~8 weeks old) were injected intraperitoneally with LPS from *E. coli*, serotype O55:B5 (0.125 μ g/ μ L; Enzo, Farmingdale, NY; Cat. No. ALX-581-013-L002) diluted in PBS or with PBS only. Mice were sacrificed 2 hours after injection. The chest cavity was immediately cut open to expose the heart, and blood was slowly withdrawn from the ventricles using a 23G needle with a 1 mL syringe, placed in a 15 mL Falcon tube and left at room temperature for ~ 1 hour to allow coagulation. The tubes were centrifuged at 2000 x g, 4°C for 10 minutes, and plasma samples were collected for cytokine analysis by enzyme-linked immunosorbent assay (ELISA). Cytokine detection was performed using mouse IL-6 ELISA MAXTM standard set from BioLegend, following the manufacturer's protocol. The liver was also removed, and

sections were stored in RNA stabilization reagent (RNAlater™, Qiagen; Cat. No. 1017980) until ready for RNA isolation.

2.3 Results

2.3.1 Pro-inflammatory cytokines downregulate MIM in RAW 264.7 cells

Immune cells are prominent players in the tumor microenvironment and MIM is highly expressed in antigen-presenting cells such as macrophages, B cells, and dendritic cells, relative to other immune cells. The mouse macrophage-like cell line, RAW 264.7, is one of a limited number of established cell lines that show high expression of MIM. LPS, a component within the cell wall of gram negative bacteria, is often used in inflammation-based research to stimulate the release of pro-inflammatory cytokines in cells. To investigate the effect of inflammation on the expression of MIM, RAW 264.7 cells were exposed to LPS and various pro-inflammatory cytokines for 24 hours. Western blot results showed that LPS, IFN γ , and IL-6 reduced the protein expression of MIM by 70-95% in RAW 264.7 cells, while only a slight decrease was induced by TNF α (**Figure 2.1 A-C**). MIM expression was also downregulated transcriptionally by LPS (**Figure 2.1 D**).

The THP-1 human cell line was derived from a patient with acute monocytic leukemia and is often used as a model for human monocytes. To determine if inflammation reduces the expression of MIM in human cells of macrophage lineage, THP-1 cells were treated with 100 ng/mL LPS and the mRNA expression of MIM was assessed by qPCR. The results were somewhat inconclusive as MIM expression in THP-

1 cells, which is low in comparison to RAW 267.4 cells, initially increased by ~8-fold over control after 4 hours of LPS treatment, but subsequently decreased to a level that was ~4-fold greater than control by 8 hours of LPS exposure (**Figure 2.1 E**).

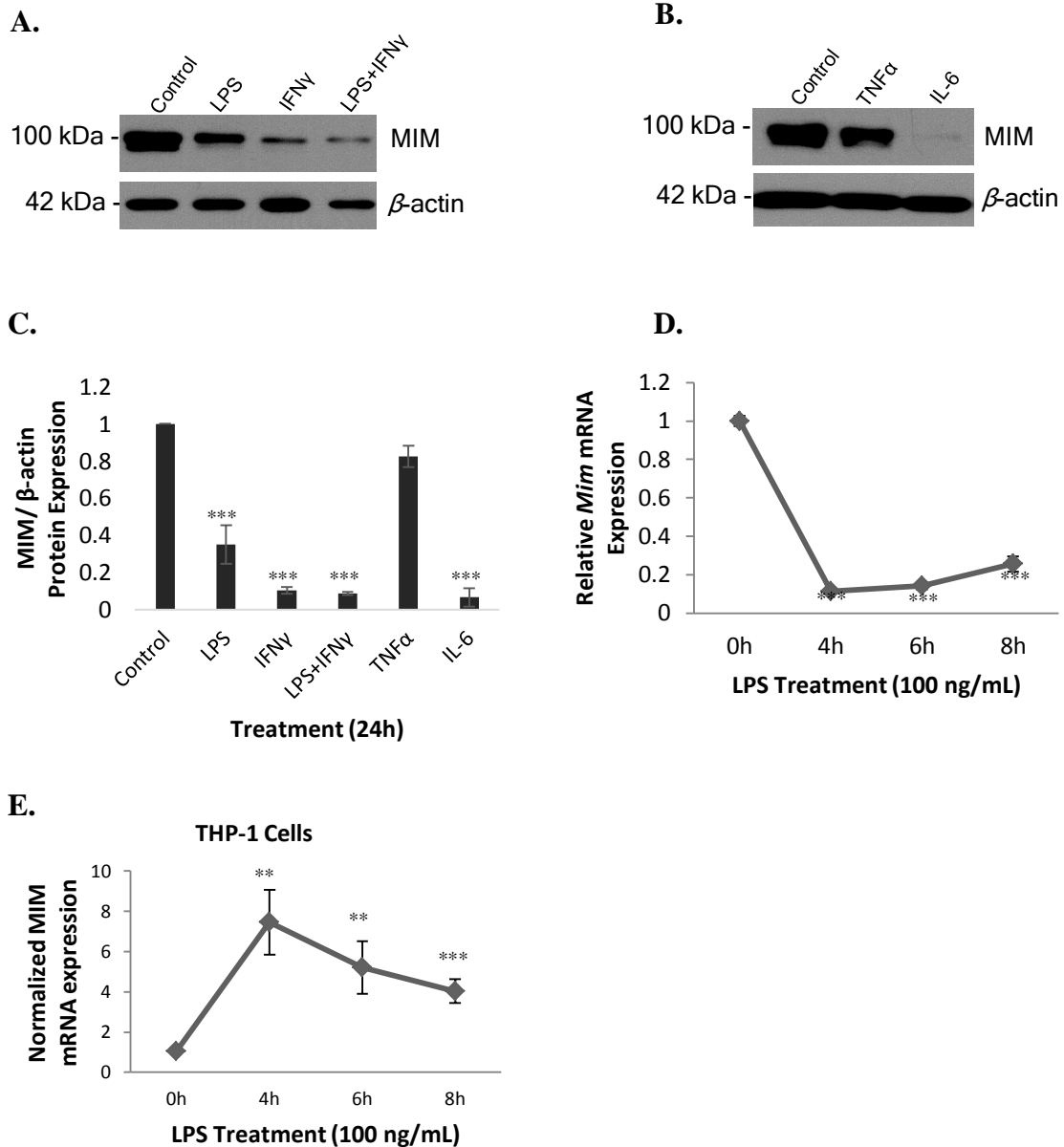


Figure 2.1 Certain pro-inflammatory cytokines downregulate MIM expression in RAW 264.7 cells. A – C. Western blot analysis of MIM expression in RAW 264.7. Cells were treated with LPS (100 ng/mL), IFN γ (50 ng/mL), or LPS plus IFN γ (A), as well as TNF α (50 ng/mL) or IL-6 (50 ng/mL) (B) for 24h. MIM levels were normalized against β -actin for 3 replicates (C). D - E. qPCR analysis of *Mim* expression normalized by *Gapdh* in RAW 264.7 cells (D) or normalized by β -actin in THP-1 cells (E) treated with LPS (100 ng/mL) for varying lengths of time. Control = no treatment. Data represented as mean \pm SD, $n=3$. **, $P < 0.01$; ***, $P < 0.001$ by Student's t -test.

2.3.2 LPS downregulates MIM in mouse bone marrow-derived macrophages

To further explore the response of MIM to inflammation in macrophages, bone marrow cells collected from wild type C57BL/6J mice were treated with M-CSF for 7 days to induce differentiation to macrophages. Western blot analysis showed that MIM expression increased over the course of M-CSF treatment (**Figure 2.2 A**). Antigens F4/80 and CD11b are widely used as markers of BMDM, so the M-CSF-treated cells were assessed by flow cytometry for CD11b and F4/80 expression to verify differentiation to macrophages. FACS results showed that 95% of the cells co-expressed these antigens at day 7 of M-CSF treatment (**Figure 2.2 B**) confirming that the cell population was mostly macrophages. The BMDMs were then exposed to 100 ng/mL LPS for varying periods. Real-time reverse transcription PCR and Western blot analysis showed that the mRNA and protein expression of MIM were downregulated in BMDMs after LPS treatment (**Figure 2.2 C & 2.2 D**). Overall, these results indicate that certain pro-inflammatory cytokines reduced the expression of MIM in mouse macrophages.

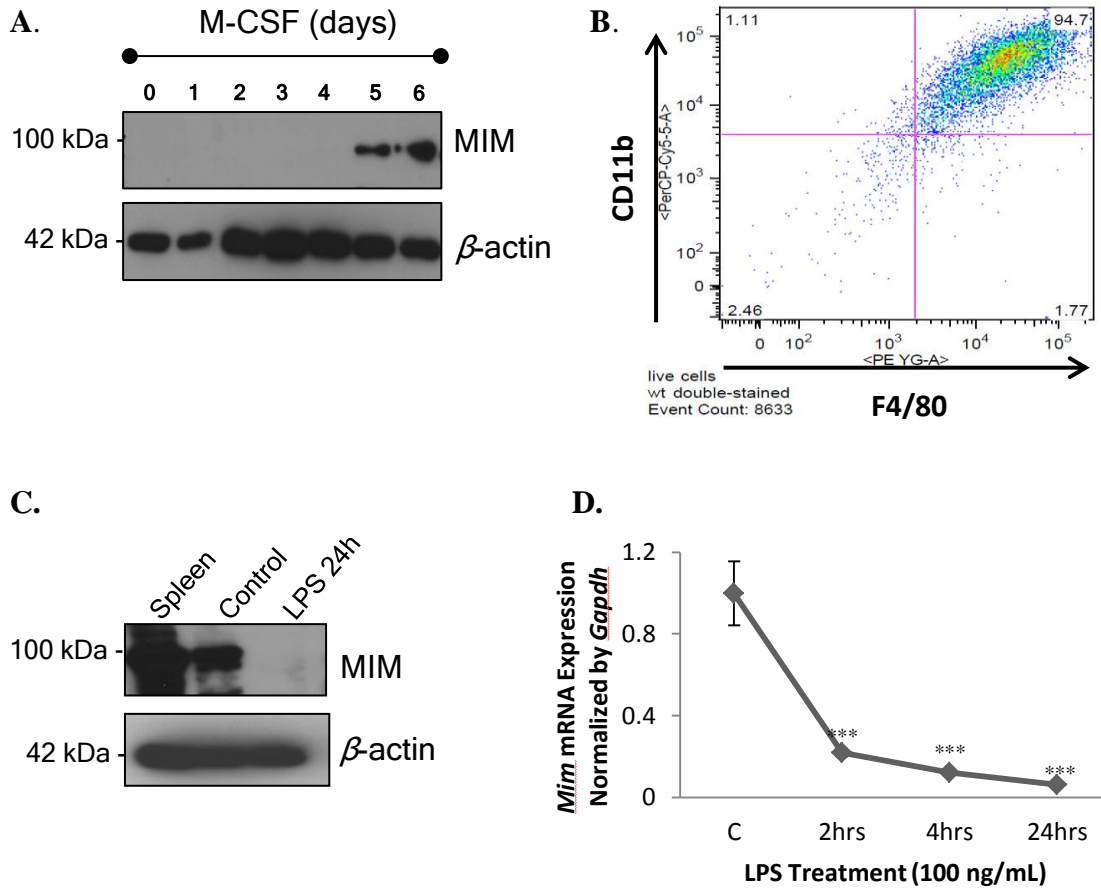
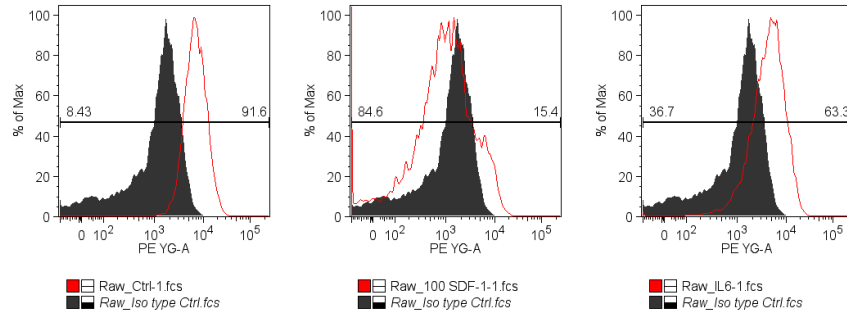


Figure 2.2 LPS downregulates MIM expression in mouse bone marrow-derived macrophages. **A.** Bone marrow cells harvested from C57BL/6J mice were treated with mouse M-CSF (20 ng/mL) for 7 days to induce differentiation into macrophages. The lysates of treated cells were analyzed by western blotting for MIM expression. **B.** Flow cytometry analysis of CD11b and F4/80 expression in cells collected after 7 days of M-CSF treatment. **C.** 1×10^6 BMDM were plated in six-well plates and treated with 100 ng/mL LPS or DMSO (vehicle-control) for 24 hours. Western blot analysis of lysates for MIM expression was performed. Lysates of mice splenic cells were used as positive control. **D.** qPCR analysis of *Mim* expression (normalized by *Gapdh*) in BMDM treated with LPS (100 ng/mL) for varying lengths of time. qPCR experiments were performed in triplicate. C = Control (no LPS). Data represented as mean \pm SD, $n=3$. ***, $P < 0.001$ by Student's *t*-test.

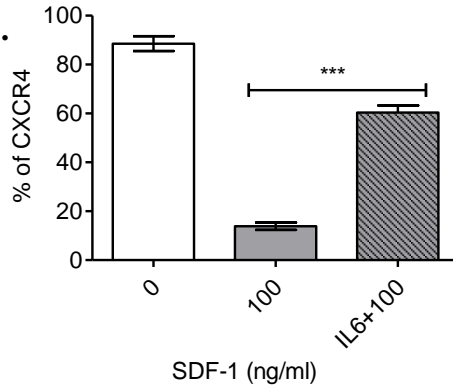
2.3.3 IL-6-induced downregulation of MIM results in impaired CXCR4 internalization and increased chemotactic response to SDF-1

Stromal cells of common metastatic niches constitutively secrete SDF-1 [118]. Given our previous findings that reduced expression of MIM led to inefficient internalization of CXCR4 and increased chemotactic response to SDF-1, the functional response to SDF-1 of RAW 264.7 cells in which expression of MIM was reduced by IL-6 was assessed. As expected, IL-6 treated RAW 264.7 cells showed impaired internalization of CXCR4 and increased chemotactic response upon exposure to SDF-1 (Figure 2.3 A - 2.3 C).

A.



B.



C.

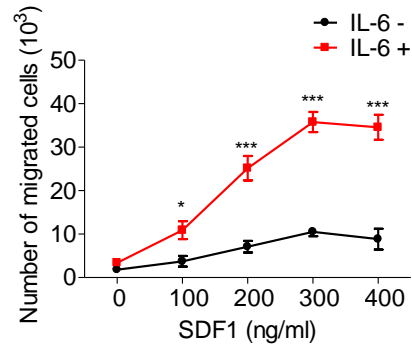


Figure 2.3 IL-6 treated RAW 264.7 cells show impaired CXCR4 internalization and increased chemotactic response to SDF-1. **A - B.** RAW 264.7 cells with or without IL-6 (50 ng/mL) pre-treatment for 24 h, were stimulated with SDF-1 (100 ng/mL) for 30 min. The percentage of cells expressing surface CXCR4 was determined by flow cytometry. **C.** RAW 264.7 cells with or without IL-6 (50 ng/mL) pre-treatment (24 h) were plated on Transwell plates in which the lower chamber was filled with medium containing SDF-1 at the indicated concentrations. After 24 h, cells were fixed and stained with 0.1% crystal violet. The number of cells that migrated to the lower chamber was compared with that of cells without SDF-1 treatment. All data represent mean \pm S.E.M. ($n = 3$). ***, $p < 0.001$ by Student's t -test.

2.3.4 Pro-inflammatory cytokines have no effect on MIM expression in B cells

MIM is highly expressed in B lymphocytes, which are another integral component of the tumor microenvironment. To determine if inflammation downregulates MIM in these immune cells, B-cells were isolated from wild-type C57BL/6J mice splenic cells using magnetic sorting technology, and treated with pro-inflammatory cytokine IL-6, for 24 hours. Western blot analysis showed the presence of phosphorylation at Tyr-705 of Stat3 in treated cells, indicating that the IL-6 signaling pathway had been activated. However, there was no difference in MIM expression between control and IL-6 treated cells (**Figure 2.4 A**). Activation of splenic B cells by IgM or IgM in combination with CD40L prior to IL-6 treatment did not change this result (**Figure 2.4 B**). Stimulation of mouse B cells with LPS and IFN γ also had no effect on MIM expression (**Figure 2.4 C**). Human lymphatic cancer cell lines Farage (non-Hodgkin's B cell lymphoma) and Reh (acute lymphocytic leukemia) have relatively high expression of MIM. Like the mice B cells, MIM expression did not change following LPS or IL-6 stimulation of these human cell lines (**Figure 2.4 D**). These results indicate that inflammation does not downregulate MIM in B cells.

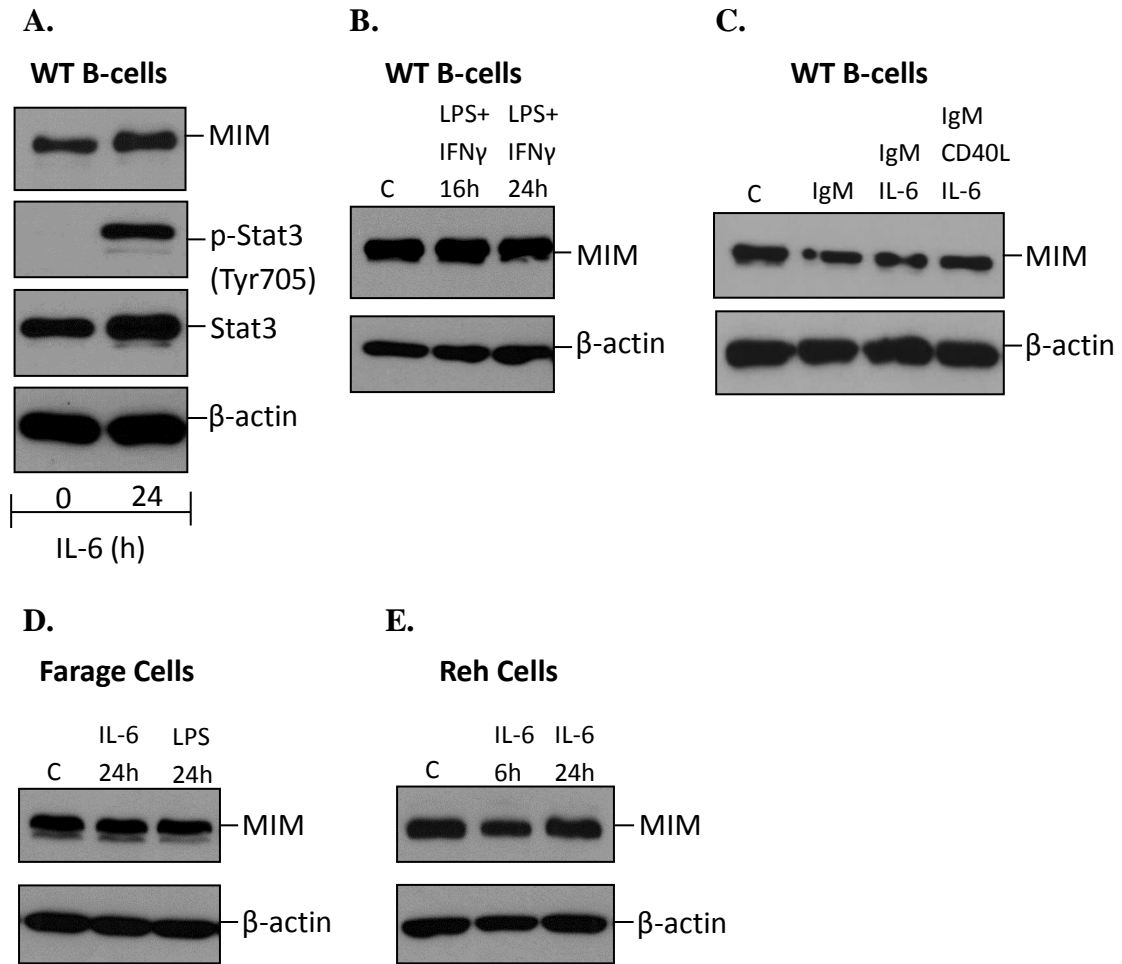


Figure 2.4 Inflammation has no effect on MIM expression in B cells. **A.** Western blot showing MIM expression in mouse B cells following 24 h exposure to IL-6. Phosphorylation of STAT3 was also assessed to confirm activation by IL-6. **B.** MIM protein expression in mouse B cells following exposure to LPS and IFN γ . **C.** Western blot analysis of MIM expression in mouse B cells that were first stimulated by IgM and CD40L for 24 hours to mimic activation by an antigen, then exposed to IL-6 for another 24 hours. **D-E.** Western blots showing MIM expression in Farage (**D**), and Reh (**E**) cells, following exposure to LPS and/or IL-6.

2.3.5 LPS-induced inflammation in mice does not alter MIM expression in liver

To assess the effect of inflammation on *Mim* expression *in vivo*, female wild type C57BL/6J mice (8 weeks old) were administered LPS intraperitoneally. After 2 hours, mice were sacrificed, and serum was collected for ELISA in order to confirm an inflammatory response. Results from ELISA showed significantly higher IL-6 in serum from mice that were injected with LPS compared to mice that were injected with PBS (**Figure 2.5 A**). Hepatocellular carcinoma is one of the inflammation-associated cancer types that often show downregulation of MIM. Given this, the expression levels of MIM in liver samples following an LPS challenge were examined to determine the effect of inflammation on MIM expression in mouse liver. Real-time quantitative PCR analysis showed no difference in *Mim* expression between mice injected with PBS and mice injected with LPS (**Figure 2.5 B**). These results suggest that acute inflammation has no effect on hepatocellular MIM expression.

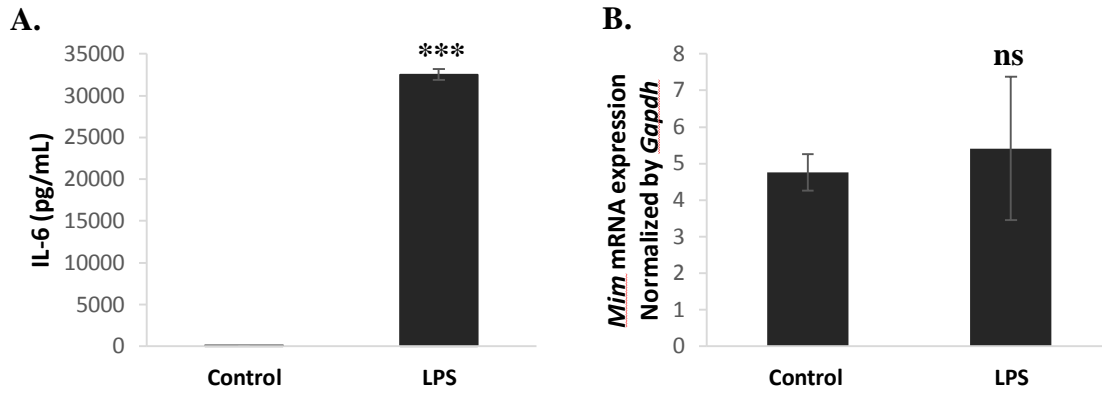


Figure 2.5 LPS-induced inflammation has no effect on MIM expression in mice liver. **A.** ELISA of IL-6 secretion. Mice were challenged with LPS and serum collected to confirm an inflammatory response. **B.** *Mim* mRNA expression in liver samples from mice injected with LPS. Control = mice injected with PBS. Data represented as mean \pm SD, $n=3$; ***, $p < 0.001$; ns, no significance

2.4 Discussion

Previous studies indicate that MIM expression may be regulated by an inflammatory microenvironment, but this theory has not been fully explored [66], [67]. In this study, we show that pro-inflammatory stimulators and cytokines such as LPS, IFN γ and IL-6 reduce MIM protein and mRNA expression in mouse BMDM and RAW 264.7 mouse macrophage-like cells, but not in mouse B cells or liver tissue. The finding of inflammation-induced downregulation of MIM in macrophages could be of therapeutic significance in MIM-related cancers as immune cells represent a major component of the tumor environment, and macrophages, specifically, coordinate various factors in the tumor microenvironment to influence proliferation, invasion and metastasis of tumor cells [119]. Microenvironmental signals generated from tumor and stromal cells can shift the functional phenotype of resident and actively recruited macrophages to a distinct phenotype that is associated with tumorigenesis [119]. These tumor-associated macrophages (TAMs) can in turn modulate the tumor microenvironment to promote tumor progression.

Cancer-related inflammation is one of the defining hallmarks of cancer, and TAMs play a significant role in the association of inflammation with cancer [120]. TAMs can produce inflammatory cytokines such as IL-6, interleukin 10 (IL-10), and TNF α that contributes to a pro-inflammatory microenvironment [119]. TAMs consists of locally proliferating macrophages (tissue-resident macrophages) and recruited macrophages derived from bone marrow monocytes, but the recruited macrophages represent the majority of TAMs [119]. Within the tumor microenvironment, peripheral blood monocytes are recruited and induced to differentiate into macrophages by various

chemokines and growth factors produced by stromal and tumor cells. This includes the chemokine CXCL12 (SDF-1), which is also secreted by the monocytes/macrophages themselves [121]. Our lab previously found that bone marrow cells from MIM-KO mice showed impaired internalization of CXCR4 and increased migration in response to SDF-1 stimulation [101]. In this study, we found that RAW 264.7 cells in which MIM expression was reduced by exposure to a pro-inflammatory stimulus (IL-6), also showed overexpression of CXCR4 and increased chemotactic response to SDF-1. Therefore, an inflammatory microenvironment could lead to reduced expression of MIM in macrophages which could potentially increase their migration to niches that secrete high levels of SDF-1. This may contribute to cancer metastasis, since one of the pro-tumor roles of TAMs is the establishment of premalignant niches in the organs to which the tumor cells will eventually metastasize [119].

To determine if inflammation also downregulates MIM in human macrophage lineage cells, we treated human monocyte-like cell line, THP-1, with LPS for various lengths of time. We found that MIM mRNA expression level initially increased in the THP-1 cells, peaking at ~4 hours before gradually decreasing over time as LPS treatment continued. LPS can induce differentiation of THP-1 cells to a more macrophage-like phenotype [122], which could explain the initial increase in MIM expression. We noted during this study that M-CSF-induced differentiation of mouse bone marrow cells to macrophages resulted in an accompanying increase in MIM expression. We speculate that the LPS-induced increase in MIM expression that was observed during the first 4 hours following LPS exposure is probably due to the cells acquiring a more mature phenotype and likely corresponds to the increase in MIM expression that was observed as

the mouse bone marrow cells differentiated into macrophages. Then once the majority of the THP-1 cells acquired a more macrophage-like phenotype, the resulting inflammation from continued exposure to LPS caused MIM expression to decrease. Further studies are needed to confirm that MIM expression increases with human monocyte differentiation, but overall these results suggest a physiological role for MIM in hematopoietic development.

B cells are another subset of immune cells that are present in the tumor microenvironment and can contribute to tumor progression and metastasis [123], and like macrophages, mouse splenic B cells have relatively high expression of MIM [78]. We investigated whether inflammation reduced MIM expression in mouse splenic B cells, and found that MIM expression did not change after exposure to LPS or pro-inflammatory cytokines. Neither did inflammation alter the expression of MIM in human lymphocytic cancer cell lines, REH or Farage. Reduced expression of MIM is associated with several inflammation-linked cancers, such as gastric cancer, pancreatic carcinoma, and hepatocellular carcinoma [11], [38], [50], [124]. To determine if the inflammatory microenvironment that is often associated with these types of cancer can reduce the expression of MIM in the local tissue milieu, we carried out an *in vivo* LPS challenge in C57BL/6J mice, and analyzed the mRNA expression of *Mim* in liver tissue harvested from the mice. We found that the acute inflammatory response that was induced by LPS did not alter *Mim* expression in liver cells.

Overall, these results imply that inflammation-driven downregulation of MIM is specific to macrophages, but further studies are needed to fully support such a conclusion. Many inflammation-associated cancers develop as a result of exposure to a

pro-inflammatory environment over an extended period of time [124]. The assays in this study only examined the effect of acute inflammation or relatively short exposure of pro-inflammatory cytokines on MIM expression. Further studies are needed to explore the effect of chronic inflammation on MIM expression.

Chapter 3¹: Rab7 is required for MIM-mediated Lysosomal Degradation of CXCR4

3.1 Introduction

Receptor-mediated endocytosis is the process by which extracellular proteins on the cell surface, such as receptors for cytokines and hormones, are selectively packaged into intracellular vesicles called endosomes [125]. During this process, the internalized proteins go through a series of sorting events that lead to either degradation in lysosomes or recycling back to the plasma membrane [126]. This process depends on post-translational modifications such as phosphorylation and ubiquitination and is guided by the activity of Rab GTPases and phosphoinositide-interacting proteins [125]. In cancer cells, the normal endocytic process is often deregulated, leading to abnormal expression of cell surface proteins and the manifestation of several of the hallmarks of cancer [127].

Overexpression of the chemokine receptor, CXCR4, has been observed in multiple cancer types and is thought to play a critical role in metastasis. CXCR4 ligand, SDF-1 (also known as CXCL12), is highly expressed at lungs, liver, brain, and the bones, which are the most common sites of metastatic spread [128]. Upon SDF-1 stimulation, CXCR4 is rapidly phosphorylated and internalized. Following internalization, CXCR4 can be recycled back to the plasma membrane or sorted to the lysosome for degradation [126].

Ubiquitination of CXCR4 by the E3 ubiquitin ligase AIP4 targets the receptor for degradation in lysosomes [129]. This process involves sorting of the receptor into early

¹ [107] Li L and Baxter SS, Zhao P, Ning G, Zhan X. (2019) Differential interactions of missing in metastasis and insulin receptor tyrosine kinase substrate with RAB proteins in the endocytosis of CXCR4. *J. Biol. Chem.* 294(16): 6494-6505

endosomes, which then mature into late endosomes or multivesicular bodies (MVBs) before fusing with lysosomes [130]. The maturation of endocytic vesicles is coordinated by Rab small GTPases such as Rab5, which associates with early endosomes; Rab7, which coordinates vesicle maturation into late endosomes; and Rab11, which is a prominent marker of recycling endosomes [131]. It is well established that Rab GTPases are essential regulators of intracellular vesicle trafficking, but the molecular mechanisms of this function have not been fully elucidated.

The CXCR4–SDF-1 axis plays an important role in regulating homeostasis of B cell compartmentalization, and high expression of CXCR4 has been linked to the development and progression of B cell lymphoma [132]. A knockout mouse strain of putative metastatic suppressor gene, MTSS1/MIM, showed a predisposition to developing a type lymphoma that resembles DLBCL at 12-24 months of age [78]. The mice also showed abnormal distribution of B lineage cells in bone marrow and spleen, suggesting a defect in homing of the cells to niches [78]. Additionally, bone marrow cells from the MIM-KO mice showed a higher cell surface expression of CXCR4 compared to cells from wild-type mice when stimulated by SDF-1 [101].

MIM is a member of the BAR domain superfamily of proteins, which are characterized by their ability to bind and deform membranes through a crescent-shaped interface [82]. Most BAR domain proteins interact through a positively charged concave surface, but MIM is one of five proteins that make up a subgroup that interacts with membranes through an inverse, or convex surface [82]. This subgroup, termed the inverse BAR (I-BAR) domain subfamily, is further subdivided based on the presence of an internal SH3 domain. The SH3-containing members include IRSp53, IRTKS, and

PINKBAR, while MIM and ABBA make up the subgroup that is lacking a SH3 domain [82]. All I-BAR domain proteins have been shown to interact with small GTPases to mediate membrane dynamics [133], [134], but the specifics of this relationship are yet to be fully determined.

Aberrant expression of MIM has been linked to cancer progression and metastasis of several types of cancer (**Table 1**). In most contexts, MIM is characterized as a tumor/metastasis suppressor, but there are examples in the literature where MIM acts as a tumor promoting factor, making its exact role in cancer progression unclear. MIM has been linked to several cellular partners and has been implicated in multiple signaling pathways [20], [29], [44], [78], [100]. There is also some evidence that MIM functions in endocytosis [98], [99], but the underlying mechanism of action has not been fully elucidated.

We recently found that upon SDF-1 stimulation, MIM binds to AIP4 and promotes ubiquitination of CXCR4, thus facilitating lysosomal degradation of the receptor [105]. We also noted that MIM interacts with Rab5 and Rab7 to facilitate the trafficking of CXCR4 into MVBs, and promotes the formation of MVBs/late endosomes [105]. In this study, we further investigated the role of Rabs in MIM-mediated CXCR4 endocytosis. We found that Rab7 is required for MIM-mediated CXCR4 lysosomal degradation. We also observed that while MIM associates with early endosomes and late endosomes through interactions with Rab5 and Rab7 respectively, MIM seemingly does not associate with recycling endosomes, as we found no evidence of any interaction with Rab11. Instead, another I-BAR family member, IRTKS, associates with Rab11 and

promotes receptor recycling in an SH3-dependent manner. This data establishes a link between I-BAR domain proteins and Rab GTPases in endocytic pathways.

3.2 Materials and Methods

Cells and cell lines

HeLa and MDA-MB-231 cells were cultured in DMEM (Corning; Corning, NY) supplemented with 10% FBS (Hyclone; Logan, UT), 100 unit/mL penicillin and 100 µg/mL streptomycin (pen/strep) (Life Technologies, Grand Island, NY; Cat. No. 15140-122) at 5% CO₂ and 37°C. Daudi, Raji, Reh cells, and primary B lymphatic cells derived from a patient, were a gift from Dr. Curt Civin. All B cells were cultured at 37 °C, 5% CO₂ in RPMI 1640 medium supplemented with 10% FBS and pen/strep. DNA-mediated transfection was performed with FuGENE transfection reagent (Active Motif Co., Carlsbad, CA; Cat. No. 32043). Stably transfected cells were selected and maintained in medium containing G418, as described previously [89]. Raji cells were transfected with pMIM-GFP using Raji Cell Avalanch transfection reagent (EZ Biosystems, College Park, MD; Cat. No. EZT-RAJI-1). The expression of transfected genes was verified by fluorescence microscopy and immunoblot analysis. SiRNA-mediated transfection was performed using Lipofectamine 2000 (Thermo Fisher Scientific, Rockford, IL) according to the manufacturer's recommendations. All the cells were tested for contamination routinely every 2 months.

Antibodies, reagents and plasmids

The polyclonal MIM antibody (PA517047), polyclonal GFP antibody (A11122), monoclonal GFP antibody (33-2600), polyclonal IRTKS antibody (PA5-22026), Alexa Fluor 488 goat anti-rabbit IgG antibody (A-11008), Alexa Fluor 568 goat anti-rabbit IgG (A11004 or A21134), Alexa Fluor 488 goat anti-mouse IgG (A32723), Alexa Fluor 568 goat anti-mouse IgG (A11011), FITC-conjugated goat anti-rabbit (INV-A21311), Alexa Fluor 568-conjugated goat anti-mouse (INV-A21134), Alexa Fluor 633-conjugated goat anti-mouse (INV-A21050), protein A-sepharose® 4B (Cat. No. 101041) and protein A/G-agarose beads (Cat. No. 20423) were purchased from Invitrogen/Thermo Scientific. The polyclonal CD63 antibody (sc-15363), polyclonal and monoclonal CXCR4 antibody (sc-9046 or sc-53534), and normal mouse IgG (sc-2025) were purchased from Santa Cruz Biotechnology (Dallas, TX). Antibody against normal rabbit IgG (729S) was purchased from Cell Signaling Technology (Danvers, MA). SDF-1 (Cat. No. 581206) and PE-conjugated anti-human CXCR4 antibodies (306506) were purchased from BioLegend (San Diego, CA). Monoclonal antibody against Rab11 (610656) was purchased from BD Biosciences (San Jose, CA). Cycloheximide (CHX, Cat. No. C4859), monoclonal antibodies against Rab7 (R8779), a set of siRNAs targeting human Rab7a at 16 different sites, and control siRNA with a scrambled sequence were purchased from Sigma-Aldrich. Phosphate-buffered saline (PBS; Cat. No. 21-040-CV) was purchased from Corning. The plasmids encoding MIM-GFP, IRTKS-GFP, IRTKS Δ SH3-GFP, IRTKS-IBAR-MIM-GFP, and MIM-IBAR-IRTKS-GFP have been described previously [135].

Western Blot analysis

Cells were lysed with RIPA lysis buffer from Millipore (Cat. No. 20-188) supplemented with anti-protease tablet (Roche, Indianapolis, IN; Cat. No. 1183617001) or Protease Inhibitor Cocktail (Sigma-Aldrich; Cat. No. P8340). Cell lysates were prepared by centrifugation at 4°C. The protein content of the cell lysates was estimated using a BCA assay kit (Thermo Fisher Scientific), and lysates were diluted appropriately for equal amounts of protein per sample. Laemmli sample buffer (Thermo Fisher Scientific; Waltham, MA) supplemented with β -mercaptoethanol (SIGMA; Cat. No. M6250) was added to lysates followed by boiling for 1-5 minutes. Aliquots of the lysates were loaded into gels for sodium dodecyl sulfate–polyacrylamide gel electrophoresis (SDS-PAGE) followed by transfer to a PVDF membrane (Millipore; Cat. No. IPVH00010). The membrane was blocked with 5% milk in TBST (10 mM Tris-HCl, pH 8.0, 150 mM NaCl and 0.1% Tween 20) at room temperature for 1 hour, then incubated with primary antibody diluted in TBST only, 5% milk-TBST solution, or 5% w/v BSA (SIGMA-Aldrich; Cat. No. A4503) -TBST solution overnight at 4°C with agitation. The PVDF membrane was rinsed with TBST and then incubated with HRP-conjugated secondary antibody at room temperature for 2 hours. After washing three times with TBST, enhanced chemiluminescence detection solution (Thermo Scientific; Cat. No. 34079) was applied to the membrane. The proteins probed were visualized by using X-
autoradiography. Densitometry analysis was performed with gel images from three independent experiments using ImageJ software.

Cell migration assay

Chemotaxis was assessed using 24-well Transwell plates with inserts of pore size 8µm from Corning (Cat. No. 3422). 2×10^5 cells/well were seeded in the migration inserts in serum-free media and placed in wells containing DMEM with SDF-1 at various concentrations. For adherent cells, following incubation at 37°C, 5% CO₂ for 16 hours, media was removed and the cells on each insert were washed with PBS twice and incubated with 4% paraformaldehyde for 5 minutes. Following additional washes with PBS, 200 µL methanol was added to the plate and inserts were incubated at room temperature for 20 minutes. Cells were then stained with 0.1% Crystal Violet for 15 minutes. After further washing with PBS, cotton swabs were used to remove non-migrated cells from the upper surface of the inserts. To count cells, the inserts were viewed under a microscope at 20× magnification, and the cells within nine microscopic fields were counted for each insert. For non-adherent cells, the cells that migrated to the lower chamber were counted using a hemocytometer.

Flow cytometry analysis

Cells were cultured in 75 cm² flasks or 10 cm tissue culture treated dishes. Adherent cells were detached using 1 mL of 0.2% EDTA Cell Dissociation Reagent (Thermo Fisher Scientific). Cells were re-suspended in 2 mL DMEM, aliquoted into equal amounts, and transferred into fresh 10 mL round bottom tubes containing 5 mL DMEM only or DMEM with SDF-1. After incubation at 37°C and 5% CO₂ for different time periods, cells were centrifuged to remove media, washed with PBS, and immediately placed on ice. The treated cells were stained with PE-conjugated anti-human-CXCR4 antibody (1 µg/mL) diluted in PBS containing 0.75% BSA and 5 mM

EDTA (FACS buffer) and incubated at 4°C for 1 hour in the dark. As the control, cells were stained with PE-conjugated anti-IgG antibody in parallel. After staining, 500 µL FACS buffer was added to the cells followed by centrifugation. The supernatant was removed by aspiration, and the cells were washed 3 times with PBS. After washing, the cells were fixed with 4% paraformaldehyde and then flow cytometry analysis performed using a BD LSRFortessa flow cytometer. The data was analyzed by using FlowJo software version 8.8.7.

Protein degradation assay

HeLa cells were plated at a density of 8×10^5 /well in a 6-well plate and incubated overnight. Cells were then treated with 0.5 mg/mL cycloheximide for 30 minutes, followed by incubation with 150 ng/mL SDF-1 for the times indicated at 37°C and 5% CO₂. The treated cells were collected using trypsin and lysed using RIPA buffer. Western blotting with anti-CXCR4 antibody (1 µg/mL) was performed to detect CXCR4 levels. The same blots were stripped and re-blotted for β-actin as the loading control.

Immunofluorescence microscopy

Glass coverslips sterilized by exposing to ultraviolet light were placed in a 6-well plate and covered with 5 µg/mL fibronectin (Life Technologies) for 30 min at room temperature. Cells were plated into each well and cultured in DMEM supplemented with 10% FBS and 1% pen/strep overnight. Cells were treated with control siRNA or siRNA against Rab7 by using FuGene Transfection Reagent (Active Motif, Carlsbad, CA) according to the manufacturer's instructions. Sixteen hours after transfection, the media was replaced by fresh DMEM supplemented with 10% FBS and cells were further incubated for 24 hours. On day of SDF-1 treatment, medium was aspirated, cells washed

with PBS, and then incubated with DMEM for 2 hours to achieve serum-starving mediated cell quiescence. The starved cells were then incubated with 100 ng/mL SDF-1 (or vehicle as control) for 30 minutes. After washing twice with PBS, cells were fixed by adding 4% paraformaldehyde at room temperature for 10 minutes, washed, and permeabilized by adding 0.05% saponin for 10 minutes. The fixed cells were blocked by 200 μ L PBS supplemented with 5% goat serum (blocking buffer). Cells were then incubated with primary antibodies (5 μ g/mL) diluted in blocking buffer for 1 hour at room temperature. Following this, cells were rinsed three times with PBS, and then incubated with Alexa Flour-conjugated secondary antibodies for 1 hour. Finally, cells were stained with DAPI for 5 minutes and the coverslip mounted on a glass slide with 20 μ L of Mounting Medium (Kirkegaard & Perry Laboratories, MD). The slide was sealed with nail polish, and the stained cells were inspected using a Zeiss LSM 510 laser scanning confocal imaging system using a Plan-Apo 63 \times /1.4 numerical aperture oil lens. The digital images were captured using an acquisition setting that was applied to all the samples analyzed in parallel. In each group, all the images were taken and presented at the same settings for brightness and contrasts. Protein co-localization was quantified based on MOC [136], which was calculated by using an ImageJ plugin. Quantification of stained puncta was also conducted by using the ImageJ software.

Co-immunoprecipitation assay

To evaluate protein-protein interactions, cell lysates were subjected immunoprecipitation (IP) followed by western blotting. Cells grown in 10-cm dishes were lysed using RIPA buffer containing protease inhibitors, and lysates collected in 1.5mL tubes. After aliquoting 30 μ L to use as input, the lysates were incubated with 20

μ L of 50% protein-A or protein-A/G beads for 90 minutes at 4°C and centrifuged at 100 x g to pre-clear. The supernatant was mixed with 5 μ g/mL anti-GFP antibody and incubated overnight at 4°C. The antibody-lysate mix was then combined with 100 μ L of protein-A or protein-A/B slurry (50%, v/v), and incubated with rotation for 2 hours at 4°C. The mixture was centrifuged at 2000 rpm for 30 seconds, and the beads washed three times with 0.5 mL RIPA lysis buffer. After carefully removing the supernatant, 60 μ L 2X SDS sample buffer was added to the bead complex, and samples were boiled for 10 minutes. The boiled samples were subjected to SDS-PAGE followed by Western blot analysis.

3.3 Results

3.3.1 MIM promotes CXCR4 internalization and reduces SDF-1 chemotactic response in multiple cell types

Our lab previous demonstrated that bone marrow cells from MIM-KO mice show increased expression of CXCR4 on the cell surface, suggesting a defect in CXCR4 internalization [101]. Given that aged MIM-KO mice are pre-disposed to developing lymphoma, internalization of CXCR4 was analyzed in human lymphatic cell lines to see if the expression of MIM correlates with the ability of the cell to endocytose CXCR4. Western blot analysis of the protein expression level of MIM in patient-derived human B lymphatic cells (PBL), Daudi (Burkitt's lymphoma), Raji (Burkitt's lymphoma) and Reh (acute lymphocytic leukemia) showed that MIM expression was relatively low in Daudi and Raji cells in comparison with PBL and Reh cells (**Figure 3.1 A**), and as expected, the

two cell lines with low expression of MIM (Daudi and Raji) did not internalize CXCR4 as efficiently as PBL and Reh cells when exposed to SDF-1 (**Figure 3.1 B**).

To confirm that MIM plays a role in CXCR4 internalization of lymphatic cells, Raji cells were transfected with a plasmid encoding MIM protein tagged with GFP (MIM-GFP) or a vector control plasmid encoding GFP only (GFP), and cells were stimulated with various concentrations of SDF-1 for 30 minutes. Flow cytometry analysis of CXCR4 cell surface expression showed that a significantly lower percentage of MIM-GFP-transfected Raji cells (~ 20%) compared with GFP-transfected Raji cells (~50%) expressed CXCR4 on the cell surface after exposure to 500 ng/mL of SDF-1 (**Figure 3.1 C**).

In our previous study, it was discovered that MIM-KO bone marrow cells displayed a more robust chemotactic response to SDF-1 than wild-type bone marrow cells [101]. Here, Transwell assays were used to examine the effect of MIM overexpression on the chemotactic response of Raji cells. There was an ~17-fold increase in the number GFP-transfected Raji cells in the lower chambers of the Transwell plates at 300 ng/mL and 400 ng/mL of SDF-1, compared to only a 6-fold increase for MIM-GFP-transfected Raji cells (**Figure 3.1 D**), indicating that MIM-overexpression reduced the chemotactic response of Raji cells to SDF-1.

CXCR4 has been reported to also play an important role in breast cancer metastasis [132]. Preferential sites of breast tumors metastasis include bones, lungs, and lymph nodes; organs that are known to secrete high levels of SDF-1 [137]. The MDA-MB-231 cell line was derived from breast cancer cells that had metastasized to the lung,

and these cells have low endogenous expression of MIM [138]. To determine if overexpression of MIM reduces the chemotactic response of these cells to SDF-1, the Transwell assay was repeated using MDA-MB-231 cells transfected with MIM-GFP or GFP. Similar to the Raji cells, significantly less MIM-GFP-transfected MDA-MB-231 cells than GFP control MDA-MB-231 migrated to the lower chambers of the Transwell plate in response to 100 ng/mL, 250 ng/mL, and 500 ng/mL SDF-1 stimulation (**Figure 3.1 E**). Overall these results confirm that MIM plays a role in CXCR4 internalization.

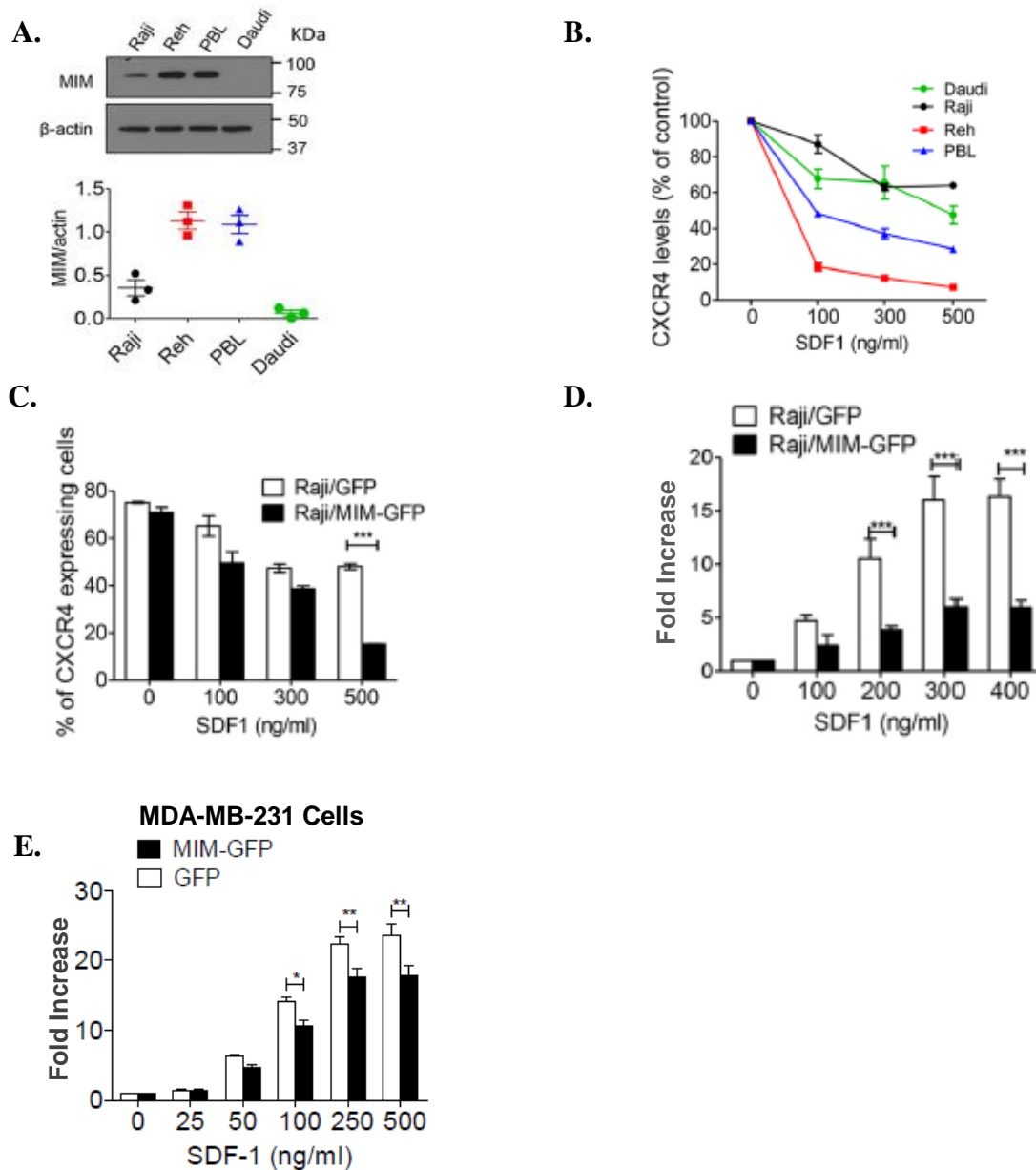


Figure 3.1 MIM promotes CXCR4 internalization and inhibits chemotactic response to SDF-1.

A. Immunoblot analysis of endogenous MIM protein in Raji, Reh, Daudi, and PBL cells. **B.** Malignant B cells were stimulated with SDF-1 at the indicated concentrations for 30 min. Surface expression of CXCR4 was analyzed by flow cytometry and normalized to that of control cells without SDF-1 treatment. **C.** Raji cells were transiently transfected with GFP or MIM-GFP and stimulated for 30 min with SDF-1 at different concentrations. The percentage of cells expressing surface CXCR4 was determined by flow cytometry. **D.** Raji cells expressing MIM-GFP or GFP were plated on Transwell plates in which the lower chamber was filled with medium containing SDF-1 at the indicated concentrations. After 24 hours, cells were fixed and stained with 0.1% crystal violet. The number of cells that migrated to the lower chamber was compared with that of cells without SDF-1 treatment. **E.** MDA-MB-231 cells expressing MIM-GFP or GFP were treated with SDF-1 at different concentrations as indicated. The motility of the treated cells was analyzed by Transwell assay as described in (D). All data represent mean \pm S.E.M. (n =3). ***, p <0.001.

3.3.2 Rab7 is indispensable for MIM-mediated CXCR4 internalization

In membrane trafficking, BAR domain proteins generate membrane curvature via re-organization of the actin cytoskeleton and signaling through small GTPases [82]. Rab small GTPases are known regulators of endocytic trafficking, and Rab5 and Rab7 are widely established markers for early and late endosomes, respectively [131]. We previously found that MIM interacts with Rab5 and Rab7 in a time-dependent manner following SDF-1 exposure [105]. We also previously showed that MIM interacted with Rab7 through the CCD of the I-BAR region, and that deletion of the CCD resulted in cell surface CXCR4 overexpression, which suggests that the MIM–Rab7 interaction is required for MIM-mediated CXCR4 internalization [105]. To further investigate the role of the MIM–Rab7 interaction in CXCR4 endocytosis, Rab7 expression was suppressed in HeLa cells overexpressing MIM-GFP or GFP only plasmids, using a set of siRNAs against *RAB7a*. (siRAB7). HeLa cells were used due to the ease of transfection compared with the lymphatic cells or MDA-MB-231. Western blot results showed that Rab7 protein expression was reduced by ~80% when compared with cells treated with scramble siRNA (Ct-siRNA) (**Figure 3.2 A**).

To assess the role of Rab7–MIM interaction in CXCR4 function, the effect of knockdown of Rab7 on the degradation of CXCR4 was measured by a cycloheximide assay. In response to SDF-1 stimulation, the half-life of CXCR4 was reduced from 4.1 hours in HeLa-GFP cells to 2.1 hours in HeLa-MIM-GFP cells treated with Ct-siRNA but was approximately the same for HeLa-GFP and HeLa-MIM-GFP cells that were treated with siRAB7 (**Figure 3.2 B**). Transwell assays were also used to analyze SDF-1-induced chemotaxis in Rab7 depleted cells. **Figure 3.2 C** shows that the attenuated chemotactic

response to SDF-1 that was seen with MIM-overexpressing cells (Figure 3.1 D – E) was not observed after treatment with siRab7 for 48 hours. Overall, these results confirm that Rab7 is required for MIM-mediated CXCR4 internalization.

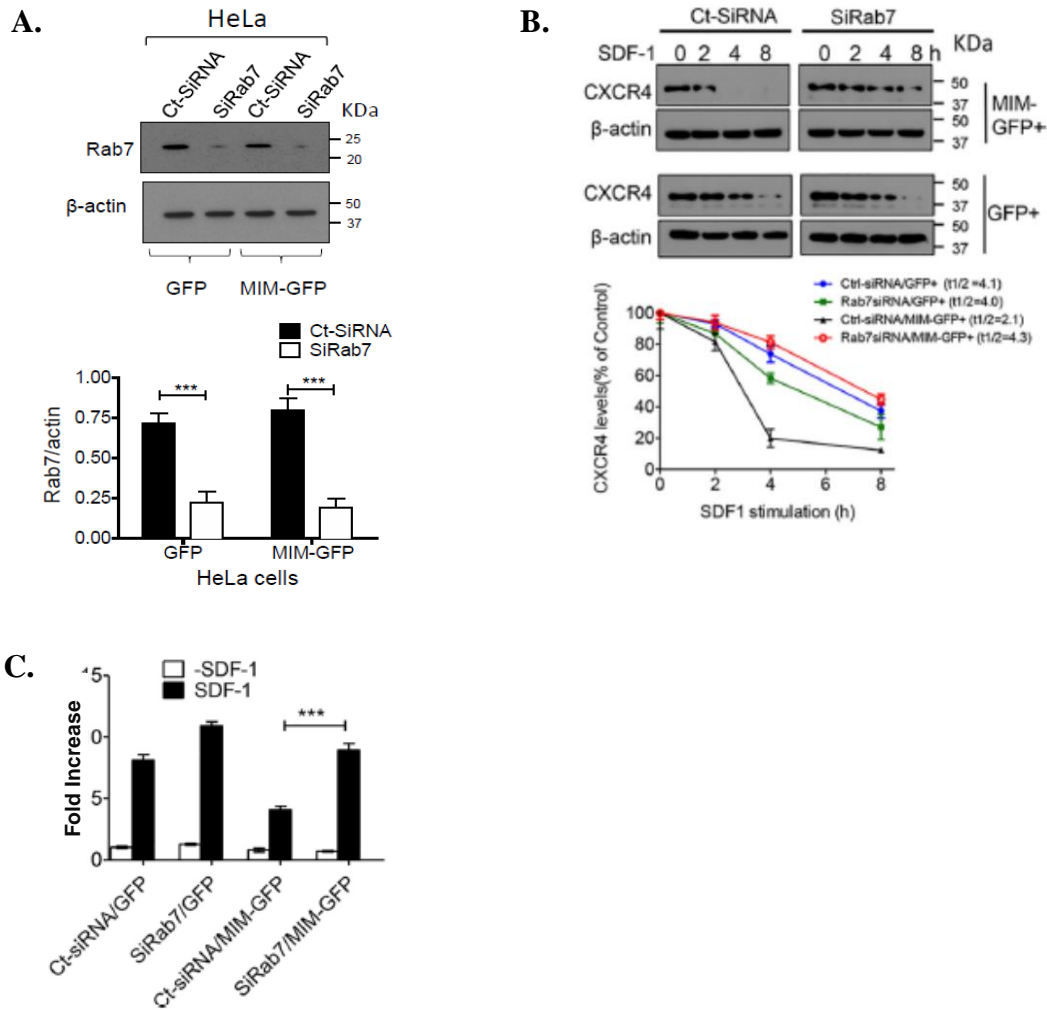


Figure 3.2 Rab7 is required for MIM-mediated CXCR4 internalization. **A.** Western blot confirmation of siRNA-mediated knockdown of Rab7 in HeLa-GFP and HeLa-MIM-GFP cells. **B.** HeLa-GFP and HeLa-MIM-GFP cells transfected with siRab7 or Ct-siRNA were pre-treated with cycloheximide 30 min prior to adding 150 ng/mL SDF-1 for the indicated times, followed by Western blot analysis of CXCR4 expression. $t^{1/2}$ was calculated using Prism software. **C.** HeLa-GFP or HeLa-MIM-GFP cells were treated with siRab7 or Ct-siRNA for 48 h and their chemotactic response to 500 ng/ml SDF-1 was assessed using a Transwell assay. The data represent mean \pm S.E.M (n=3). IB, immunoblot.

3.3.3 Rab7 is required for MIM-mediated recruitment of CXCR4 to late endosomes

Rab7 is known to regulate late endocytic trafficking [139] and we previously found that MIM promotes sorting of CXCR4 into late endosomes [105]. Therefore, we investigated the effect of Rab7 depletion on MIM-mediated recruitment of CXCR4 to late endosomes, by assessing the co-localization of CXCR4 with CD63, a late endosome marker. Immunofluorescence staining showed that 72% of CD63 co-localized with CXCR4 in HeLa-MIM-GFP cells treated with control siRNA compared to 17% with siRab7 treatment (**Figure 3.3 C, 3.3 D and 3.3 E**), while CD63 co-localization remained at approximately 20% in HeLa-GFP cells whether pre-treated with control or siRab7 (**Figure 3.3 A, 3.3 B and 3.3 E**). In the absence of SDF-1 stimulation, HeLa-MIM-GFP and HeLa-GFP cells showed low co-localization of CXCR4 and CD63 whether cells were pre-treated with control siRNA or siRab7 (**Figure 3.3**). SDF-1 stimulation also increased CD63 puncta in HeLa-MIM-GFP cells, indicating that MIM promotes the formation of late endosomes (**Figure 3.3 F**). Rab7 depletion significantly decreased CD63 puncta in HeLa-MIM-GFP cells, but not in HeLa-GFP cells (**Figure 3.3 F**). Overall, these results showed Rab7 is required for MIM-mediated recruitment of CXCR4 to late endosomes.

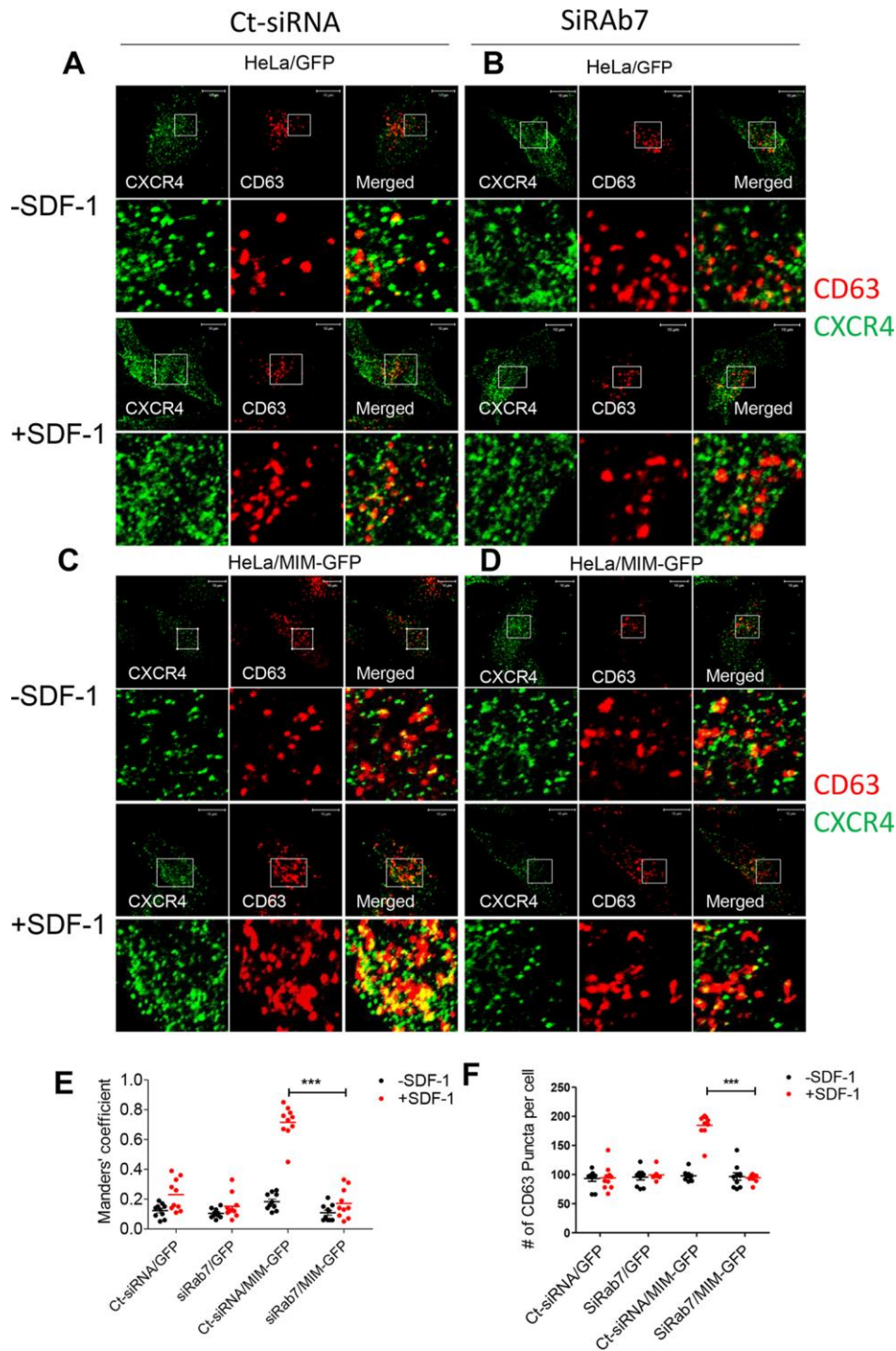


Figure 3.3 Rab7 is essential for MIM to promote CXCR4 sorting into late endosomes. A–D. HeLa cells expressing GFP (*A* and *B*) or MIM-GFP (*C* and *D*) were plated in 6-well plates, treated with Ct-siRNA (*A* and *C*) or siRab7 (*B* and *D*) for 48 h, and stimulated with 500 ng/ml SDF-1 for 30 min. The treated cells were co-stained with monoclonal CXCR4 antibody (*green*) and polyclonal CD63 antibody (*red*) and inspected by confocal microscopy. The *boxed areas* of images were amplified and are presented below. **E.** Co-localization of CXCR4 and CD63 was quantitatively analyzed based on Manders' coefficient. **F.** The amount of CD63 puncta of the acquired images was also quantified. Scale bars = 10 μ m. ***, $p < 0.001$ ($n = 10$).

3.3.4 Rab7 is required for recruitment of MIM into late endosomes

We previously observed that MIM associates with late endosomes in response to SDF-1 stimulation [105]. Here, we analyzed the effect of RNAi-mediated reduction of Rab7 on the recruitment of MIM to late endosomes. HeLa-GFP cells showed diffused staining with or without SDF-1 treatment of si-Rab7 pre-treatment (**Figure 3.4 A and 3.4 B**). As expected, based on our previous results, SDF-1 stimulation led to about 70% co-localization of CD63 with MIM compared to approximately 17% without SDF-1 treatment (**Figure 3.4 C and 3.4 E**). Depletion of Rab7 reduced MIM-CXCR4 co-localization to control levels (**Figure 3.4 D and 3.4 E**), indicating that Rab7 is required for sorting of MIM into late endosomes.

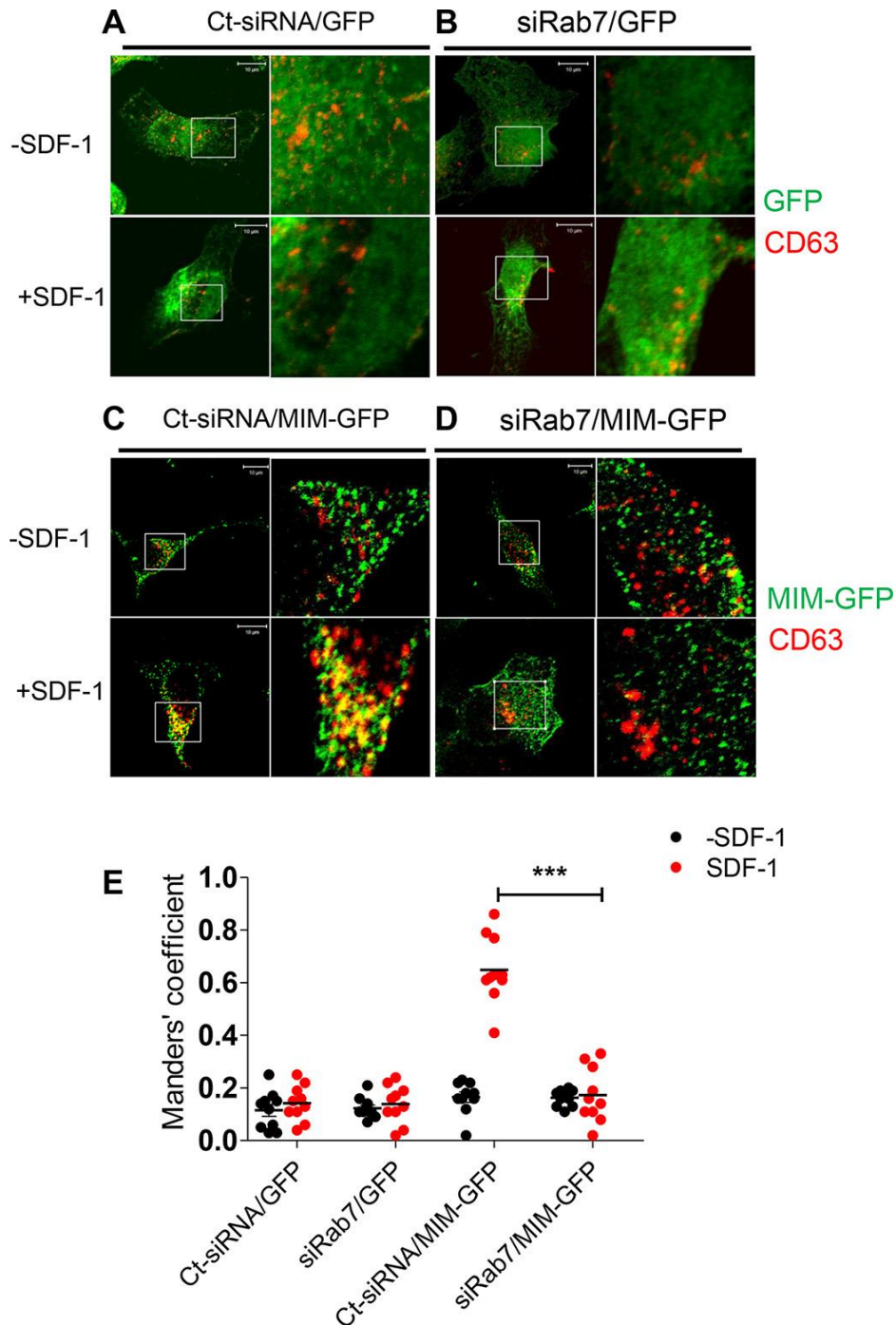


Figure 3.4 RAB7 is indispensable for recruitment of MIM into late endosomes. A–D. HeLa cells expressing GFP (A and B) or MIM-GFP (C and D) were treated with control siRNA (A and C) or siRab7 (B and D) for 2 days prior to treatment with 500 ng/ml SDF-1 for 30 min. The treated cells were co-stained with GFP antibody (green) and CD63 antibody (red) and inspected by confocal microscopy. The boxed areas were amplified and are presented to the left of the corresponding images. E. Co-localization of CD63 and GFP or MIM-GFP was quantitatively analyzed based on Manders' coefficient. Data represent mean. ***, $p < 0.001$ ($n = 10$). Scale bars = 10 μ m.

3.3.5 MIM regulates CXCR4 degradation while IRTKS regulates CXCR4 recycling

The small GTPase Rab11 is the most commonly used marker for recycling endosomes. To determine if MIM also participates in the recycling pathway, interactions between MIM and Rab11 were analyzed by co-IP assays. The results indicate that SDF-1 stimulation of HeLa-MIM-GFP cells does not induce an interaction between Rab11 and MIM (**Figure 3.5 A**), which suggests that MIM does not participate in the recycling pathway. This is as expected, given that receptor recycling generally results in increased cell surface expression of the receptor, and the absence of MIM leads to CXCR4 overexpression on cell surface.

In an earlier study, this lab found that HeLa cells overexpressing another I-BAR domain protein, IRTKS, showed increased migration in response SDF-1 when compared with control cells [135]. To determine if IRTKS participates in the recycling pathway, interactions between IRTKS and Rab11 were analyzed by co-IP assays using stably transfected HeLa cell lines in which a GFP tagged IRTKS plasmid was overexpressed (HeLa-IRTKS-GFP). Interestingly, an interaction between IRTKS and Rab11 was observed 30 minutes after SDF-1 stimulation. (**Figure 3.5 A**). Also, microscopic examination of fluorescent-labeled Rab11 and CXCR4 showed that 30 minutes of SDF-1 treatment increased the co-localization of CXCR4 and Rab11 in HeLa-IRTKS-GFP cells (**Figure 3.5 B**). These results indicate that IRTKS may play a key role in CXCR4 recycling.

To determine if IRTKS also associates with early or late endosomes, co-IP assays were performed to examine the interaction between IRTKS and Rab5 or Rab7. Similar to MIM, IRTKS bound Rab5 five minutes after SDF-1 exposure (**Figure 3.5 C**), but unlike MIM, there was no interaction detected between Rab7 and IRTKS at 30 minutes of SDF-1 treatment (**Figure 3.5 D**). IRTKS also showed an opposite effect on chemotaxis than MIM. As was previously observed [135], HeLa-IRTKS-GFP cells showed increased migration in response to SDF-1 compared to HeLa-GFP cells (**Figure 3.5 E**).

To further explore the influence of IRTKS on the function of CXCR4, cell surface expression of CXCR4 was assessed by flow cytometry, following inhibition of proteolysis with cycloheximide and CXCR4 activation by SDF-1 for different lengths of time. At 30 minutes of SDF-1 treatment, CXCR4 levels fell to approximately 62% in HeLa-IRTKS-GFP cells, compared with ~53% for control cells, and 20% for HeLa-MIM-GFP cells (**Figure 3.5 F**). However, by one hour, CXCR4 levels recovered to ~80% in HeLa-IRTKS-GFP cells, while remaining around 50% for control cells, and falling to almost zero for HeLa-MIM-GFP cells (**Figure 3.5 G**). This indicates that IRTKS is not involved the CXCR4 degradation process.

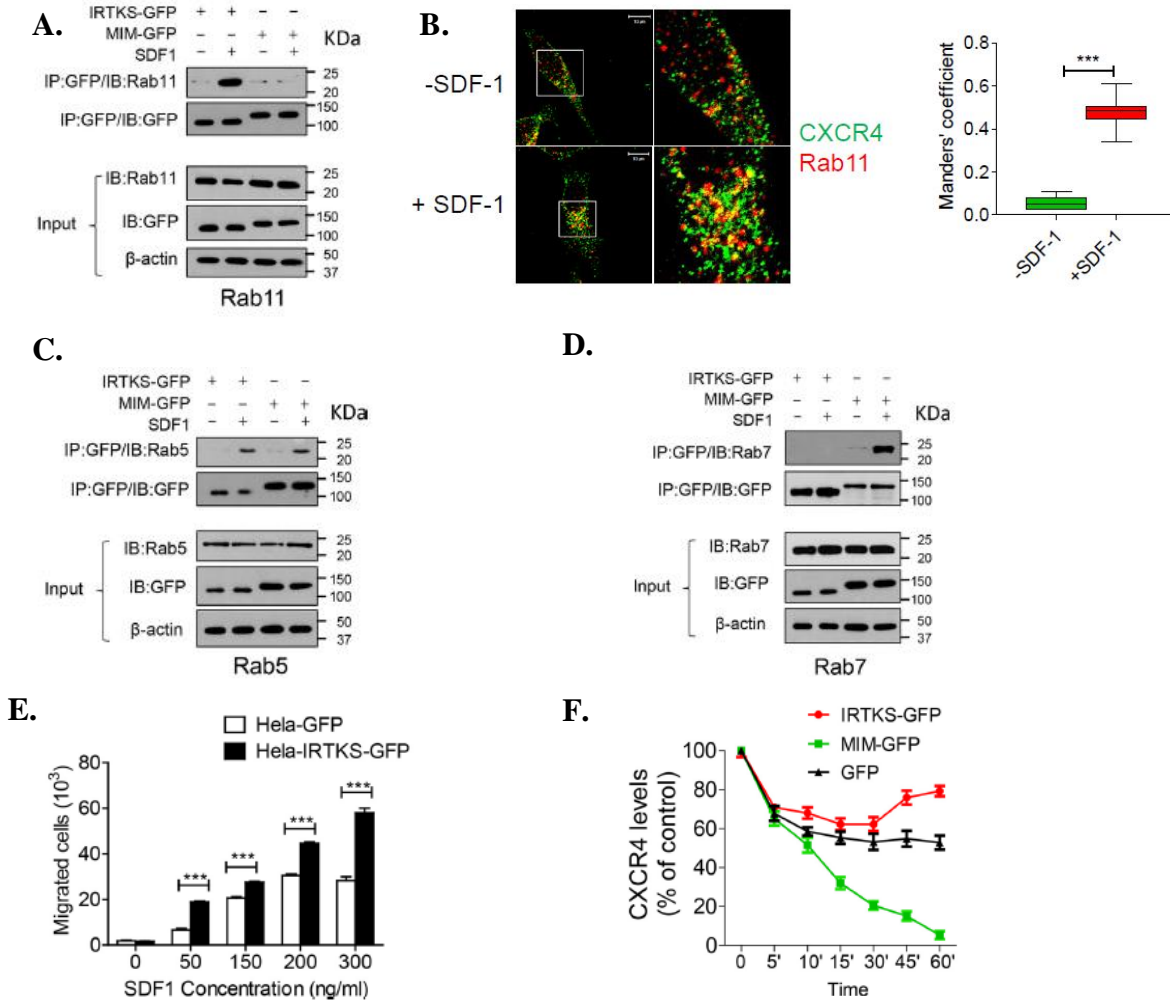


Figure 3.5 MIM and IRTKS are targeted by different Rabs. **A.** HeLa cells expressing MIM-GFP or IRTKS-GFP were treated with 150 ng/mL SDF-1 for 30 min and interaction of MIM or IRTKS with Rab11 were analyzed by co-IP. **B.** HeLa-IRTKS-GFP cells were treated with 500 ng/mL SDF-1 for 30 min, followed by co-staining with anti-CXCR4 (green) and anti-Rab11 (red). The stained cells were inspected by confocal microscopy. Quantification of co-localization of CXCR4 and Rab11 was performed based on Mander's coefficient. **C-D.** HeLa cells expressing MIM-GFP or IRTKS-GFP were treated with 150 ng/mL SDF-1 for 5 min (**C**) or 30 min (**D**). Interactions between MIM or IRTKS with Rab5 (**C**) and Rab7 (**D**) were analyzed by co-IP. **E.** HeLa cells expressing GFP or IRTKS-GFP were plated in upper chambers Transwell plates, and chemotaxis was assessed by quantifying the number of cells that migrated to the lower chambers in response to different concentrations of SDF-1. **F.** HeLa cells expressing GFP, MIM-GFP, or IRTKS-GFP, were incubated with 500 μ g/mL cycloheximide for 30 min prior to treatment with 150 ng/mL SDF-1 for the indicated times. The levels of CXCR4 on the surface of treated cells were estimated by flow cytometry. All data represent mean \pm S.E.M. ($n=3$). ***, $p<0.001$, except (**B**), ($n=10$).

3.3.6 The SH3 domain determines the interaction with Rab11

A major structural difference between MIM and IRTKS is that IRTKS contains a SH3 domain. To determine if the SH3 domain plays a role in the interaction of these I-BAR proteins and Rab GTPases, various mutants of MIM and IRTKS were created (**Figure 3.6 A**). The mutant of IRTKS in which the SH3 domain was deleted (IRTKS Δ SH3) still interacted with Rab5 after five minutes of SDF-1 exposure, but it failed to bind to Rab11 at 30 minutes of SDF-1 exposure (**Figure 3.6 B**). Instead, unlike full length IRTKS, and similar to MIM, it interacted with Rab7 (**Figure 3.6 B**). Also, the IRTKS Δ SH3 mutants were able to internalize CXCR4 with approximately the same efficiency as MIM-GFP-overexpressing cells, while IRTKS-GFP-overexpressing cells were significantly less efficient at internalizing CXCR4 (**Figure 3.6 C**).

The sequence responsible for the MIM–Rab7 interaction is located in the I-BAR domain of MIM [105]. To interrogate the role of the I-BAR domain in determining Rab7 versus Rab11 binding, two chimeric mutants were created in which the MIM I-BAR domain replaced the I-BAR domain in IRTKS (MIM-IBAR-IRTKS), and vice versa (IRTKS-IBAR-MIM) (**Figure 3.6 A**). **Figure 3.6 D** shows that the IRTKS-IBAR-MIM mutant interacted with Rab7 but not Rab11, while the MIM-IBAR-IRTKS mutant bound Rab11, but not Rab7. Overall, this data indicates that the SH3 domain mediates the IRTKS–Rab11 interaction and the function of IRTKS in CXCR4 intracellular trafficking.

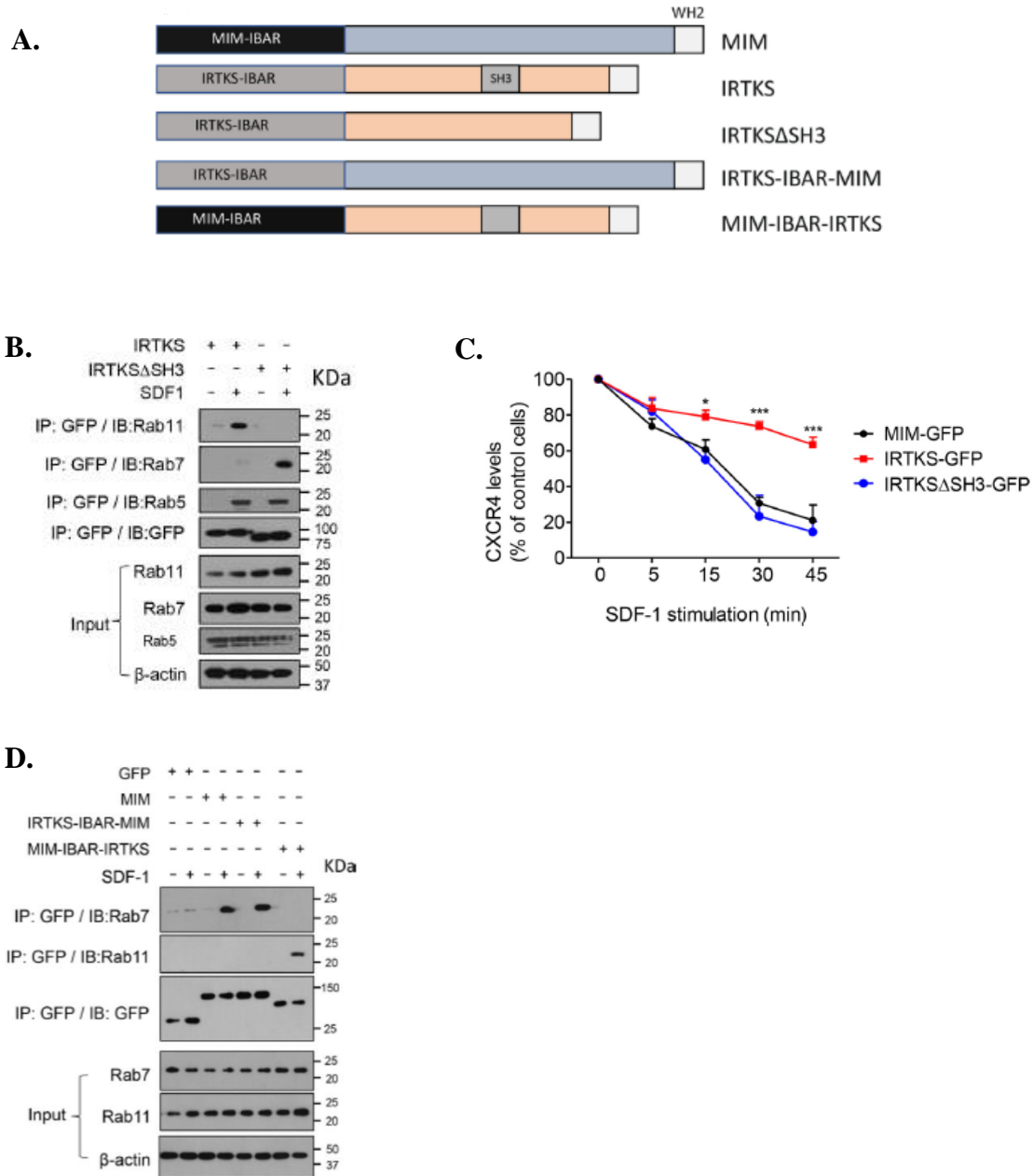


Figure 3.6 The SH3 domain determines recruitment of IRTKS to Rab11. **A.** Schematic of MIM, IRTKS, and their fusion mutants. *WH2*, WASP homology 2. **B.** HeLa cells expressing IRTKS-GFP or IRTKS Δ SH3-GFP were stimulated with 150 ng/ml SDF-1 for 30 min. The cell lysates were subjected to immunoprecipitation (IP) with GFP antibody, followed by immunoblot (IB) using anti-RAB11, RAB5, or RAB7, as indicated. **C.** Cells expressing MIM-GFP, IRTKS-GFP, and IRTKS Δ SH3-GFP were treated with 500 ng/ml SDF-1 for up to 45 min. The levels of surface CXCR4 were estimated by flow cytometry. The data represent mean \pm S.E.M. ($n=3$). *, $p < 0.05$; ***, $p < 0.001$; referring to the differences between cells expressing IRTKS-GFP and those expressing IRTKS Δ SH3-GFP. **D.** Cells expressing MIM-GFP, IRTKS-GFP or their fusions were treated with 150 ng/ml SDF-1 for 30 min. The interactions of MIM and its fusions with RAB7 and RAB11 were analyzed by co-IP.

3.4 Discussion

As a protein that is aberrantly expressed in several cancer types, MIM has been the subject of a significant amount of research aimed at understanding its mechanism of action. Numerous biological functions have been attributed to MIM, including roles as a cytoskeletal scaffold and as a signaling molecule in growth factor, chemokine and hedgehog signaling pathways [68]. However, exactly how MIM functions in these pathways is yet to be fully defined. In this study, we further investigated the mechanism through which MIM regulates the intracellular trafficking of chemokine receptor, CXCR4, to influence the chemotactic response of cells to the chemokine, SDF-1.

Previously, this lab found that bone marrow cells derived from MIM-KO mice showed a defect in internalizing CXCR4, establishing a link between MIM and CXCR4 endocytosis [101]. We also found that MIM facilitates the internalization and lysosomal degradation of CXCR4 by forming a complex with AIP4 and CXCR4 to promote ubiquitination of the receptor, and by interacting with small GTPases, Rab5 and Rab7 to promote sorting into the lysosomal degradation pathway [105]. GPCRs such as CXCR4 are primarily internalized via clathrin mediated endocytosis, which involves the recruitment of receptors into clathrin coated pits [140]. Clathrin polymerization leads to progressive invagination of each pit until it is released into the cytoplasm as an endocytic vesicle or early endosome. Early endosomes essentially act as sorting stations where the fate of the receptor is decided [141]. The receptor can be guided to lysosomal degradation, recycling to the plasma membrane, or retro-transportation to the Golgi. Rab GTPases play a significant role in determining the sorting fate of the receptor, with different Rabs having specific responsibilities. For example, sorting to lysosomes is

primarily dependent on Rab7 activity, while sorting to recycling routes is dependent on Rab4, Rab8, and Rab11 [141].

MIM seems to play a role in the sorting of CXCR4 into the lysosomal degradation pathway. During endocytic trafficking, Rab5 is generally associated with early endosomes, where it regulates early events, such as cargo selection for the forming vesicles and early endosome fusion and motility [142]. Rab7, on the other hand, is localized mainly to late endosomes and is responsible for maturation of early endosomes into late endosomes, as well as transport from late endosomes to lysosomes [142]. We previously observed that MIM interacted with Rab5 and co-localized with EEA1 (an early endosome marker) and CXCR4 shortly after SDF-1 treatment, suggesting that MIM is bound to CXCR4 as it is sorted into early endosomes [105]. Several minutes after SDF-1 exposure, MIM remained associated with CXCR4 as well as AIP4, but was bound to Rab7 instead of Rab5, and co-localized with late endosome marker CD63 [105]. In this study, Rab7 was shown to be necessary for MIM-mediated CXCR4 internalization and lysosomal degradation, as well as for sorting of CXCR4 and MIM to late endosomes. No interaction was observed between MIM and Rab11, the primary Rab GTPase associated with receptor recycling.

I-BAR domain proteins bind through a convex or inversely curved surface, thus sensing and generating negatively curved membranes. This feature of I-BAR proteins raises the possibility that MIM and other I-BAR domain proteins may participate in the membrane remodeling that is necessary for the formation and maturation of endosomes. Interestingly, we found that another I-BAR domain protein, IRTKS, interacted with Rab5 at five minutes and Rab11 at 30 minutes after exposure SDF-1 exposure. The association

of IRTKS with Rab5 in the early response to SDF-1 stimulation indicates that IRTKS may also be involved in early endosome formation.

We found that IRTKS showed no affinity for Rab7, and IRTKS-overexpressing cells showed a faster recovery of CXCR4 cell surface expression following SDF-1-induced internalization. IRTKS contains a SH3 domain that is not present in MIM, and this seem to be the determinant of whether Rab7 or Rab11 is engaged by the respective I-BAR domain protein, since deletion of the SH3 domain abolished the ability of IRTKS to bind Rab11, but rendered it capable of binding Rab7. These findings point to IRTKS being involved in the recycling pathway, but further experimentation is needed to verify if this is the case, and to determine how the SH3 domain recruits Rab11 to IRTKS. Taken together, the data supports a model for CXCR4 endocytosis where MIM mediates trafficking of the receptor from internalization to lysosomal degradation, while IRTKS likely mediates recycling of the receptor to the plasma membrane (**Figure 3.7**).

MIM could promote lysosomal degradation in receptor-mediated endocytosis of other receptors, particularly other GPCRs. In a previous study [78], it was observed that B cells isolated from MIM-KO mice failed to internalize CXCR5 after exposure to its ligand, C-X-C motif chemokine ligand 13 (CXCL13). The CXCR5 endocytic pathway is not as extensively studied as CXCR4, but as GPCRs, the two receptors likely share many similarities in their pathways, particularly in the activity of Rab GTPases. Abnormal expression of epidermal growth factor receptor (EGFR) is also linked to MIM dysregulation [20], [29], and while EGFR is not a GPCR, AIP4 ubiquitinates and targets EGFR for lysosomal degradation [142]. MIM binds directly to AIP4 via its WW domain, but its interaction CXCR4 seems to be indirect [105]. This indicates that specificity lies

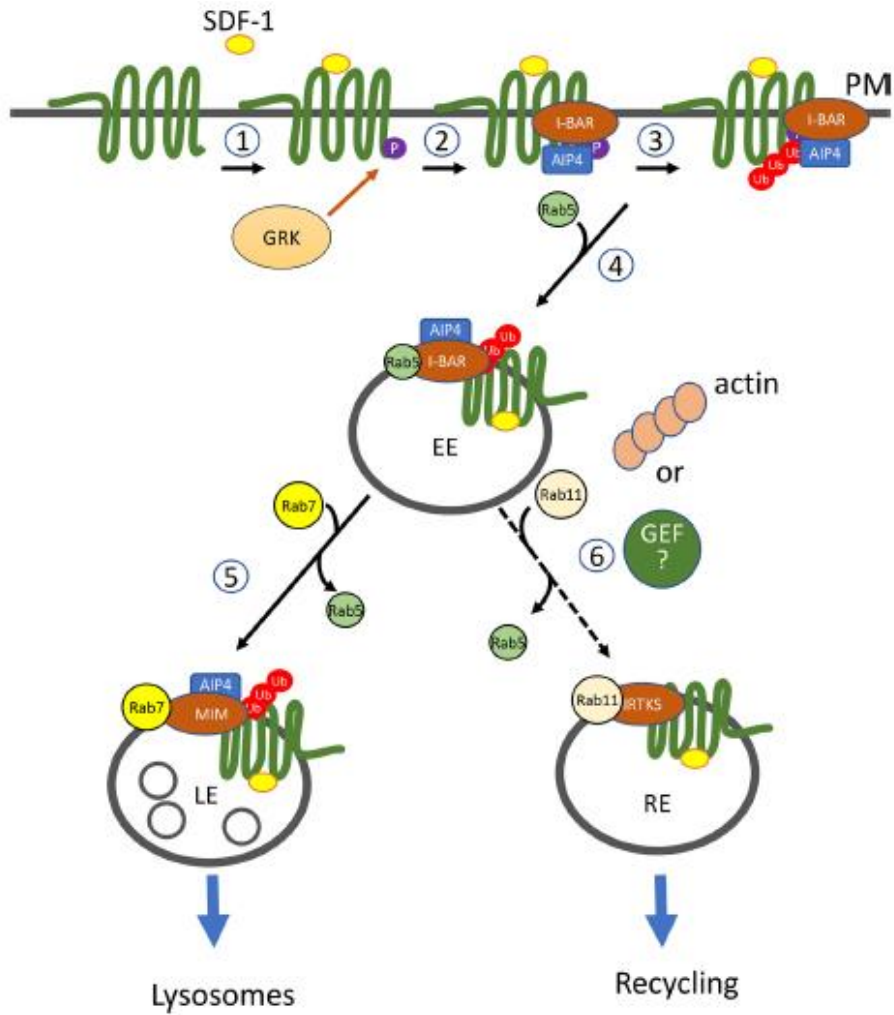


Figure 3.7 A model depicting the function of I-BAR domain proteins in the regulation of CXCR4. CXCR4 is a G protein–coupled receptor with seven transmembrane domains. Upon SDF-1 stimulation, CXCR4 is phosphorylated at its C terminus by a G protein–coupled receptor kinase (*GRK*) (1). The phosphorylated CXCR4 allows its association with the E3 ubiquitin ligase AIP4, which is promoted by the I-BAR domain protein MIM or IRTKS. This results in formation of a complex of the CXCR4, AIP4, and I-BAR proteins (2) and a subsequent increase in ubiquitination of the receptor (3). Because of the ability to bind to RAB5 and RAB7, MIM facilitates sorting of the ubiquitinated receptor complex from early endosomes (*EE*) to late endosomes (*LE*) (5). On the other hand, IRTKS facilitates sorting of the receptor complex into a type of RAB11-coated endocytic vesicles, such as recycling vesicles (*RE*) (6). This step may be facilitated by actin assembly or an unidentified GEF of RAB11.

with the E3 ubiquitin ligase, and not with receptor. This means that MIM could possibly function in the endocytosis of any receptor whose expression is regulated by ubiquitination via a WW domain-containing E3 ubiquitin ligase. AIP4 is a member of the neural precursor cell expressed developmentally downregulated protein 4 (NEDD4) family of E3 HECT ubiquitin ligases which consists of nine members in humans [143]. In a recent paper, MIM was shown to suppress transforming growth factor beta 1 (TGF- β 1)-induced epithelial-mesenchymal transition (EMT) in gastric cancer cells, but the mechanism of action was not described [38]. TGF- β 1 receptor signaling depends on the activity of SMURFs, which are also WW domain-containing E3 ubiquitin ligases from the NEDD4 family. Thus, MIM could potentially regulate TGF- β receptor signaling as well, via interactions with SMURFs.

A lack of specific binding to a particular receptor could explain the complexities of the role of MIM in cancer biology. If the activity of MIM is dependent on interactions with E3 ubiquitin ligases or with Rab7, then MIM could be involved in a plethora of signaling pathways. As such, MIM could seem to be an oncogene, tumor suppressor, or a metastasis suppressor, depending on the receptor function that is disrupted when MIM is deregulated. Exploring whether MIM regulates the signaling of other receptors by facilitating lysosomal degradation could lead to ways of utilizing MIM as a prognostic marker and provide alternative therapeutic approaches for treating MIM-linked cancers.

Chapter 4: Overexpression of MIM Suppresses Basal Autophagy

4.1 Introduction

Autophagy is a highly conserved catabolic process in which cellular content is digested in lysosomes to maintain homeostasis and normal cellular physiology. There are three main types of autophagy: macro-autophagy, micro-autophagy and chaperone-mediated autophagy (CMA), but the term autophagy is often used in reference to macro-autophagy. While both micro-autophagy and CMA involve direct uptake by the lysosome, macro-autophagy involves the engulfment of cellular contents into double-membraned vesicles called autophagosomes, which eventually fuse with lysosomes, resulting in degradation and the recycling of macromolecules [144]. Although autophagy is commonly induced by stresses such as starvation, hypoxia and pathogen infection, constitutive (basal) autophagy also occurs at a low rate as part of the cellular housekeeping mechanisms. Basal autophagy assists in maintaining the health of the cell through activities such as clearance of misfolded proteins, damaged organelles and toxic metabolites from the cell, and contributes to the maintenance of key physiological processes, including development, programmed cell death, metabolism and aging [145]. Deregulation of autophagy has been implicated in a number of human diseases, including cancer and neurodegenerative disorders.

Autophagy has been linked to various aspects of tumorigenesis, including proliferation, invasion, metastasis, and drug resistance [104]. Its role in cancer cells is strongly context-dependent. It can either promote tumorigenesis or act as a tumor suppressor, depending on factors such as those associated with the tumor

microenvironment [104]. For example, autophagy is usually considered to be a survival-promoting pathway, as it helps to maintain the health of the cell by preserving organelle function, removing toxic cellular waste products and providing substrates to support metabolism during starvation. The removal of harmful materials by autophagy protects the cell from genomic instability, and the loss of autophagy has been associated with increased risk of cancer, which indicates a tumor suppressive role for autophagy [104]. However, cancer cells can also take advantage of the pro-survival activity of autophagy to withstand microenvironmental stresses, allowing them to thrive under suboptimal conditions, and providing them with fuel to meet their massive nutrient and energy demands [104]. Autophagy also demonstrates a paradoxical role in response to cancer therapy, where it can cause either resistance or increased sensitivity to chemotherapy and radiation treatment [146]. Autophagy in cancer has significant therapeutic implications, and it remains a challenge in cancer therapy.

Autophagy and endocytosis are both intracellular membrane trafficking pathways, and as such, they share some of the same trafficking machinery and associated proteins [147]. Notably, small GTPase activity and post-translation modifications are regulatory mechanisms utilized by both processes. Ubiquitination, in particular, plays a major role in autophagy regulation with a number of different E3 ubiquitin ligases recently identified as being involved in autophagy [148]. Our lab has recently established that the MIM protein regulates CXCR4 endocytosis through an interaction with Rab7 and AIP4 E3 ubiquitin ligase [105]. Given this finding, we speculated that MIM may play a similar role in autophagy. Indeed, several yeast studies have linked Ivy1 (yeast ortholog of MIM) to autophagy, as it interacts with autophagy-related proteins, including ypt7 (Rab7) [149],

Gtr1/Gtr2/ Ego complex (Rag GTPases /Ragulator) [150], vacuolar protein sorting (Vps) proteins [150], and Fab1 (PIKfyve) [151], and seem to regulate TORC1 (target of rapamycin complex 1) activity and vacuole membrane homeostasis. However, there is little evidence for a role of MIM in mammalian autophagy.

In this study, we sought to establish the role of MIM in mammalian autophagy. We found that MIM overexpression increased the levels of autophagy markers LC3-II and p62 in mammalian cells under normal conditions indicating an effect of MIM on basal autophagy. Immunofluorescence assays showed that the increase in LC3-II was due to an accumulation of autophagosomes. This most likely resulted from an impairment of autophagosome maturation or lysosomal fusion, which prevented autophagic degradation. When a stressor such starvation was introduced, autophagy was induced in both control and MIM-overexpressing cells. However, the response was different in each group, as autophagy occurred at a slower rate in the MIM-overexpressing cells than in control cells. Overall, the results indicate that high MIM expression inhibits basal autophagy and alters cellular response to autophagy inducers.

4.2 Materials and Methods

Cell Culture and Drug Treatment

HeLa and RAW 264.7 cells were cultured in DMEM (Corning; Corning, NY) supplemented with 10% FBS (Hyclone; Logan, UT), 100 unit/mL penicillin / 100 µg/mL streptomycin (pen/strep) (Life Technologies, Grand Island, NY; Cat. No. 15140-122), and 50 mM HEPES (GIBCO, Life Technologies; Cat. No. 15630-080) at 37°C and 5%

CO₂. The following drugs obtained from Sigma-Aldrich (St. Louis, MO) were used to induce or inhibit autophagy: Rapamycin (Cat. No. R0395), Bafilomycin A1 (Cat. No. B1793) and N-Acetyl-D-sphingosine (C2- Ceramide; Cat. No. A7191). Starvation medium was EBSS (Hyclone; Cat. No. SH30029.02) supplemented with 50 mM HEPES.

Antibodies and Western Blotting

Western blot analysis was performed as described in **Chapter 2.2**. Briefly, cells were solubilized in RIPA buffer supplemented with protease inhibitors, and the protein concentration was determined by BCA Assay. Protein samples were loaded on 10% or 15% gels and transferred onto PVDF membranes. The following primary antibodies were used for protein detection: rabbit polyclonal anti-MIM (Invitrogen; Cat. No. PA517047), mouse monoclonal anti- microtubule-associated protein 1 light chain 3B (LC3B) (CST, Danvers, MA; Cat. No. 83506S), mouse monoclonal anti- sequestosome-1/ubiquitin-binding protein p62 (SQTM1/p62) (CST; Cat. No. 88588S), rabbit polyclonal anti-p62 (BioLegend, San Diego, CA; Cat. No. 647702), rabbit polyclonal anti-LC3 (SIGMA; Cat. No. L8918), or mouse monoclonal anti- β -actin (SIGMA; Cat. No. A5441). The proteins probed were visualized using X-autoradiography, and densitometry analysis was performed on gel images from three independent experiments using ImageJ software.

Plasmids and siRNA transfection

MAP1LC3B with N-terminal RFP tag (RFP-LC3) transfection-grade plasmid for autophagosome marking (Cat. No. RC100053) and Mtss1 Mouse siRNA Oligo Duplex (Cat. No. SR419894) were purchased from OriGene Technologies (Rockville, MD). Tandem RFP-GFP-LC3 plasmid was a gift from Anne Hamacher-Brady at Johns Hopkins University, Baltimore, MD. Transfections were performed using Lipofectamine

2000 Transfection Reagent (Cat. No. 11668027) or Lipofectamine RNAiMAX Transfection Reagent (Cat. No. 13778075) from Invitrogen (Thermo Fisher Scientific, Waltham, MA) according to manufacturer's protocol.

Immunofluorescence microscopy

Cells in 2 mL DMEM supplemented with 10% FBS and 1% pen/strep were added to each well of a 6-well plate and cultured overnight at 37°C, 5% CO₂. For RFP-GFP-LC3 analysis, sterilized fibronectin-coated glass coverslips were placed into wells prior to adding cells. For transient RFP-LC3 or RFP-GFP-LC3 expression, cells were transfected with plasmids using Lipofectamine 2000 Transfection Reagent according to the manufacturer's instructions. After 16 hours, transfection media was replaced by fresh DMEM supplemented with FBS and cells were further incubated for 24 hours. To create slides, coverslips were washed twice with PBS and cells were fixed by adding 4% paraformaldehyde at room temperature for 10 minutes. Cells were stained with DAPI for 5 minutes before coverslips were mounted onto glass slides with 20 µL of Mounting Medium (Kirkegaard & Perry Laboratories, MD), and the slides were sealed with nail polish. Cells were viewed under a fluorescent microscope at 40× magnification, and images of cells within nine microscopic fields were taken.

Quantitative RT-PCR

Total RNA was isolated using RNAeasy kit (QIAGEN, Hilden, Germany), and the RNA (100 ng) was reverse transcribed into cDNA using the High Capacity cDNA Reverse Transcription Kit from Applied Biosystems (Thermo Fisher Scientific, Waltham, MA; Cat. No. 4368814) following the respective manufacturers' guidelines. Quantitative PCR for gene expression of mouse *Mim* and *Gapdh* was performed using the synthesized

cDNA as the template and Power SYBR® Green PCR Master Mix from Applied Biosystems (Life Technologies, Carlsbad, CA; Cat. No. 4367659). Reactions were carried out on an ABI 7900HT Real-Time PCR System (Applied Biosystems, Foster City, CA). The following primer pairs were used: mouse *Mtss1* forward 5'-GCG TCT TGG ATT GGG ACT TG-3'; *Mtss1* reverse 5'-TCC TTC TCG ATC ACA GCC TC-3' and mouse *Gapdh* forward 5'-CCG CAT CTT CTT GTG CAG TG-3'; *Gapdh* reverse 5'-GAC TGT GCC GTT GAA TTT GC-3'. Relative mRNA expression was calculated as *Mim* expression normalized to *Gapdh* expression. Samples were run in triplicate.

Cytotoxicity Assay

The cytotoxic effect of C2-ceramide was analyzed using the CytoTox 96® Non-Radio Cytotoxicity Assay kit (Cat. No. G1781) from Promega (Madison, WI), following the manufacturer's instructions. Briefly, cells were treated with C2-ceramide for 24 hours, and 50 µL of the supernatant was transferred to a fresh 96-well plate. An equal volume of CytoTox 96® Reagent from kit was added to each well and incubated at room temperature for 30 minutes. Stop Solution (50 µL) provided in the kit was added to neutralize the reaction. The absorbance signal was measured at 490nm in a plate reader. Experiments were performed in triplicate, and the average absorbance was calculated.

4.3 Results

4.3.1 MIM overexpression induces LC3 accumulation

To determine whether MIM participates in mammalian autophagy, LC3 protein levels were assessed by Western blot analysis of cell lysates from stable cell lines of

HeLa cells expressing MIM-GFP (HeLa-MIM-GFP) or GFP only (HeLa-GFP). During the course of autophagosome formation and maturation, the cytosolic form of LC3 protein (LC3-I) is conjugated to a phosphatidylethanolamine form (LC3-II), which is incorporated in autophagosomal membranes, thus making LC3 protein a great marker for autophagy [152]. Results from immunoblotting of LC3 protein showed that MIM overexpression in HeLa significantly increased the levels of LC3-II (**Figure 4.1 A and 4.1 B**), suggesting a buildup of autophagosomal structures. Another method to assess autophagy is to monitor the conversion of LC3-I to LC3-II, where an increase in LC3-II to LC3-I ratio would indicate an increase in the formation of autophagosomes. LC3-II to LC3-I ratio was also significantly greater in MIM-overexpressing cells compared to control cells (**Figure 4.1 A and 4.1 C**). Live fluorescent microscopy of HeLa-GFP and HeLa-MIM-GFP cells transiently transfected with a RFP-LC3 plasmid also showed about a 3-fold increase of LC3-positive vesicles, which appear as bright cytoplasmic dots, in MIM-overexpressing cells (**Figure 4.1 D**). These results indicate a role of MIM in the autophagic pathway.

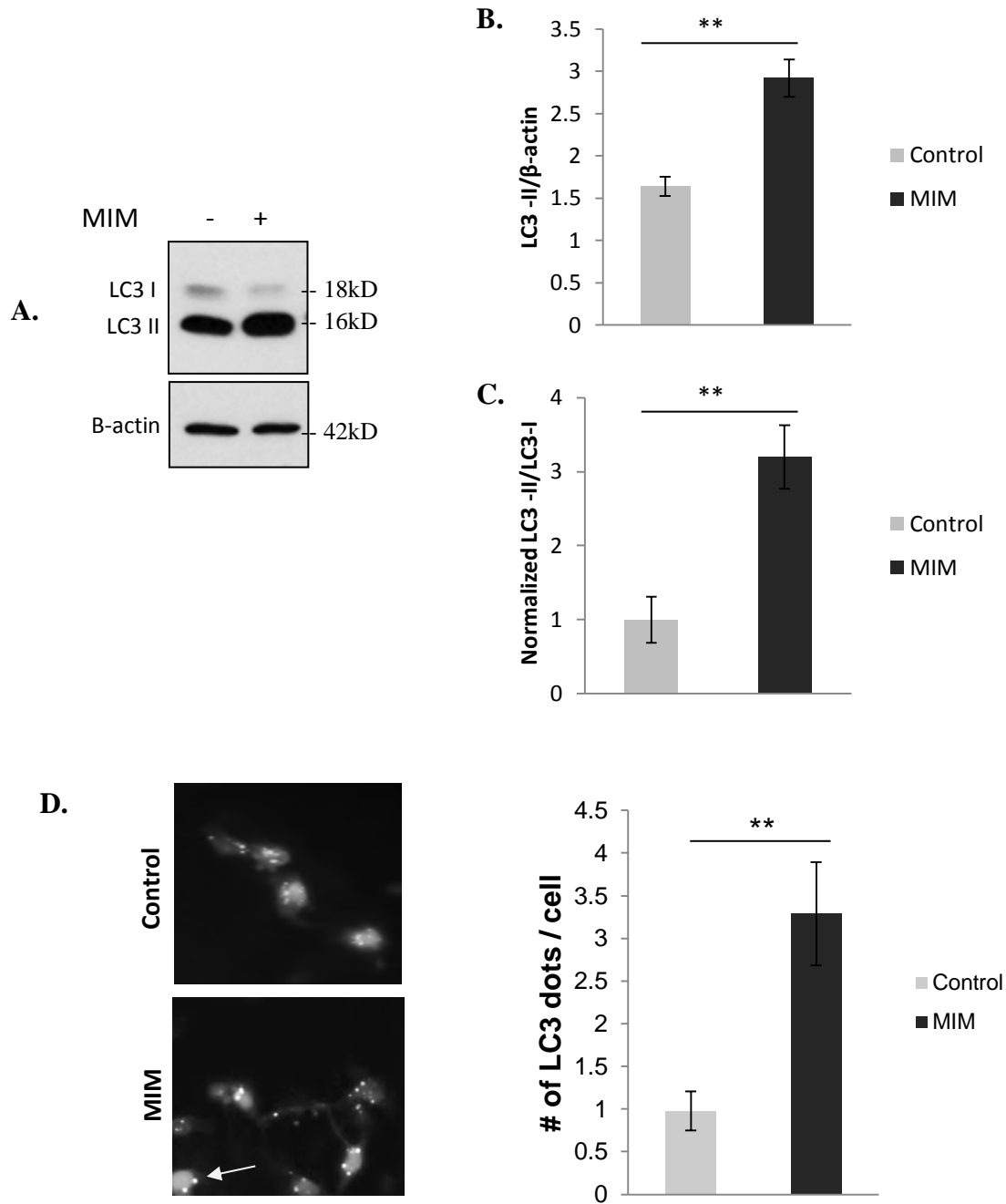


Figure 4.1 MIM overexpression induces LC3 accumulation. **A.** Western blot analysis of LC3 levels in HeLa cells stably transfected with GFP only (control) or MIM-GFP plasmid (MIM). **B.** Graph representing average intensity of LC3-II normalized by β -actin from 3 independent experiments. **C.** Graph representing average normalized LC3 ratio from 3 independent experiments. **D.** Stable MIM-overexpressing and control HeLa cells were transiently transfected with a RFP-LC3B plasmid and representative images taken under 40X objective. Quantification of number of LC3 dots per cell is shown. *Arrow* indicates representative of size and shape of dots counted; ~ 50 cells per group, mean \pm SD. ** $P \leq 0.005$ using Student's *t*-test.

4.3.2 MIM overexpression inhibits autophagic degradation

The LC3-positive dots observed in the cytoplasm of MIM-overexpressing cells (Figure 4.1 D) most likely represent autophagosomes or autolysosomes (autophagosomes fused with lysosomes), generation of which could be due to either increased autophagy activation or inhibition of autophagosome clearance. To determine whether MIM promotes autophagy activation or inhibits autophagic degradation, HeLa-GFP and HeLa-MIM-GFP cells were treated with bafilomycin A1 (BA1; a lysosomal inhibitor) for 4 hours and LC3-II levels were then assessed by Western blot. As shown in **Figure 4.2 A and 4.2 B**, BA1 treatment resulted in increased LC3-II accumulation in control HeLa cells, indicating basal autophagic activity in these cells, and MIM overexpression resulted in significantly higher LC3-II level even without BA1 treatment, a result that is consistent with that of Figure 4.1 B. However, there was no significant difference in LC3-II accumulation between vehicle-control treated and BA1 treated HeLa-MIM-GFP cells (**Figure 4.2 A and 4.2 B**), indicating an impairment in autophagic flux in MIM-overexpressing cells. BA1 treatment also resulted in an increase in LC3-II to LC3-I ratio in control HeLa cells, while there was no significant difference between vehicle-control and BA1 treated HeLa-MIM-GFP cells (**Figure 4.2 A and 4.2 C**). Average LC3 ratio in MIM-overexpressing cells was less than the ratio in control cells, which is inconsistent with results in Figure 4.1, but this is likely due to high variability among the independent replicates (**Figure 4.2 C**).

To further support the above observations, sequestosome-1 (SQSTM1 or p62) was also analyzed. P62 is often used as an alternative marker of autophagy as it binds directly to LC3 and is degraded in the lysosome along with LC3-II [153]. Western blot

analysis showed that p62 was significantly greater in HeLa-MIM-GFP cells when compared to HeLa-GFP control cells, and while BA1 treatment of HeLa-GFP cells resulted in increased p62 accumulation, there was no significant difference between vehicle-treated and BA1-treated HeLa-MIM-GFP cells (**Figure 4.2 A & 4.2 D**). These findings concur with the LC3 results.

To address whether the effect of MIM is cell type specific, MIM-overexpressing MDA-MB-231 cells were analyzed. As shown in **Figure 4.2 E – 4.2 H**, MIM overexpression resulted in elevated LC3-II and p62 levels as well as increased LC3 ratio and no significant change in the accumulation of both proteins or LC3 ratio in response to BA1 when compared to control cells. Taken together, the data suggest that the higher levels of LC3-II and p62 observed in MIM overexpressing cells are likely due to an inhibition of autophagosome clearance rather than increased autophagy activation.

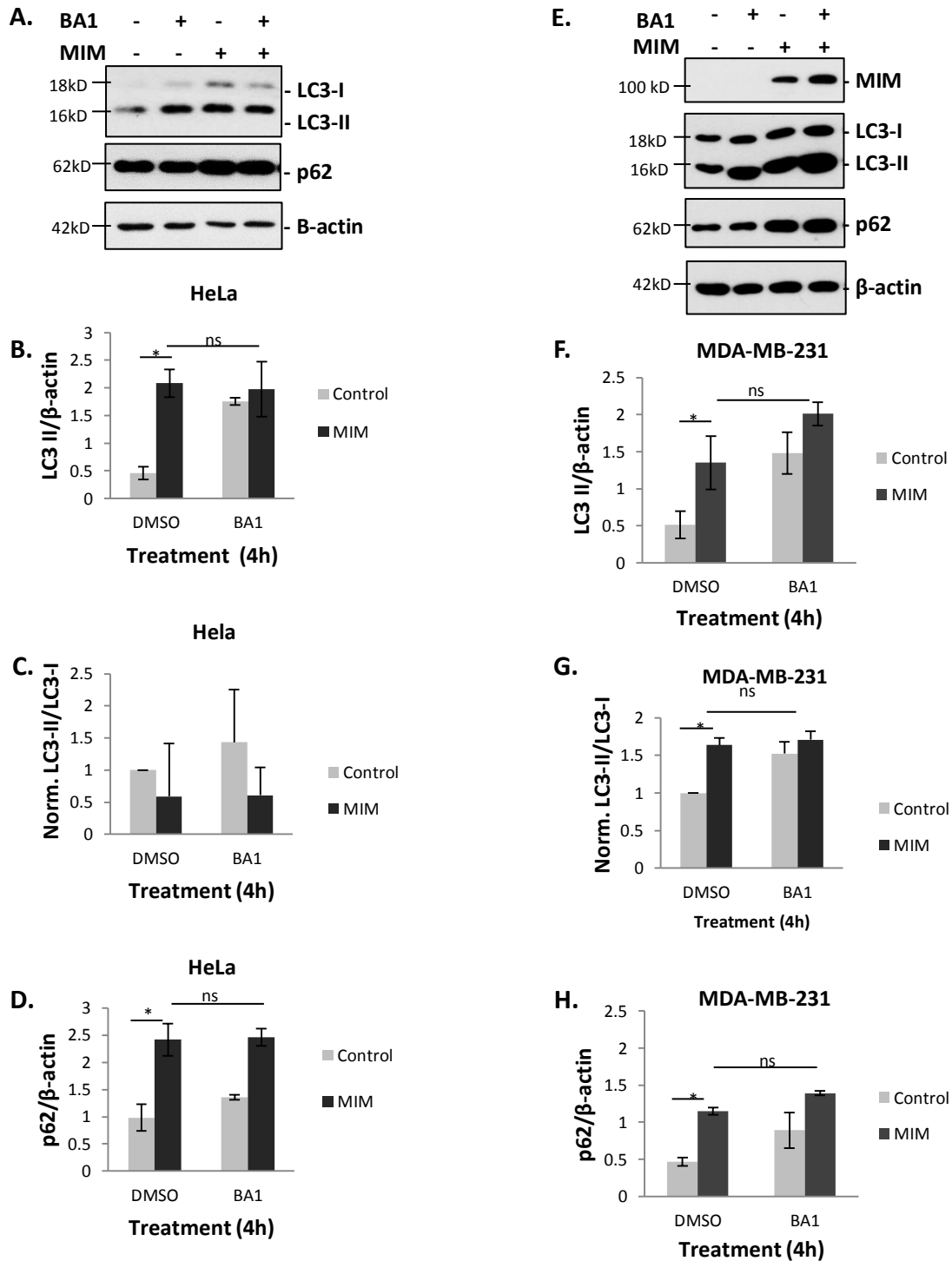


Figure 4.2 MIM overexpression inhibits autophagic degradation. Western blot analysis of endogenous LC3 and p62 expression in HeLa cells or MDA-MB-231 cells stably transfected with GFP only (control) or MIM-GFP plasmid (MIM), with or without BA1 treatment (400 nM). **A.** Representative Western blot of HeLa cell lysates. **B-D.** Quantification of LC3-II level (**B**), LC3-II to LC3-I ratio (normalized by DMSO-treated control) (**C**) and p62 level (**D**) in HeLa cells. **E.** Representative Western blot of MDA-MB-231 cell lysates. **F-H.** Quantification of LC3-II level (**F**), LC3-II to LC3-I ratio (**G**) and p62 level (**H**) in MDA-MB-231 cells. Graphs represent mean \pm SD, 3 independent experiments, * $P \leq 0.005$ using Student's *t*-test.

4.3.3 MIM overexpression induces accumulation of autophagosomes

To determine whether the LC3 positive structures observed in HeLa-MIM-GFP cells are autophagosomes or autolysosomes, control and MIM-overexpressing cells were transfected with a tandem RFP-GFP-LC3 plasmid, and LC3 punctate dots were inspected and quantified by fluorescent microscopy. As GFP, but not RFP fluorescence, is susceptible to the acidic pH environment in lysosomes, RFP-positive/GFP-positive puncta would represent autophagosomes, whereas RFP-positive/GFP-negative puncta would represent autolysosomes [152]. **Figure 4.3 A & 4.3 B** showed that the majority of the LC3 positive puncta in MIM-overexpressing cells were positive for both RFP and GFP, indicating that they are autophagosomes. Thus, MIM-overexpression inhibits the maturation of autophagosomes into autolysosomes in mammalian cells, which is consistent with the biochemical result showing that MIM inhibits degradation of LC3-II and p62 (4.3.2).

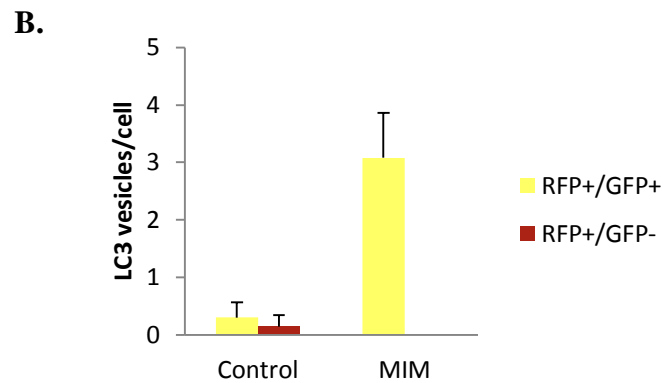
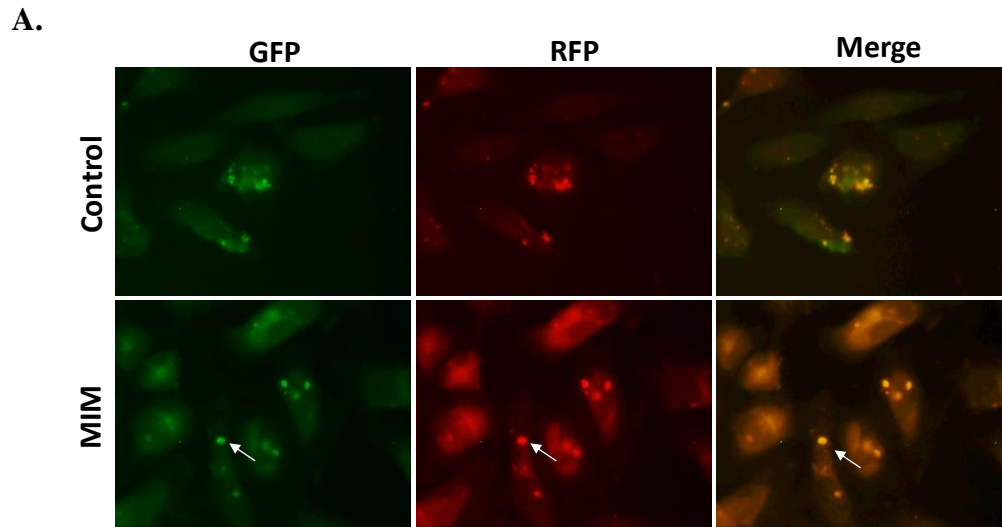


Figure 4.3 MIM overexpression prevents autophagosome maturation/ fusion. **A.** Stable MIM-overexpressing and control HeLa cells were transiently transfected with RFP-GFP-LC3 plasmid and visualized by fluorescent microscopy. Representative images were taken under 40X objective **B.** The numbers of red-positive and green-positive vesicles (RFP+/GFP+) and red-positive and green-negative vesicles (RFP+/GFP-) were quantified in ~ 50 cells per group. *Arrow* indicates representative of size and shape of dots counted. Graph represent mean \pm SD.

4.3.4 Overexpression of MIM alters autophagic response to starvation

The observed accumulation of autophagosomes in HeLa-MIM-GFP cells occurred under nutrient-rich conditions, suggesting that MIM-overexpression inhibited basal autophagy. To investigate the effect of MIM overexpression on starvation-induced autophagy, LC3 protein levels were assessed by immunoblotting after nutrient starvation for different time periods. Starvation induced autophagy in HeLa-GFP cells as indicated by an initial accumulation of LC3-II at 30 minutes and 1 hour, followed by a decrease at 2 hours (**Figure 4.4 A & 4.4 B**). The initial increase in LC3-II represents the formation and maturation of autophagosomes, while the decrease at 2 hours indicates lysosomal degradation. In contrast to control cells, HeLa-MIM-GFP cells showed an increase in LC3-II level even prior to starvation and were able to maintain this level until 2 hours when a significant decrease was observed (**Figure 4.4 A & 4.4 B**). Quantification of LC3-II/ LC3-I in HeLa-GFP cells showed that starvation induced a significant 2-fold and 2.5 fold increase in LC3 ratio at 30 minutes and 1 hour respectively, followed by a decrease at 2 hours (**Figure 4.4 A & 4.4 C**). In HeLa-MIM-GFP cells, starvation also induced higher LC3 ratio at 30 minutes and 1 hour, although this increase was not significant. However, the LC3 ratio further increased to about 5-fold at 2 hours (**Figure 4.4 A & 4.4 C**).

To further evaluate the impact of MIM on starvation-induced autophagy, changes in LC3-II levels were assessed by Western blot following starvation for 4 hours in the presence or absence of BA1. As expected, BA1 treatment caused an increase in LC3-II in non-starved control cells, but did not increase LC3-II in non-starved MIM-overexpressing cells (**Figure 4.4 D & 4.4 E**), a result that is consistent that of Figure 4.2.

However, starvation caused a reduction in LC3-II in both HeLa-GFP and HeLa-MIM-GFP cells, indicating that autophagic degradation occurred even with MIM overexpression (**Figure 4.4 D & 4.4 E**). This was confirmed as BA1 treatment of starved cells resulted in increased accumulation of LC3-II in both control and MIM-overexpressing cells when compared to vehicle-treated starved cells, although the degree of increase was less in HeLa-MIM-GFP cells than in HeLa-GFP cells (**Figure 4.4 D & 4.4 E**). The LC3-II to LC3-I ratio also indicated that there was a less robust autophagic response to starvation in MIM-overexpressing, as LC3 ratio in control cells was 3.7-fold greater in BA1-treated starved cells than in non-starved cells, compared to a 2-fold difference in MIM overexpressing cells (**Figure 4.4 F**). Taken together, the results suggest that overexpression of MIM created a block that slowed down the normal autophagic response to starvation, but the cells were able to overcome the block after extended nutrient deprivation. However, it was noted that the exogenous MIM expression decreased over time with nutrient deprivation (**Figure 4.4 A**). This could account partially for the recovery of the MIM-mediated autophagy inhibition observed under nutrient-rich conditions or short periods of starvation.

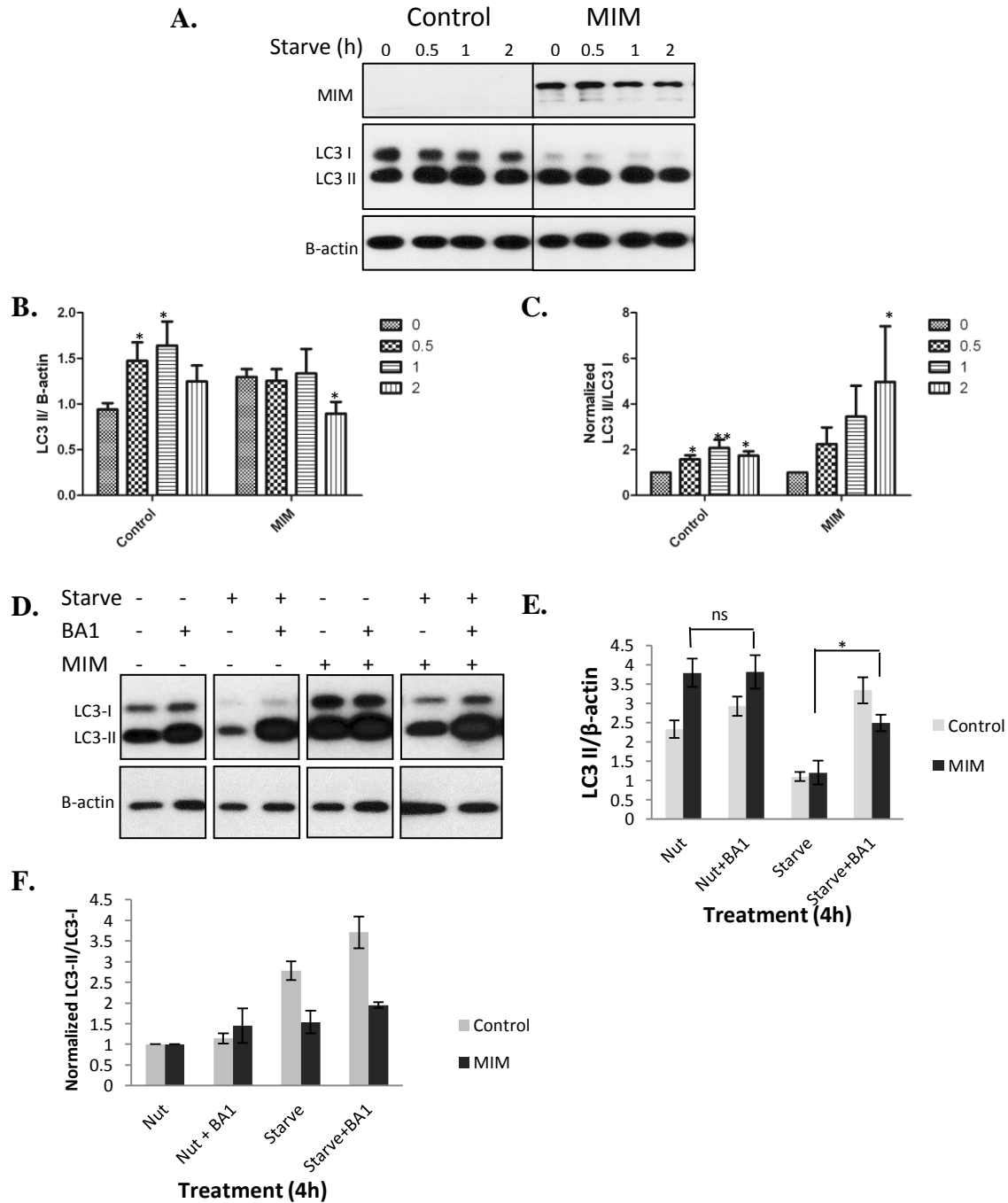


Figure 4.4 Starvation induces autophagy in MIM-overexpressing cells. **A.** Representative immunoblot showing LC3 levels in control and MIM-overexpressing HeLa cells following incubation in nutrient-free EBSS (starve) for different time periods (0.5h, 1h, 2h). Three independent experiments were performed. **B.** Graphical representation of (A) showing quantification of LC3-II intensity (relative to β -actin). **C.** Quantification of LC3-I: LC3-II ratio in (A) normalized by no starvation (0h). **D.** Western blot of LC3 levels in control and MIM-overexpressing cells cultured with or without nutrients for 4h in the presence or absence of BA1 (200 nM). **E.** Quantification of LC3-II relative to β -actin in (D). **F.** Quantification of LC3-II to LC3-I ratio in (D) normalized by control (Nut). Nut = nutrients. Graphs represent mean \pm SD, $n = 3$. * $P < 0.05$ using Student's t -test.

4.3.5 RNAi-mediated reduction of MIM in RAW 264.7 cells increases LC3-II degradation under normal conditions

To further investigate the effect of MIM on autophagic response, MIM expression was reduced by siRNA treatment in RAW 264.7 cells, a mouse macrophage-like cell line with high expression of MIM. RNA interference of *Mim* resulted in decreased LC3-II levels and LC3-II to LC3-I ratio under normal conditions (**Figure 4.5 C, 4.5 D & 4.5 E**). This decrease correlated with the levels of MIM downregulation achieved by two different RNAi oligomers (**Figure 4.5 A & 4.5 B**). However, when cells were exposed to BA1, the level of LC3-II/ β -actin and LC3-II/LC3-I increased in siMIM-treated cells at a degree that was higher than that of cells treated with scrambled (SC) siRNA (**Figure 4.5 F, 4.5 G & 4.5 H**). This result indicates that the siMIM-induced decrease of LC3-II was likely due to increased autophagic flux and not reduced LC3-II production, a view that is consistent with that obtained with MIM overexpression.

Mammalian target of rapamycin (mTOR) signaling inhibits autophagy under nutrient-rich conditions, so inhibiting mTOR is an alternative method to nutrient starvation for inducing autophagy in cells. To assess the effect of MIM downregulation on mTOR regulated autophagy, siMIM-treated and SC-treated RAW 264.7 cells were exposed to rapamycin (an mTOR inhibitor) for 4 hours, in the presence or absence of BA1. Western blot analysis showed that there was no significant difference in LC3-II levels between SC-treated and siMIM-treated RAW 264.7 cells after exposure to rapamycin plus BA1 (**Figure 4.5 F & 4.5 G**), but LC3 conversion results indicated that the RAW cells became more sensitive to rapamycin after MIM depletion (**Figure 4.5 F & 4.5 H**). Exposure to rapamycin induced a 1.6-fold increase in LC3-II/LC3-I in BA1-

treated siMIM cells, but LC3-II/LC3-I did not change significantly in BA1-treated control cells after exposure to rapamycin (**Figure 4.5 F & 4.5 H**). It was also noted that rapamycin treatment, as well as starvation, decreased the protein expression of MIM in RAW 264.7 (**Figure 4.5 I**). Overall, these findings complement the results from MIM overexpression in HeLa cells.

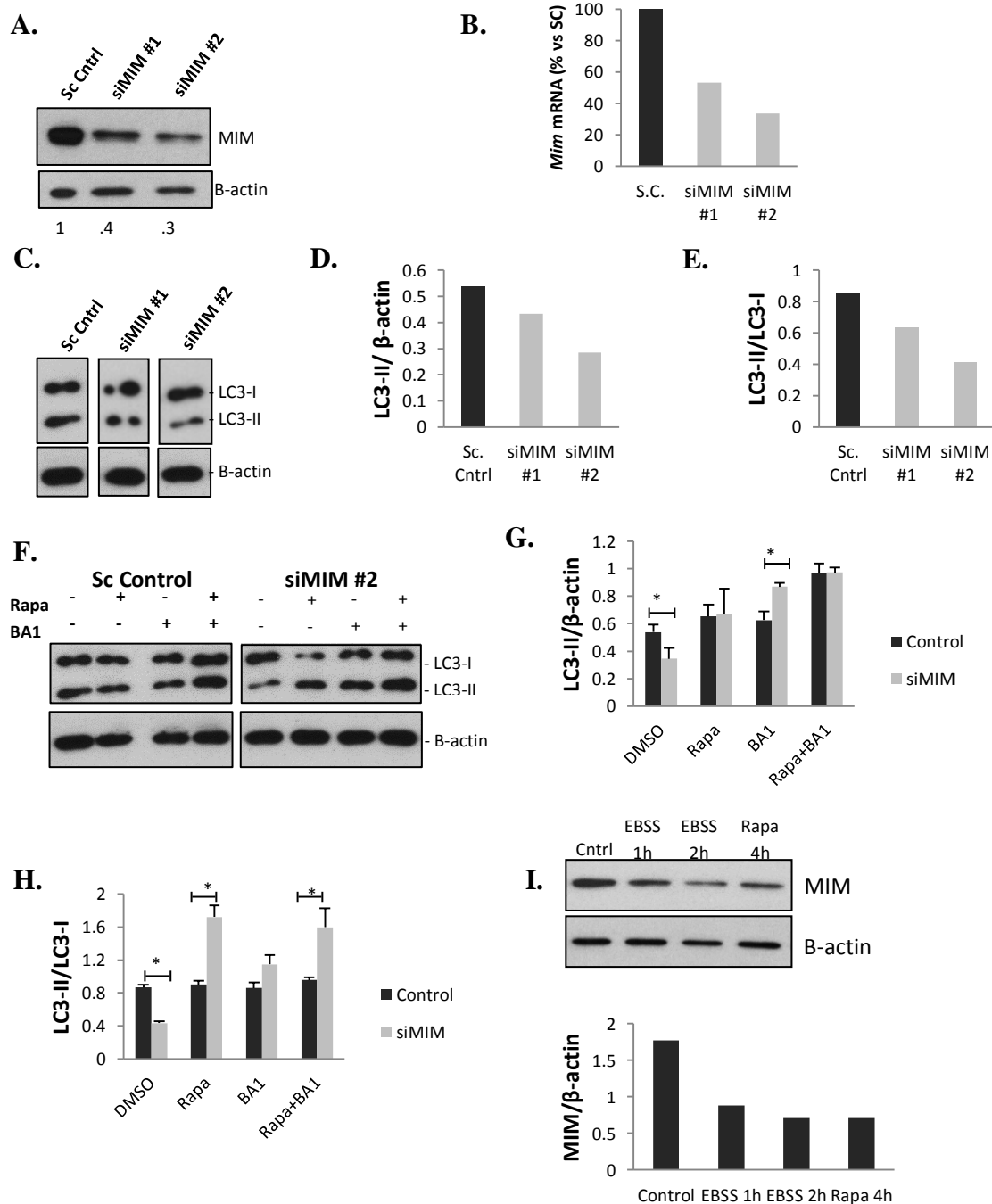


Figure 4.5 siMIM-treated RAW 264.7 cells show increased LC3-II degradation. **A.** Western blot showing MIM protein expression in RAW 264.7 cells transfected with siRNA oligomers targeting MIM or a scrambled sequence (Sc cntrl/S.C.). **B.** *Mim* mRNA levels normalized by *Gapdh* in S.C.-treated or siMIM-treated RAW 264.7 cells. **C.** LC3 protein levels in cell lysates from (A). **D.** Quantification of LC3-II level in (C) normalized by β -actin. **E.** Quantification of LC3 ratio in (C). **F-H.** Western blot of LC3 levels in S.C. and siMIM-treated RAW 264.7 cells following exposure to 200 nM rapamycin (Rapa) for 4 hours in the presence or absence of BA1 (200 nM). Graphs represent averages of LC3-II normalized by β -actin (**G**) and LC3 ratio (**H**) from 3 independent experiments. DMSO: vehicle-control. Error bar: SD, *, $P \leq 0.05$ using Student's *t*-test. **I.** MIM protein levels in RAW 264.7 cells after starvation (EBSS) or treatment with rapamycin (200 nM).

4.3.6 Overexpression of MIM impedes C2-ceramide-induced autophagy and promotes ceramide-mediated cytotoxicity

Our results indicate that MIM overexpression inhibited basal autophagy, but interpretation of the effect of MIM on induced autophagy was confounded by the finding that both starvation and rapamycin reduced the expression of MIM over time. To further investigate the role MIM may play in induced autophagy, HeLa-GFP and HeLa-MIM-GFP cells were treated with serial dilutions of the synthetic ceramide, n-acetylsphingosine (C2-ceramide) (**Figure 4.6**). C2-ceramide is known to induce autophagy under nutrient-rich conditions, and it does not reduce the expression of MIM (**Figure 4.6 A**). Western blot analysis of HeLa-GFP cell lysates showed a maximum of a ~2-fold increase over vehicle-control (DMSO) in both LC3-II levels and LC3-II to LC3-I ratio, while analysis of HeLa-MIM-GFP cell lysates showed very little difference in LC3 levels or ratio, even at high concentration of C2-ceramide (**Figure 4.6 A - 4.6 C**). P62 protein level was also analyzed, and the results showed that C2-ceramide treatment increased p62 by as much as 1.7 fold at low concentrations (6.25 μ M and 12.5 μ M), but reduced it at concentrations above 25 μ M in HeLa-GFP cells (**Figure 4.6 A & 4.6 D**). In contrast, C2-ceramide induced only a slight increase in p62 at low concentrations in HeLa-MIM-GFP cells, even though it also decreased p62 levels at high concentrations (**Figure 4.6 A & 4.6 D**). Although the precise reason for the reduction of p62 at high concentrations of C2-Ceramide in both MIM-overexpressing and control cells is currently unknown, the overall data agree with the view that MIM impedes autophagic flux in many aspects of autophagy.

Ceramides are bioactive sphingolipids that have garnered some interest as they may be used as chemotherapy agents due to their ability to induce cell death and cell cycle arrest [109]. However, ceramides can also induce autophagy, which potentially promotes cancer cell survival. Given that MIM overexpression inhibits C2-ceramide-induced autophagy, we performed a cytotoxicity assay to determine if MIM overexpression promoted C2-ceramide-induced cell death. HeLa-GFP and HeLa-MIM-GFP cells were treated with increasing concentrations of C2-ceramide ranging from 6.25 μM to 100 μM and the cytotoxicity was assessed by LDH release (**Figure 4.6 E**). The results showed very little change in the cytotoxicity for both HeLa-GFP and HeLa-MIM-GFP cells at 6.25 μM and 12.5 μM of C2-ceramide treatment (**Figure 4.6 E**). However, at 25 μM , the cytotoxicity was increased by 1.5-fold over the vehicle-control in HeLa-MIM-GFP cells, while remaining unchanged in HeLa-GFP cells. The degree of cytotoxicity remained greater in HeLa-MIM-GFP cells than in HeLa-GFP cells at high concentrations of C2-ceramide (50 μM and 100 μM). This data indicates that MIM overexpression enhances C2-ceramide-induced cytotoxicity, although the relationship between the increased cytotoxicity and MIM-mediated autophagy inhibition remains to be established.

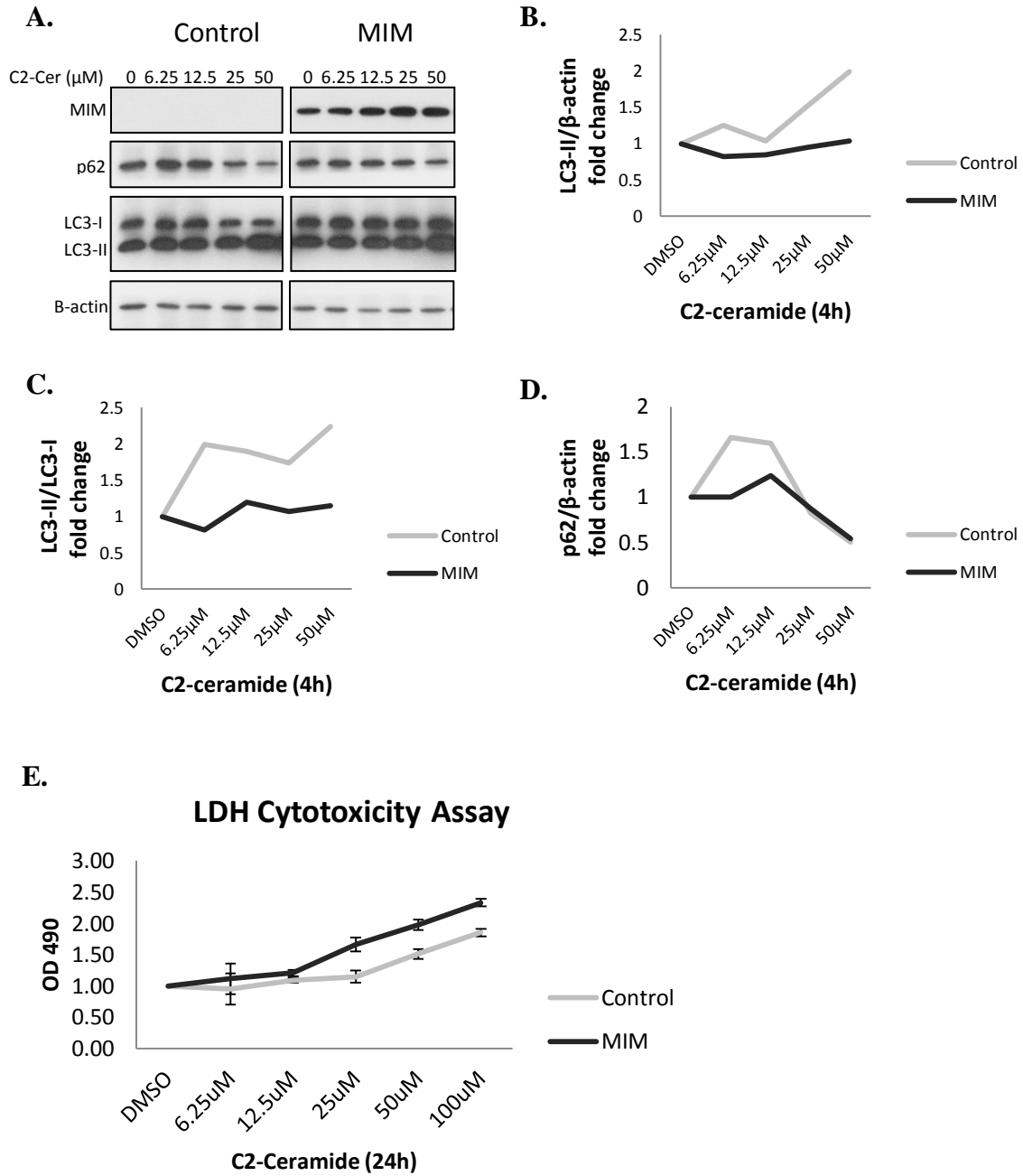


Figure 4.6 MIM overexpression inhibits autophagy activation and enhances cytotoxicity induced by C2-ceramide. Control and MIM-overexpressing HeLa cells treated with different concentrations of C2-ceramide for 4 or 24 hours. **A.** Immunoblot showing LC3 and p62 levels **B.** Graph showing mean LC3-II levels normalized by β -actin from 2 independent experiments. **C.** Graph showing LC3-II to LC3-I ratio. **D.** Graph showing p62 levels normalized by β -actin. **E.** CytoTox 96® Non-Radioactive Cytotoxicity Assay used to measure LDH release by cells after 24 h of treatment with C2-ceramide. Graph represents average of OD 490 values from three independent assays.

4.4 Discussion

Although autophagy was initially identified in mammals, the molecular machinery of autophagy was largely determined through genetic studies in yeast, as over 30 autophagy-related genes were identified in this model system [145]. Recent studies in yeast suggest that Iyyl1 is implicated in autophagy, but this is yet to be established in mammals. In this study, we found that overexpression of MIM induced the accumulation of autophagosomes by a mechanism that may involve inhibition of autophagosome maturation into autolysosomes, a finding that supports a role of MIM in autophagy regulation.

The process of autophagy starts with the formation of an isolation membrane called a phagophore, which expands to engulf cytoplasmic contents until it eventually forms a closed double-membraned vesicle called an autophagosome [144]. The autophagosome matures through the final stage of autophagy when it fuses with the lysosome to form an autolysosome, where autophagosomal contents are degraded. Models of autophagosome-lysosome fusion present two possible pathways: autophagosomes may fuse directly to lysosomes to form autolysosomes; or alternatively, autophagosomes may first fuse with late endosomes or MVBs to form hybrid structures called amphisomes, which then fuses with lysosomes to form autolysosomes [154]. Suppression of the maturation and fusion process results in a build-up of autophagosomes and inhibition of autophagic flux. Our results show that overexpression of MIM induced the accumulation of autophagosomes and impaired autolysosome formation during basal autophagy (Figure 4.3). This indicates that MIM inhibits an autophagic process downstream of the autophagosome formation. The nature of the autophagic process

involving MIM and the mechanism by which MIM inhibits autophagy are currently unknown.

Previous studies from this lab showed that MIM interacts with Rab5, Rab7 and the E3 ubiquitin ligase AIP4 to promote internalization of the chemokine receptor CXCR4 [105]. Several Rab GTPases function in both endocytosis and autophagy, including Rab5 and Rab7. Rab5 is thought to be involved in autophagosome formation while Rab7 is involved in autophagosome maturation and fusion events [155]. To explore the possibility that MIM inhibits autophagy perhaps by sequestering Rab7, we examined if induction of autophagy by starvation, rapamycin, or by treatment with CCCP, a mitochondrial oxidative phosphorylation uncoupler, had any effect on the interaction between MIM and Rab7. Early results revealed no change in MIM–Rab7 interaction upon autophagy induction (data not shown). A recent paper predicts a LC3-interacting (LIR) motif present in the MIM protein based on a computational analysis [156]. Therefore, we also looked for the potential interactions between MIM and LC3 or p62 by co-IP and immunofluorescence assays. Results from these experiments showed no evidence of any interactions among these proteins (data not shown).

Given our previous findings of MIM-mediated regulation of CXCR4 endocytosis through an interaction with a WW domain-containing E3 ligase, it is possible that MIM could alter autophagy through participation in an ubiquitination event. Ubiquitination is a key regulatory mechanism in autophagy, and several E3 ligase has been identified to be involved in the autophagic process, including two WW domain-containing E3 ligases, NEDD4 and SMURF1 [148]. The potential of MIM to interact with an ubiquitin ligase complex involved in autophagy will be explored in a future effort.

In a recent study using the yeast model system, Ivy1 was found to bind and inhibit the Fab1 complex [151]. Interestingly, the interaction between Ivy1 and Fab1 is interrupted by membrane stresses, resulting in vacuole fission. In yeasts, Fab1 is a kinase that acts as part of a complex responsible for the generation of phosphatidylinositol 3,5-bisphosphate (PI-3,5-P₂) on the surface of lysosomes, thereby promoting lysosomal membrane homeostasis [151]. In humans, PIKfyve (mammalian Fab1) is thought to participate in autophagosome maturation/fusion, as treatment of mammalian cells with PIKfyve inhibitors leads to an accumulation of autophagosomes [157]. It is possible that the interaction between Ivy1 and Fab1 may be conserved in mammalian cells, and that the possible interaction between MIM and PIKfyve may also be subjected to regulation by cellular stresses. In light of this, it is interesting to note our finding that autophagic stressors such as starvation can remove the autophagy inhibition imposed by MIM overexpression. This finding seems analogous to the reported inhibitory activity of Ivy1 for Fab1, which is released by osmotic stress in yeast. Future studies should verify the interaction between MIM and PIKfyve under conditions with and without autophagic stresses.

As discussed above, MIM imposes inhibitory activity on basal autophagy. However, overexpression of MIM does not block the autophagy induced by starvation, which could be partially due to the fact that either exogenous or endogenous MIM proteins are downregulated by starvation or rapamycin treatment. Starvation-mediated MIM downregulation may provide a biological advantage as it allows autophagy to proceed under cellular stresses. Yet, not all autophagy is associated with MIM downregulation as we have observed that C2-ceramide induces autophagy without

downregulating MIM. In addition to autophagy, ceramides also induce apoptotic cell death and are released during chemotherapy [158], thereby recently gaining great interests in cancer therapy. In light of this fact, our observation that overexpression of MIM impedes ceramide-induced autophagy while promoting its cytotoxicity is of considerable clinical significance. Further efforts will be made to explore the potential of modulating MIM expression to increase the sensitivity of cells to the cytotoxic effect of ceramides.

Chapter 5: Summary and Conclusion

In MIM-linked cancers, MIM is most commonly downregulated in tumors versus healthy tissues, and reduced expression of MIM is most often associated with metastasis and poor prognosis (**Table 1**). Despite the numerous studies showing this association, how MIM contributes to metastasis and poor prognosis is not fully understood. There is much that is still unknown about the regulation and function of MIM, which increases the challenge of understanding MIM's role in cancer progression. In this study, we proposed that microenvironment stressors can impact MIM expression, which may in turn influence the interaction and crosstalk between tumor cells and stromal cells (**Figure 5.1**). We focused on the effect of inflammation to determine if factors within the tumor microenvironment can alter MIM expression, and focused on elucidating the function of MIM in CXCR4 endocytosis and in autophagy, two processes that can influence microenvironment interactions.

Previous work in the lab showed that MIM promoted lysosomal degradation of CXCR4 by facilitating ubiquitination and endosomal sorting of the internalized receptor in cells that have been stimulated by its ligand, SDF-1[105]. Therefore, when MIM is downregulated, CXCR4 internalization and degradation are impaired, leading to overexpression of CXCR4 on cell surfaces. In this study, we found that certain pro-inflammatory cytokines decrease MIM expression in mouse macrophages and indirectly lead to overexpression of cell surface CXCR4. This finding could be important to determining MIM's role in cancer progression and metastasis, since macrophages play a significant role in promoting different aspects of metastasis, including the formation of pre-metastatic niches, extravasation of circulating cancer cells and colonization of

secondary sites [159]. Also, SDF-1 is secreted by stromal cells in the tumor microenvironment and metastatic niches [160]. Therefore, downregulation of MIM in macrophages may potentially facilitate the tumor-promoting role of macrophages through its regulation of CXCR4 expression. Future studies will focus on investigating the impact of inflammation on MIM expression in human macrophages, and on determining the mechanism through which inflammation regulates MIM in macrophages. The effect of chronic inflammation on MIM expression will also be explored.

MIM is thought to function in intracellular membrane trafficking pathways such as endocytosis and autophagy, given that it is a member of the BAR domain family of proteins. As mentioned above, our lab has recently described a mechanism by which MIM regulates CXCR4 endocytosis through interactions with E3 ligase AIP4 and small GTPases Rab5 and Rab7 to promote sorting of the receptor into endocytic vesicles of the lysosomal degradation pathway [105]. In this study, we found that Rab7 is necessary for MIM-mediated sorting of CXCR4 into the lysosomal degradation pathway, and that the interaction between I-BAR proteins and Rabs is important in determining the sorting fate of the internalized receptor. These findings are significant because Rabs function in multiple membrane trafficking pathways [161]. Therefore, MIM could potentially regulate other growth factor and chemokine receptors that similarly utilize endocytic intracellular trafficking as a regulatory mechanism, as well as regulate other trafficking pathways such as autophagy. Future directions of this study will include determining if MIM interacts with Rab7 to control other signaling pathways.

Given its role in CXCR4 regulation, aberrant MIM expression could have a major impact on interactions within the tumor microenvironment. In this study, we showed that

MIM-deficient cells had a stronger response to SDF-1 gradient, indicating increased metastatic potential for cells with low MIM expression. Although more in depth association studies are needed to confirm that CXCR4-overexpressing cancers have low MIM expression (or vice versa), CXCR4-overexpressing cancers [132] and MIM-downregulated cancers (**Table 1**) seem to overlap. The next step is to use *in vivo* mouse models to confirm that MIM-deficient tumor cells are more likely to migrate from the primary tumor bulk to secondary sites in response to a SDF-1 gradient.

The microenvironment may also impact the function of MIM in tumor progression via autophagy. We have discovered that high expression of MIM inhibits basal autophagy in cells by preventing autophagosome maturation and/or fusion with the lysosome. Basal autophagy is thought to play a tumor suppressive role because it can remove certain cancer-promoting factors such as misfolded proteins, damaged organelles, pathogens and toxins [162]. Overexpression of MIM is commonly associated with low-grade tumors and early TNM stages. Our finding suggests that the MIM-mediated inhibition of basal autophagy may contribute to tumor progression at early stages. Interestingly, we found that MIM expression is reduced by nutrient deprivation or mTOR inhibition, which could account for the significant variation in the level of MIM expression observed within tumor samples. When the tumor bulk increases, the reduced MIM expression as a result of microenvironmental factors could increase the migratory potential of the cancer cells, thus promoting metastasis.

While this study strongly suggests a role of MIM in autophagy, there is much to be determined about the mechanism through which MIM regulates autophagy. Future studies will focus on elucidating this mechanism. Furthermore, our results indicate that

MIM could be implicated in the pharmacologic function of ceramides, as overexpression of MIM promotes the cytotoxicity of C2-ceramide while inhibiting ceramide-induced autophagy. This finding could have significant implications for cancer therapy as increased ceramide production is a common side effect of chemotherapy and radiation [163].

Elucidating the role of MIM in mammalian autophagy could also have therapeutic implications for certain neurodegenerative disorders. A recent paper has reported that MIM-KO mice develop progressive ataxia, and neurons from these mice show some autophagy defects [79]. It would be interesting to define whether the defect in autophagy is a direct result of the lack of MIM expression.

Overall, the results presented here offer further insights into the role of MIM in cancer biology. Our findings provide several avenues to pursue in utilizing MIM as a cancer prognostic predictor or therapeutic target, and could also be beneficial to the treatment of other diseases such as neurodegenerative disorders.

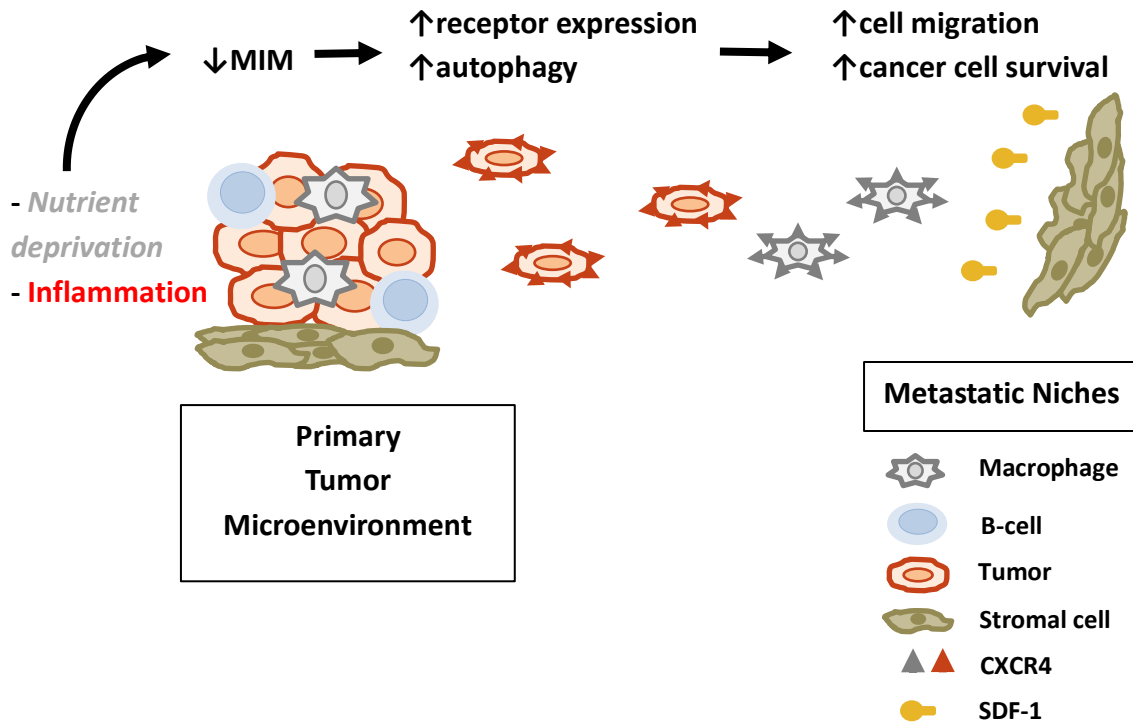


Figure 5.1 A model depicting the role of the tumor microenvironment in MIM expression and function. Inflammation and nutrient deprivation downregulate MIM expression in cells resulting in overexpression of cell surface CXCR4 and increased autophagy, thus promoting cell migration and cancer cell survival.

References

- [1] N. Riggi, M. Aguet, and I. Stamenkovic, “Cancer Metastasis: A Reappraisal of Its Underlying Mechanisms and Their Relevance to Treatment,” *Annu. Rev. Pathol. Mech. Dis.*, vol. 13, no. 1, pp. 117–140, 2018.
- [2] T. N. Seyfried and L. C. Huysentruyt, “On the origin of cancer metastasis,” *Crit. Rev. Oncog.*, vol. 18, no. 1–2, pp. 43–73, 2013.
- [3] C. L. Chaffer and R. A. Weinberg, “A perspective on cancer cell metastasis,” *Science (80-.)*, vol. 331, no. 6024, pp. 1559–1564, Mar. 2011.
- [4] N. N. Howlader *et al.*, “(SEER Cancer Statistics Review, 1975-2016,” *National Cancer Institute. Bethesda, MD, based on November 2018 SEER data submission, posted to the SEER web site, April 2019*, 2019. [Online]. Available: https://seer.cancer.gov/csr/1975_2016/.
- [5] C. Holohan, S. Van Schaeybroeck, D. B. Longley, and P. G. Johnston, “Cancer drug resistance: An evolving paradigm,” *Nat. Rev. Cancer*, vol. 13, no. 10, pp. 714–726, 2013.
- [6] Y. G. L. J. A. Macoska, S. Korenchuk, and K. J. Pienta, “MIM, a potential metastasis suppressor gene in bladder cancer,” *Neoplasia*, vol. 4, no. 4, pp. 291–294, 2002.
- [7] S. Nixdorf *et al.*, “Expression and regulation of MIM (Missing in Metastasis), a novel putative metastasis suppressor gene, and MIM-B, in bladder cancer cell lines,” *Cancer Lett.*, vol. 215, no. 2, pp. 209–220, 2004.
- [8] R. D. Loberg *et al.*, “Differential expression analysis of MIM (MTSS1) splice variants and a functional role of MIM in prostate cancer cell biology,” *Int. J. Oncol.*, vol. 26, no. 6, pp. 1699–1705, 2005.
- [9] P. Du, L. Ye, F. Ruge, Y. Yang, and W. G. Jiang, “Metastasis suppressor-1, MTSS1, acts as a putative tumour suppressor in human bladder cancer,” *Anticancer Res.*, vol. 31, no. 10, pp. 3205–3212, 2011.
- [10] F. Xie *et al.*, “The impact of Metastasis Suppressor-1, MTSS1, on oesophageal squamous cell carcinoma and its clinical significance,” *J. Transl. Med.*, vol. 9, no. 1, 2011.
- [11] H. Fan *et al.*, “MTSS1, a novel target of DNA methyltransferase 3B, functions as a tumor suppressor in hepatocellular carcinoma,” *Oncogene*, vol. 31, no. 18, pp. 2298–2308, 2012.
- [12] R. Liu, T. A. Martin, N. J. Jordan, F. Ruge, L. Ye, and W. G. Jiang, “Metastasis suppressor 1 expression in human ovarian cancer: The impact on cellular migration and metastasis,” *Int. J. Oncol.*, vol. 47, no. 4, pp. 1429–1439, 2015.

- [13] M. Schemionek *et al.*, “Identification of the adapter molecule MTSS1 as a potential oncogene-specific tumor suppressor in acute myeloid leukemia,” *PLoS One*, vol. 10, no. 5, 2015.
- [14] M. Schemionek *et al.*, “Mtss1 is a critical epigenetically regulated tumor suppressor in CML,” *Leukemia*, vol. 30, no. 4, pp. 823–832, 2016.
- [15] P. Du, S. Wang, X. Tang, C. An, Y. Yang, and W. G. Jiang, “Reduced expression of metastasis suppressor-1 (MTSS1) accelerates progression of human bladder uroepithelium cell carcinoma,” *Anticancer Res.*, vol. 37, no. 8, pp. 4499–4505, 2017.
- [16] H. Wang, X. Yu, X. Wang, X. Li, and S. Yang, “Missing in metastasis B, regulated by DNMT1, functions as a putative cancer suppressor in human lung giant-cell carcinoma,” *Acta Biochim. Biophys. Sin. (Shanghai)*, vol. 49, no. 3, pp. 238–245, 2017.
- [17] S. Ma, X. Y. Guan, T. K. Lee, and K. W. Chan, “Clinicopathological significance of missing in metastasis B expression in hepatocellular carcinoma,” *Hum. Pathol.*, vol. 38, no. 8, pp. 1201–1206, 2007.
- [18] K. D. Mertz *et al.*, “MTSS1 is a metastasis driver in a subset of human melanomas,” *Nat. Commun.*, vol. 5, 2014.
- [19] D. Wang, M. Xu, T. Wang, T. Li, and J. wei Zhu, “MTSS1 Overexpression Correlates with Poor Prognosis in Colorectal Cancer,” *J. Gastrointest. Surg.*, vol. 15, no. 7, pp. 1205–1212, 2011.
- [20] J. C. Dawson, P. Timpson, G. Kalna, and L. M. Machesky, “Mtss1 regulates epidermal growth factor signaling in head and neck squamous carcinoma cells,” *Oncogene*, vol. 31, no. 14, pp. 1781–1793, 2012.
- [21] J. Zhang, Y. Tong, L. Ren, and C. D. Li, “Expression of metastasis suppressor 1 in cervical carcinoma and the clinical significance,” *Oncol. Lett.*, vol. 8, no. 5, pp. 2145–2149, 2014.
- [22] G. Kayser *et al.*, “Downregulation of MTSS1 expression is an independent prognosticator in squamous cell carcinoma of the lung,” *Br. J. Cancer*, vol. 112, no. 5, pp. 866–873, 2015.
- [23] X. Y. Huang *et al.*, “Elevated MTSS1 expression associated with metastasis and poor prognosis of residual hepatitis B-related hepatocellular carcinoma,” *J. Exp. Clin. Cancer Res.*, vol. 35, no. 1, 2016.
- [24] X. Y. Huang *et al.*, “Missing-in-metastasis B (MIM-B) combined with caveolin-1 promotes metastasis of hepatocellular carcinoma,” *Oncotarget*, vol. 8, no. 56, pp. 95450–95465, 2017.
- [25] M. A. A. Koike Folgueira *et al.*, “Gene expression profile associated with response to doxorubicin-based therapy in breast cancer,” *Clin. Cancer Res.*, vol. 11, no. 20,

pp. 7434–7443, 2005.

- [26] C. Parr and W. G. Jiang, “Metastasis suppressor 1 (MTSS1) demonstrates prognostic value and anti-metastatic properties in breast cancer,” *Eur. J. Cancer*, vol. 45, no. 9, pp. 1673–1683, 2009.
- [27] M. C. Barros Filho *et al.*, “Gene trio signatures as molecular markers to predict response to doxorubicin cyclophosphamide neoadjuvant chemotherapy in breast cancer patients,” *Brazilian J. Med. Biol. Res.*, vol. 43, no. 12, pp. 1225–1231, 2010.
- [28] W. Xie, F. Sun, L. Chen, and X. Cao, “MiR-96 promotes breast cancer metastasis by suppressing MTSS1,” *Oncol. Lett.*, vol. 15, no. 3, pp. 3464–3471, 2018.
- [29] M. Kedmi *et al.*, “EGF induces microRNAs that target suppressors of cell migration: MiR-15b targets MTSS1 in breast cancer,” *Sci. Signal.*, vol. 8, no. 368, p. ra29, 2015.
- [30] J. Vadakekolathu *et al.*, “MTSS1 and SCAMP1 cooperate to prevent invasion in breast cancer,” *Cell Death Dis.*, vol. 9, no. 3, 2018.
- [31] S. Jahid *et al.*, “miR-23a promotes the transition from indolent to invasive colorectal cancer,” *Cancer Discov.*, vol. 2, no. 6, pp. 540–553, 2012.
- [32] W. Wu *et al.*, “MicroRNA-135b regulates metastasis suppressor 1 expression and promotes migration and invasion in colorectal cancer,” *Mol. Cell. Biochem.*, vol. 388, no. 1–2, pp. 249–259, 2014.
- [33] J. Li *et al.*, “Inhibition of miR-15b decreases cell migration and metastasis in colorectal cancer,” *Tumor Biol.*, vol. 37, no. 7, pp. 8765–8773, 2016.
- [34] E. Agarwal *et al.*, “Role of Akt2 in regulation of metastasis suppressor 1 expression and colorectal cancer metastasis,” *Oncogene*, vol. 36, no. 22, pp. 3104–3118, 2017.
- [35] M. Xu and T. A. O. Xu, “Expression and clinical significance of miR-23a and MTSS1 in diffuse large B-cell lymphoma,” *Oncol. Lett.*, vol. 16, no. 1, pp. 371–377, 2018.
- [36] S. Yamashita, Y. Tsujino, K. Moriguchi, M. Tatematsu, and T. Ushijima, “Chemical genomic screening for methylation-silenced genes in gastric cancer cell lines using 5-aza-2'-deoxycytidine treatment and oligonucleotide microarray,” *Cancer Sci.*, vol. 97, no. 1, pp. 64–71, 2006.
- [37] K. Liu, G. Wang, H. Ding, Y. Chen, G. Yu, and J. Wang, “Downregulation of metastasis suppressor 1(MTSS1) is associated with nodal metastasis and poor outcome in Chinese patients with gastric cancer,” *BMC Cancer*, vol. 10, 2010.
- [38] H. Wang, Y. Zhao, L. Cao, J. Zhang, Y. Wang, and M. Xu, “Metastasis suppressor protein 1 regulated by PTEN suppresses invasion, migration, and EMT of gastric

- carcinoma by inactivating PI3K/AKT signaling,” *J. Cell. Biochem.*, vol. 120, no. 3, pp. 3447–3454, 2019.
- [39] S. Zhang and Q. Qi, “MTSS1 suppresses cell migration and invasion by targeting CTTN in glioblastoma,” *J. Neurooncol.*, vol. 121, no. 3, pp. 425–431, 2015.
- [40] D. Luxen *et al.*, “MTSS1 is epigenetically regulated in glioma cells and inhibits glioma cell motility,” *Transl. Oncol.*, vol. 10, no. 1, pp. 70–79, 2017.
- [41] J. Wang, J. Li, J. Shen, C. Wang, L. Yang, and X. Zhang, “MicroRNA-182 downregulates metastasis suppressor 1 and contributes to metastasis of hepatocellular carcinoma,” *BMC Cancer*, vol. 12, 2012.
- [42] F. Wang, Y. Liu, and H. Zhang, “Loss of MTSS1 expression is an independent prognostic factor for hilar cholangiocarcinoma,” *Pathol. Oncol. Res.*, vol. 19, no. 4, pp. 815–820, 2013.
- [43] W. Shi, G. Hasimu, Y. Wang, N. Li, M. Chen, and H. Zhang, “MTSS1 is an independent prognostic biomarker for survival in intrahepatic cholangiocarcinoma patients,” *Am. J. Transl. Res.*, vol. 7, no. 10, pp. 1974–1983, 2015.
- [44] P. Du, L. Ye, H. Li, Y. Yang, and W. G. Jiang, “The tumour suppressive role of Metastasis Suppressor-1, MTSS1, in human kidney cancer, a possible connection with the SHH pathway,” *J. Exp. Ther. Oncol.*, vol. 10, no. 2, pp. 91–99, 2012.
- [45] M. D. Taylor, O. Bollt, S. C. Iyer, and G. P. Robertson, “Metastasis suppressor 1 (MTSS1) expression is associated with reduced in-vivo metastasis and enhanced patient survival in lung adenocarcinoma,” *Clin. Exp. Metastasis*, vol. 35, no. 1–2, pp. 15–23, 2018.
- [46] H. Zhao, J. Xue, J. Liu, Y. Liu, and Y. Cheng, “Effect of metastasis suppressor 1 on H1299 cells and its clinical significance in non-small cell lung cancer,” *Oncol. Rep.*, vol. 36, no. 5, pp. 2814–2822, 2016.
- [47] M. Liu *et al.*, “MiRNA-29a in lung cancer by Inhibiting MTSS1,” *Eur. Rev. Med. Pharmacol. Sci.*, vol. 22, no. 17, pp. 5531–5538, 2018.
- [48] N. Xu, W. Yang, Y. Liu, F. Yan, and Z. Yu, “MicroRNA-411 promoted the osteosarcoma progression by suppressing MTSS1 expression,” *Environ. Sci. Pollut. Res.*, vol. 25, no. 12, pp. 12064–12071, 2018.
- [49] H. S. Isaksson, B. Sorbe, and T. K. Nilsson, “Whole genome expression profiling of blood cells in ovarian cancer patients -Prognostic impact of the CYP1B1, MTSS1, NCALD, and NOP14 genes,” *Oncotarget*, vol. 5, no. 12, pp. 4040–4049, 2014.
- [50] L. Zhou *et al.*, “Expression and Significances of MTSS1 in Pancreatic Cancer,” *Pathol. Oncol. Res.*, vol. 22, no. 1, pp. 7–14, 2016.
- [51] L. Xu *et al.*, “miR-96 promotes the growth of prostate carcinoma cells by

- suppressing MTSS1,” *Tumor Biol.*, vol. 37, no. 9, pp. 12023–12032, 2016.
- [52] J. Chen, L. Huang, Q. Zhu, Z. Wang, and Z. Tang, “MTSS1 hypermethylation is associated with prostate cancer progression,” *J. Cell. Physiol.*, 2019.
- [53] Y. Guo, M. S. Ren, C. Shang, L. Zhu, and M. Zhong, “MTSS1 gene regulated by miR-96 inhibits cell proliferation and metastasis in tongue squamous cellular carcinoma Tca8113 cell line,” *Int. J. Clin. Exp. Med.*, vol. 8, no. 9, pp. 15441–15449, 2015.
- [54] J. Utikal *et al.*, “The expression of metastasis suppressor MIM/MTSS1 is regulated by DNA methylation,” *Int. J. Cancer*, vol. 119, no. 10, pp. 2287–2293, 2006.
- [55] N. Bethge *et al.*, “Identification of highly methylated genes across various types of B-cell non-hodgkin lymphoma,” *PLoS One*, vol. 8, no. 11, 2013.
- [56] J. Zhong *et al.*, “SCF β -TRCP targets MTSS1 for ubiquitination-mediated destruction to regulate cancer cell proliferation and migration,” *Oncotarget*, vol. 4, no. 12, pp. 2339–2353, 2013.
- [57] A. Giacobbe *et al.*, “p63 controls cell migration and invasion by transcriptional regulation of MTSS1,” *Oncogene*, vol. 35, no. 12, pp. 1602–1608, 2016.
- [58] R. Lei *et al.*, “Suppression of MIM by microRNA-182 activates RhoA and promotes breast cancer metastasis,” *Oncogene*, vol. 33, no. 10, pp. 1287–1296, 2014.
- [59] Q. Jiang, Y. Ren, J. Cheng, J. Cheng, J. Qin, and Y. Li, “Effect of miR-182 targeting MTSS1 on the proliferation and metastasis of esophageal cancer,” *Int. J. Clin. Exp. Pathol.*, vol. 9, no. 11, pp. 10871–10877, 2016.
- [60] Z. Liu *et al.*, “MiR-182 overexpression in tumorigenesis of high-grade serous ovarian carcinoma,” *J. Pathol.*, vol. 228, no. 2, pp. 204–215, 2012.
- [61] H. Hirata *et al.*, “MicroRNA-182-5p Promotes Cell Invasion and Proliferation by Down Regulating FOXF2, RECK and MTSS1 Genes in Human Prostate Cancer,” *PLoS One*, vol. 8, no. 1, 2013.
- [62] W. Zhou *et al.*, “MiR-135a promotes growth and invasion of colorectal cancer via metastasis suppressor 1 in vitro,” *Acta Biochim. Biophys. Sin. (Shanghai)*, vol. 44, no. 10, pp. 838–846, 2012.
- [63] S. Liu *et al.*, “MicroRNA-135a contributes to the development of portal vein tumor thrombus by promoting metastasis in hepatocellular carcinoma,” *J. Hepatol.*, vol. 56, no. 2, pp. 389–396, 2012.
- [64] M. De Yan *et al.*, “Fucoidan elevates MicroRNA-29b to regulate DNMT3B-MTSS1 axis and inhibit EMT in human hepatocellular carcinoma cells,” *Mar. Drugs*, vol. 13, no. 10, pp. 6099–6116, 2015.

- [65] <https://clinicaltrials.gov/ct2/show/NCT03601052>, “Efficacy, Safety, and Tolerability of Reamlarsen (MRG-201) Following Intradermal Injection in Subjects With a History of Keloids - Full Text View - ClinicalTrials.gov.” [Online]. Available: <https://clinicaltrials.gov/ct2/show/NCT03601052>. [Accessed: 19-Dec-2019].
- [66] A. E. Zeleniak, W. Huang, M. K. Brinkman, M. L. Fishel, and R. Hill, “Loss of MTSS1 results in increased metastatic potential in pancreatic cancer,” *Oncotarget*, vol. 8, no. 10, pp. 16473–16487, 2017.
- [67] A. E. Zeleniak, W. Huang, M. L. Fishel, and R. Hill, “PTEN-Dependent Stabilization of MTSS1 Inhibits Metastatic Phenotype in Pancreatic Ductal Adenocarcinoma,” *Neoplasia (United States)*, vol. 20, no. 1, pp. 12–24, 2018.
- [68] F. Xie, L. Ye, M. Ta, L. Zhang, and W. G. Jiang, “MTSS1: A multifunctional protein and its role in cancer invasion and metastasis,” *Front. Biosci. - Sch.*, vol. 3 S, no. 2, pp. 621–631, 2011.
- [69] A. Glassmann *et al.*, “Developmental expression and differentiation-related neuron-specific splicing of metastasis suppressor 1 (Mtss1) in normal and transformed cerebellar cells,” *BMC Dev. Biol.*, vol. 7, 2007.
- [70] G. Hayn-Leichsenring *et al.*, “Cellular distribution of metastasis suppressor 1 and the shape of cell bodies are temporarily altered in Engrailed-2 overexpressing cerebellar Purkinje cells,” *Neuroscience*, vol. 189, pp. 68–78, 2011.
- [71] T. Sistig, F. Lang, S. Wrobel, S. L. Baader, K. Schilling, and B. Eiberger, “Mtss1 promotes maturation and maintenance of cerebellar neurons via splice variant-specific effects,” *Brain Struct. Funct.*, vol. 222, no. 6, pp. 2787–2805, 2017.
- [72] W. Liu, Y. Komiya, C. Mezzacappa, D. K. Khadka, L. Runnels, and R. Habas, “MIM regulates vertebrate neural tube closure,” *Development*, vol. 138, no. 10, pp. 2035–2047, 2011.
- [73] K. Kawabata Galbraith *et al.*, “MTSS1 Regulation of Actin-Nucleating Formin DAAM1 in Dendritic Filopodia Determines Final Dendritic Configuration of Purkinje Cells,” *Cell Rep.*, vol. 24, no. 1, pp. 95-106.e9, 2018.
- [74] J. Saarikangas *et al.*, “MIM-Induced Membrane Bending Promotes Dendritic Spine Initiation,” *Dev. Cell*, vol. 33, no. 6, pp. 644–659, 2015.
- [75] J. Yu *et al.*, “Metastasis suppressor 1 regulates neurite outgrowth in primary neuron cultures,” *Neuroscience*, vol. 333, pp. 123–131, 2016.
- [76] H. S. Isaksson *et al.*, “Differential interactions of missing in metastasis and insulin receptor tyrosine kinase substrate with RAB proteins in the endocytosis of CXCR4,” *Oncogene*, vol. 8, no. 1, pp. 6494–6505, 2016.
- [77] J. Saarikangas *et al.*, “Missing-in-metastasis MIM/MTSS1 promotes actin assembly at intercellular junctions and is required for integrity of kidney

- epithelia,” *J. Cell Sci.*, vol. 124, no. 8, pp. 1245–1255, 2011.
- [78] D. Yu *et al.*, “Mice deficient in MIM expression are predisposed to lymphomagenesis,” *Oncogene*, vol. 31, no. 30, pp. 3561–3568, 2012.
- [79] A. S. Brown *et al.*, “MTSS1/Src family kinase dysregulation underlies multiple inherited ataxias,” *Proc. Natl. Acad. Sci. U. S. A.*, vol. 115, no. 52, pp. E12407–E12416, 2018.
- [80] D. Sakamuro, K. J. Elliott, R. Wechsler-Reya, and G. C. Prendergast, “BIN1 is a novel MYC-interacting protein with features of a tumour suppressor,” *Nat. Genet.*, vol. 14, no. 1, pp. 69–77, 1996.
- [81] T. B. Stanishneva-Konovalova, N. I. Derkacheva, S. V. Polevova, and O. S. Sokolova, “The Role of BAR Domain Proteins in the Regulation of Membrane Dynamics,” *Acta Naturae*, vol. 8, no. 4, pp. 60–69, 2016.
- [82] F. Safari and S. Suetsugu, “The BAR domain superfamily proteins from subcellular structures to human diseases,” *Membranes (Basel)*, vol. 2, no. 1, pp. 91–117, 2012.
- [83] C. Mim and V. M. Unger, “Membrane curvature and its generation by BAR proteins,” *Trends in Biochemical Sciences*, vol. 37, no. 12, pp. 526–533, 2012.
- [84] U. Salzer, J. Kostan, and K. Djinović-Carugo, “Deciphering the BAR code of membrane modulators,” *Cell. Mol. Life Sci.*, vol. 74, no. 13, pp. 2413–2438, 2017.
- [85] H. Zhao, A. Pykäläinen, and P. Lappalainen, “I-BAR domain proteins: Linking actin and plasma membrane dynamics,” *Current Opinion in Cell Biology*, vol. 23, no. 1, pp. 14–21, 2011.
- [86] L. M. Machesky and S. A. Johnston, “MIM: A multifunctional scaffold protein,” *J. Mol. Med.*, vol. 85, no. 6, pp. 569–576, 2007.
- [87] G. Bompard, S. J. Sharp, G. Freiss, and L. M. Machesky, “Involvement of Rac in actin cytoskeleton rearrangements induced by MIM-B,” *J. Cell Sci.*, vol. 118, no. 22, pp. 5393–5403, 2005.
- [88] J. C. Dawson, S. Bruche, H. J. Spence, V. M. M. Braga, and L. M. Machesky, “Mtss1 promotes cell-cell junction assembly and stability through the small GTPase Rac1,” *PLoS One*, vol. 7, no. 3, 2012.
- [89] J. Lin *et al.*, “Differential regulation of cortactin and N-WASP-mediated actin polymerization by missing in metastasis (MIM) protein,” *Oncogene*, vol. 24, no. 12, pp. 2059–2066, 2005.
- [90] J. A. Woodings, S. J. Sharp, and L. M. Machesky, “MIM-B, a putative metastasis suppressor protein, binds to actin and to protein tyrosine phosphatase δ ,” *Biochem. J.*, vol. 371, no. 2, pp. 463–471, 2003.

- [91] R. Gonzalez-Quevedo, M. Shoffer, L. Horng, and A. E. Oro, "Receptor tyrosine phosphatase-dependent cytoskeletal remodeling by the hedgehog-responsive gene MIM/BEG4," *J. Cell Biol.*, vol. 168, no. 3, pp. 453–463, 2005.
- [92] J. Saarikangas *et al.*, "Molecular Mechanisms of Membrane Deformation by I-BAR Domain Proteins," *Curr. Biol.*, vol. 19, no. 2, pp. 95–107, 2009.
- [93] X. Lin, H. Wang, Z. Lou, M. Cao, Z. Zhang, and N. Gu, "Roles of PIP2 in the membrane binding of MIM I-BAR: insights from molecular dynamics simulations," *FEBS Lett.*, vol. 592, no. 15, pp. 2533–2542, 2018.
- [94] P. K. Mattila, M. Salminen, T. Yamashiro, and P. Lappalainen, "Mouse MIM, a tissue-specific regulator of cytoskeletal dynamics, interacts with ATP-actin monomers through its C-terminal WH2 domain," *J. Biol. Chem.*, vol. 278, no. 10, pp. 8452–8459, 2003.
- [95] A. Yamagishi, M. Masuda, T. Ohki, H. Onishi, and N. Mochizuki, "A Novel Actin Bundling/Filopodium-forming Domain Conserved in Insulin Receptor Tyrosine Kinase Substrate p53 and Missing in Metastasis Protein," *J. Biol. Chem.*, vol. 279, no. 15, pp. 14929–14936, 2004.
- [96] S. H. Lee, F. Kerff, D. Chereau, F. Ferron, A. Klug, and R. Dominguez, "Structural Basis for the Actin-Binding Function of Missing-in-Metastasis," *Structure*, vol. 15, no. 2, pp. 145–155, 2007.
- [97] M. P. Maddugoda *et al.*, "CAMP signaling by Anthrax edema toxin induces transendothelial cell tunnels, which Are resealed by MIM via Arp2/3-Driven actin polymerization," *Cell Host Microbe*, vol. 10, no. 5, pp. 464–474, 2011.
- [98] M. Cao, T. Zhan, M. Ji, and X. Zhan, "Dimerization is necessary for MIM-mediated membrane deformation and endocytosis," *Biochem. J.*, vol. 446, no. 3, pp. 469–475, 2012.
- [99] G. A. Quinones, J. Jin, and A. E. Oro, "I-BAR protein antagonism of endocytosis mediates directional sensing during guided cell migration," *J. Cell Biol.*, vol. 189, no. 2, pp. 353–367, 2010.
- [100] Y. Wang, K. Zhou, X. Zeng, J. Lin, and X. Zhan, "Tyrosine phosphorylation of missing in metastasis protein is implicated in platelet-derived growth factor-mediated cell shape changes," *J. Biol. Chem.*, vol. 282, no. 10, pp. 7624–7631, 2007.
- [101] T. Zhan, C. Cao, L. Li, N. Gu, C. I. Civin, and X. Zhan, "MIM regulates the trafficking of bone marrow cells via modulating surface expression of CXCR4," *Leukemia*, vol. 30, no. 6, pp. 1327–1334, 2016.
- [102] M. Bershteyn, S. X. Atwood, W. M. Woo, M. Li, and A. E. Oro, "MIM and cortactin antagonism regulates ciliogenesis and hedgehog signaling," *Dev. Cell*, vol. 19, no. 2, pp. 270–283, 2010.

- [103] C. A. Callahan *et al.*, “MIM/BEG4, a Sonic hedgehog-responsive gene that potentiates Gli-dependent transcription,” *Genes Dev.*, vol. 18, no. 22, pp. 2724–2729, 2004.
- [104] S. S. Singh *et al.*, “Dual role of autophagy in hallmarks of cancer,” *Oncogene*, vol. 37, no. 9, pp. 1142–1158, 2018.
- [105] L. Li, S. S. Baxter, N. Gu, M. Ji, and X. Zhan, “Missing-in-metastasis protein downregulates CXCR4 by promoting ubiquitylation and interaction with small Rab GTPases,” *J. Cell Sci.*, vol. 130, no. 8, pp. 1475–1485, 2017.
- [106] S. Takahashi *et al.*, “Rab11 regulates exocytosis of recycling vesicles at the plasma membrane,” *J. Cell Sci.*, vol. 125, no. 17, pp. 4049–4057, 2012.
- [107] L. Li, S. S. Baxter, P. Zhao, N. Gu, and X. Zhan, “Differential interactions of missing in metastasis and insulin receptor tyrosine kinase substrate with RAB proteins in the endocytosis of CXCR4,” *J. Biol. Chem.*, vol. 294, no. 16, pp. 6494–6505, 2019.
- [108] E. Tasdemir *et al.*, “Methods for assessing autophagy and autophagic cell death,” *Methods Mol. Biol.*, vol. 445, pp. 29–76, 2008.
- [109] S. A. F. Morad and M. C. Cabot, “Ceramide-orchestrated signalling in cancer cells,” *Nat. Rev. Cancer*, vol. 13, no. 1, pp. 51–65, 2013.
- [110] W. Zhu, X. Wang, Y. Zhou, and H. Wang, “C2-ceramide induces cell death and protective autophagy in head and neck squamous cell carcinoma cells,” *Int. J. Mol. Sci.*, vol. 15, no. 2, pp. 3336–3355, 2014.
- [111] Y. Yuan, Y. C. Jiang, C. K. Sun, and Q. M. Chen, “Role of the tumor microenvironment in tumor progression and the clinical applications (Review),” *Oncol. Rep.*, vol. 35, no. 5, pp. 2499–2515, May 2016.
- [112] M. J. Oudin and V. M. Weaver, “Physical and chemical gradients in the tumor microenvironment regulate tumor cell invasion, migration, and metastasis,” *Cold Spring Harb. Symp. Quant. Biol.*, vol. 81, no. 1, pp. 189–205, Jan. 2016.
- [113] M. Wang *et al.*, “Role of tumor microenvironment in tumorigenesis,” *Journal of Cancer*, vol. 8, no. 5, pp. 761–773, 2017.
- [114] F. R. Balkwill, M. Capasso, and T. Hagemann, “The tumor microenvironment at a glance,” *J. Cell Sci.*, vol. 125, no. 23, pp. 5591–5596, 2012.
- [115] N. E. Sounni and A. Noel, “Targeting the tumor microenvironment for cancer therapy,” *Clin. Chem.*, vol. 59, no. 1, pp. 85–93, Jan. 2013.
- [116] A. Palumbo, N. de Oliveira Meireles Da Costa, M. H. Bonamino, L. F. Ribeiro Pinto, and L. E. Nasciutti, “Genetic instability in the tumor microenvironment: A new look at an old neighbor,” *Molecular Cancer*, vol. 14, no. 1, 2015.

- [117] X. Zhang, R. Goncalves, and D. M. Mosser, "The isolation and characterization of murine macrophages," *Current Protocols in Immunology*, no. SUPPL. 83. 2008.
- [118] C. Calatuzzolo, E. Ciusani, E. Corsini, F. Di Meco, B. Pollo, and A. Salmaggi, "Involvement of the CXCL12/CXCR4/CXCR7 Axis in Brain Metastases," in *Brain Metastases from Primary Tumors: Epidemiology, Biology, and Therapy*, Elsevier Inc., 2014, pp. 25–36.
- [119] L. Yang and Y. Zhang, "Tumor-associated macrophages: from basic research to clinical application," *J. Hematol. Oncol.*, vol. 10, no. 1, p. 58, 2017.
- [120] D. Hanahan and R. A. Weinberg, "Hallmarks of cancer: The next generation," *Cell*, vol. 144, no. 5, pp. 646–674, 2011.
- [121] J. L. Owen and M. Mohamadzadeh, "Macrophages and chemokines as mediators of angiogenesis," *Front. Physiol.*, vol. 4 JUL, 2013.
- [122] J. Wan *et al.*, "NFB inhibition attenuates LPS-induced TLR4 activation in monocyte cells," *Mol. Med. Rep.*, vol. 14, no. 5, pp. 4505–4510, Nov. 2016.
- [123] P. Tsou, H. Katayama, E. J. Ostrin, and S. M. Hanash, "The emerging role of b cells in tumor immunity," *Cancer Research*, vol. 76, no. 19. American Association for Cancer Research Inc., pp. 5591–5601, 01-Oct-2016.
- [124] G. Multhoff, M. Molls, and J. Radons, "Chronic inflammation in cancer development," *Front. Immunol.*, vol. 2, no. JAN, 2012.
- [125] I. Mellman and Y. Yarden, "Endocytosis and cancer," *Cold Spring Harb. Perspect. Biol.*, vol. 5, no. 12, 2013.
- [126] S. R. Elkin, A. M. Lakoduk, and S. L. Schmid, "Endocytic pathways and endosomal trafficking: a primer," *Wiener Medizinische Wochenschrift*, vol. 166, no. 7–8, pp. 196–204, 2016.
- [127] Y. Mosesson, G. B. Mills, and Y. Yarden, "Derailed endocytosis: An emerging feature of cancer," *Nat. Rev. Cancer*, vol. 8, no. 11, pp. 835–850, Nov. 2008.
- [128] J. A. Burger and T. J. Kipps, "CXCR4: A key receptor in the crosstalk between tumor cells and their microenvironment," *Blood*, vol. 107, no. 5, pp. 1761–1767, 2006.
- [129] A. Marchese, C. Raiborg, F. Santini, J. H. Keen, H. Stenmark, and J. L. Benovic, "The E3 ubiquitin ligase AIP4 mediates ubiquitination and sorting of the G protein-coupled receptor CXCR4," *Dev. Cell*, vol. 5, no. 5, pp. 709–722, Nov. 2003.
- [130] A. Marchese, "Endocytic trafficking of chemokine receptors," *Current Opinion in Cell Biology*, vol. 27, no. 1. pp. 72–77, 2014.
- [131] H. Stenmark, "Rab GTPases as coordinators of vesicle traffic," *Nat. Rev. Mol. Cell*

Biol., vol. 10, no. 8, pp. 513–525, Aug. 2009.

- [132] S. Chatterjee, B. Behnam Azad, and S. Nimmagadda, “The intricate role of CXCR4 in cancer,” *Advances in Cancer Research*, vol. 124, pp. 31–82, 2014.
- [133] P. Aspenstrom, “BAR domain proteins regulate Rho GTPase signaling,” *Small GTPases*, vol. 5, no. 2, Dec. 2014.
- [134] T. Sudhakaran *et al.*, “The rho GTPase signals through IRTKS, EPS8 and WAVE2 to generate dorsal membrane ruffles and filopodia,” *J. Cell Sci.*, vol. 129, no. 14, pp. 2829–2840, 2016.
- [135] L. Li, H. Liu, S. S. Baxter, N. Gu, M. Ji, and X. Zhan, “The SH3 domain distinguishes the role of I-BAR proteins IRTKS and MIM in chemotactic response to serum,” *Biochem. Biophys. Res. Commun.*, vol. 479, no. 4, pp. 787–792, 2016.
- [136] K. W. Dunn, M. M. Kamocka, and J. H. McDonald, “A practical guide to evaluating colocalization in biological microscopy,” *Am. J. Physiol. - Cell Physiol.*, vol. 300, no. 4, Apr. 2011.
- [137] K. E. Luker and G. D. Luker, “Functions of CXCL12 and CXCR4 in breast cancer,” *Cancer Lett.*, vol. 238, no. 1, pp. 30–41, Jul. 2006.
- [138] Y. Wang *et al.*, “Downregulation of missing in metastasis gene (MIM) is associated with the progression of bladder transitional carcinomas,” *Cancer Invest.*, vol. 25, no. 2, pp. 79–86, 2007.
- [139] P. A. Vanlandingham and B. P. Ceresa, “Rab7 regulates late endocytic trafficking downstream of multivesicular body biogenesis and cargo sequestration,” *J. Biol. Chem.*, vol. 284, no. 18, pp. 12110–12124, May 2009.
- [140] B. L. Wolfe and J. A. Trejo, “Clathrin-dependent mechanisms of G protein-coupled receptor endocytosis,” *Traffic*, vol. 8, no. 5, pp. 462–470, May-2007.
- [141] S. Sigismund, S. Confalonieri, A. Ciliberto, S. Polo, G. Scita, and P. P. di Fiore, “Endocytosis and signaling: Cell logistics shape the eukaryotic cell plan,” *Physiol. Rev.*, vol. 92, no. 1, pp. 273–366, Jan. 2012.
- [142] F. Guerra and C. Bucci, “Multiple Roles of the Small GTPase Rab7,” *Cells*, vol. 5, no. 3, p. 34, Aug. 2016.
- [143] R. J. Ingham, G. Gish, and T. Pawson, “The Nedd4 family of E3 ubiquitin ligases: Functional diversity within a common modular architecture,” *Oncogene*, vol. 23, no. 11 REV. ISS. 1, pp. 1972–1984, Mar. 2004.
- [144] D. Glick, S. Barth, and K. F. Macleod, “Autophagy: Cellular and molecular mechanisms,” *J. Pathol.*, vol. 221, no. 1, pp. 3–12, 2010.
- [145] N. Mizushima, “Autophagy: Process and function,” *Genes and Development*, vol.

21, no. 22. pp. 2861–2873, 15-Nov-2007.

- [146] X. Sui *et al.*, “Autophagy and chemotherapy resistance: A promising therapeutic target for cancer treatment,” *Cell Death Dis.*, vol. 4, no. 10, 2013.
- [147] S. A. Tooze, A. Abada, and Z. Elazar, “Endocytosis and autophagy: Exploitation or cooperation?,” *Cold Spring Harb. Perspect. Biol.*, vol. 6, no. 5, pp. 18358–18359, 2014.
- [148] E. Kuang, J. Qi, and Z. Ronai, “Emerging roles of E3 ubiquitin ligases in autophagy,” *Trends Biochem. Sci.*, vol. 38, no. 9, pp. 453–460, 2013.
- [149] J. Numrich *et al.*, “The I-BAR protein Ivy1 is an effector of the Rab7 GTPase Ypt7 involved in vacuole membrane homeostasis,” *J. Cell Sci.*, vol. 128, no. 13, pp. 2278–2292, 2015.
- [150] N. V. Varlakhanova, B. A. Tornabene, and M. G. J. Ford, “Ivy1 is a negative regulator of Gtr-dependent TORC1 activation,” *J. Cell Sci.*, vol. 131, no. 17, Sep. 2018.
- [151] P. C. Malia, J. Numrich, T. Nishimura, A. G. Montoro, C. J. Stefan, and C. Ungermann, “Control of vacuole membrane homeostasis by a resident PI-3,5-kinase inhibitor,” *Proc. Natl. Acad. Sci. U. S. A.*, vol. 115, no. 18, pp. 4684–4689, May 2018.
- [152] S. R. Yoshii and N. Mizushima, “Monitoring and measuring autophagy,” *International Journal of Molecular Sciences*, vol. 18, no. 9. MDPI AG, 01-Sep-2017.
- [153] I. Orhon and F. Reggiori, “Assays to Monitor Autophagy Progression in Cell Cultures,” *Cells*, vol. 6, no. 3, p. 20, 2017.
- [154] B. Ravikumar *et al.*, “Regulation of mammalian autophagy in physiology and pathophysiology,” *Physiol. Rev.*, vol. 90, no. 4, pp. 1383–1435, 2010.
- [155] I. G. Ganley, “Autophagosome maturation and lysosomal fusion,” *Essays Biochem.*, vol. 55, no. 1, pp. 65–78, 2013.
- [156] P. Petrov *et al.*, “Computational analysis of the evolutionarily conserved Missing In Metastasis/Metastasis Suppressor 1 gene predicts novel interactions, regulatory regions and transcriptional control,” *Sci. Rep.*, vol. 9, no. 1, 2019.
- [157] F. Reggiori and C. Ungermann, “Autophagosome Maturation and Fusion,” *Journal of Molecular Biology*, vol. 429, no. 4. Academic Press, pp. 486–496, 17-Feb-2017.
- [158] S. Pattingre, C. Bauvy, T. Levade, B. Levine, and P. Codogno, “Ceramide-induced autophagy: To junk or to protect cells?,” *Autophagy*, vol. 5, no. 4, pp. 558–560, May 2009.
- [159] G. R. Doak, K. L. Schwertfeger, and D. K. Wood, “Distant Relations: Macrophage

Functions in the Metastatic Niche,” *Trends in Cancer*, vol. 4, no. 6, pp. 445–459, Jun. 2018.

- [160] W. Meng, S. Xue, and Y. Chen, “The role of CXCL12 in tumor microenvironment,” *Gene*, vol. 641. Elsevier B.V., pp. 105–110, 30-Jan-2018.
- [161] J. C. Hervé and N. Bourmeyster, “Rab GTPases, master controllers of eukaryotic trafficking,” *Small GTPases*, vol. 9, no. 1–2. pp. 1–4, 2018.
- [162] C. W. Yun and S. H. Lee, “The Roles of Autophagy in Cancer,” *International journal of molecular sciences*, vol. 19, no. 11. NLM (Medline), 05-Nov-2018.
- [163] R. Nganga, N. Oleinik, and B. Ogretmen, “Mechanisms of Ceramide-Dependent Cancer Cell Death,” *Adv. Cancer Res.*, vol. 140, pp. 1–25, Jan. 2018.